NASA TECHNICAL NOTE

NASA TN D-3203

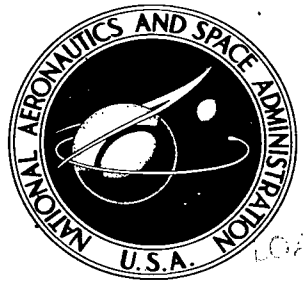

TRANSONIC AERODYNAMIC CHARACTERISTICS OF A SERIES OF RELATED BODIES WITH CROSS-SECTIONAL ELLIPTICITY

by Bernard Spencer, Jr.

Langley Research Center
Langley Station, Hampton, Va.

NATIONAL AERONAUTICS AND SPACE ADMINISTRATION • WASHINGTON, D. C. • FEBRUARY 1966

TRANSONIC AERODYNAMIC CHARACTERISTICS OF A SERIES OF RELATED BODIES WITH CROSS-SECTIONAL ELLIPTICITY

By Bernard Spencer, Jr.

Langley Research Center
Langley Station, Hampton, Va.

NATIONAL AERONAUTICS AND SPACE ADMINISTRATION

For sale by the Clearinghouse for Federal Scientific and Technical Information
Springfield, Virginia 22151 – Price $3.00

TRANSONIC AERODYNAMIC CHARACTERISTICS OF A SERIES OF RELATED BODIES WITH CROSS-SECTIONAL ELLIPTICITY

By Bernard Spencer, Jr.
Langley Research Center

SUMMARY

An investigation has been made to determine the transonic aerodynamic characteristics of a series of power-law bodies and a theoretical hypersonic minimum-wave-drag body of equal length and equal volume. Also included in the investigation are the effects of altering cross-sectional ellipticity for a given body, while maintaining a constant longitudinal distribution of cross-sectional area. The Mach number range of the investigation was from 0.50 to 1.12, and the angle of attack was varied from approximately -6° to 28° at 0° of sideslip.

Increasing power-body exponent for a given value of ellipticity results in increases in the lift-curve slope at low angles of attack and in the overall lift variation with angle of attack throughout the Mach number range. Large increases in minimum drag at a given Mach number also occur with increasing body exponent primarily because of the large increase in base area. The maximum lift-drag ratio for the series of power-law bodies was obtained with the lowest power-body exponent (smallest base area) at all Mach numbers. Increasing body exponent also resulted in large rearward shifts in longitudinal center-of-pressure location at all Mach numbers.

Increasing ellipticity for any given power-law body resulted in large increases in lift and maximum lift-drag ratio and only slight effects on center-of-pressure location.

A comparison between a theoretically determined body shape for minimized pressure drag at hypersonic speeds and the series of power-law bodies investigated indicates that the overall aerodynamic characteristics of the theoretical body are similar to those experienced with a power-law body having an exponent of 0.50. The values of maximum lift-drag ratio at transonic speeds for the theoretical body were slightly higher than those for the power-law bodies for all values of ellipticity.

INTRODUCTION

Extensive research has been done and is presently being done by the National Aeronautics and Space Administration and others relating to theoretical and experimental

determination of the aerodynamic characteristics of volumetrically efficient lifting-body configurations. (See refs. 1 to 12.) Configurations of this type may have application to vehicles designed for hypersonic cruise or glide, or for operations between earth and near-earth orbiting laboratories. Since some portion of the aforementioned missions will be made at low-subsonic, transonic, and supersonic speeds, aerodynamic efficiency is desired at all speeds for maneuvering ability and range control (refs. 13 and 14).

In the continuing study of practical body shapes for hypersonic flight, the present investigation was made to determine the transonic aerodynamic characteristics of a series of power-law bodies and a theoretical body for minimizing zero-lift pressure drag at hypersonic speeds; the power-law bodies and the theoretical body have equal length and equal volume. The power-law bodies have values of the exponent of 0.25, 0.50, 0.66, 0.75, and 1.00. The hypersonic minimum-wave-drag shapes were determined by using the methods described in references 11 and 12. For a given power-law body or the minimum-wave-drag body, cross-sectional shape was altered from circular to elliptic, while maintaining a constant longitudinal distribution of cross-sectional area. Horizontal- to vertical-axis ratios of 1.0, 2.0, and 3.0 were investigated for each of the power-law bodies and the minimum-wave-drag body. The experiments were made in the Langley high-speed 7- by 10-foot tunnel at Mach numbers from 0.50 to 1.12, corresponding to a range of average test Reynolds numbers from 6.25×10^6 to 9.00×10^6 based on body length. Angle-of-attack range was from approximately -6° to 28° at 0° of sideslip.

SYMBOLS

Longitudinal data are presented about the stability and body axes, and all coefficients are normalized with respect to each body projected planform area and length (25.00 in., or 0.635 m). The longitudinal location of the moment reference point was located at 66.67 percent of the total length for each configuration; the vertical moment reference point was located on the body center line.

$C_{A,b}$ base-axial-force coefficient

C_L lift coefficient, $\frac{\text{Lift}}{qS}$

C_N normal-force coefficient, $\frac{\text{Normal force}}{qS}$

C_D drag coefficient, $\frac{\text{Drag}}{qS}$

C_m pitching-moment coefficient, $\frac{\text{Pitching moment}}{qS\ell}$

$C_{D,min}$	minimum drag coefficient
C_{L_α}	lift-curve slope ($\alpha \approx 0^o$)
C_{N_α}	normal-force-curve slope ($\alpha \approx 0^o$), per deg
C_{m_α}	longitudinal stability parameter, per deg
a	semimajor (horizontal) axis length of elliptic-cross-section bodies, radius for a/b = 1.0 bodies, $a = \frac{a_{max}}{l^n} x^n$, ft (m)
a_{max}	body maximum semispan, ft (m)
b	semiminor (vertical) axis length of elliptic-cross-section bodies, ft (m)
l	total body length, 25.00 in. (0.635 m)
L/D	lift-drag ratio
$(L/D)_{max}$	maximum lift-drag ratio
A	aspect ratio, $\frac{(2a_{max})^2}{S}$
A_b	body base area, sq ft (sq m)
M	Mach number
q	free-stream dynamic pressure, lb/sq ft (N/sq m)
S	body projected planform area, sq ft (sq m)
S_{cross}	cross-sectional area of bodies, sq ft (sq m)
S_{wet}	wetted area of bodies (excluding base area), sq ft (sq m)
x	longitudinal coordinate of bodies, ft (m)
x_o	longitudinal coordinate of moment reference point, ft (m)

x_{cp}/l	longitudinal center-of-pressure location ($\alpha = 0$), $x_o/l - C_{m_\alpha}/C_{N_\alpha}$
α	angle of attack, deg
n	power-body exponent

MODELS

Three-view drawings of the power-law bodies used in the investigation are shown in figure 1 along with pertinent geometric characteristics. Photographs of the bodies are shown as figure 2. Normalized design ordinates for each body are presented in table I.

All the bodies used in the investigation had either circular or elliptic cross sections with horizontal- to vertical-axis ratios (a/b) of 1.0, 2.0, and 3.0 held constant along the length of the body. The planform of the power-law bodies was defined by the relation $a = a_{max}(x/l)^n$ with values of the exponent n of 0.25, 0.50, 0.66, 0.75, and 1.00. The planform of the theoretical hypersonic minimum-wave-drag bodies was defined as described in reference 12 and does not conform to a power relation. The constraints of equal length and equal volume have been imposed on all bodies.

TESTS AND CORRECTIONS

The present investigation was conducted in the Langley high-speed 7- by 10-foot tunnel at Mach numbers from 0.50 to 1.12, corresponding to a range of average test Reynolds numbers from approximately 6.25×10^6 to 9.00×10^6 based on body length. The angle-of-attack range of the investigation was from approximately -5^o to 28^o at 0^o of sideslip.

Forces and moments were measured by use of a sting-supported, internally mounted, six-component strain-gage balance.

Transition was fixed on all bodies tested at a distance of 1.0 inch aft of the body apex by a 1/8-inch-wide circumferential band of carborundum grains having a nominal diameter of 0.0117 inch. Transition was also fixed along the body length on the lower surface at a distance from the body center line equal to one-eighth the local perimeter.

Corrections have been applied to the angle of attack to account for deflection of the sting and balance under load. Drag coefficients presented herein are for total drag of the configuration, including base drag. In order to indicate the magnitude of the base-axial-force coefficients for the power-law bodies with $a/b = 1.0$ and $a/b = 2.0$ and for the minimum-wave-drag body, $C_{A,b}$ values are presented in figure 3, as a function of angle

of attack, for the various test Mach numbers. No base-axial-force data were obtained on the $a/b = 3.0$ bodies.

The bases of the models were concaved in an effort to obtain a uniform pressure at the base. No attempt has been made to correct the drag data for the induced effect of sting-support interference. Support interference effects on various types of configurations are shown in references 8, 15, and 16.

RESULTS AND DISCUSSION

Figures 4 to 9 present the basic longitudinal aerodynamic data at Mach numbers from 0.50 to 1.12 for each configuration. Figures 10 to 14 present a summary of pertinent longitudinal aerodynamic parameters as functions of Mach number, power-law-body exponent, and ellipticity. The major portion of the discussion is confined to observations of the summary data except for significant results noted in the basic data.

Increasing the power-body exponent (decreasing bluntness and increasing span, figs. 1(b) and 1(c)) for a given value of ellipticity results in large increases in the lift-curve slope at low angles of attack (fig. 10(b)) and in the overall lift variation with angle of attack at all Mach numbers (figs. 4 to 9). There are only minor effects of increasing Mach number on the lift-curve slope at low angles of attack for any of the configurations, however. (See fig. 10(b).) Increasing the value of a/b for any given power-law body or the minimum-wave-drag body results in large increases in lift; the percentage increase in the lift referenced to that of the circular body is almost constant for a given value of ellipticity. (See fig. 10(c).) The lift characteristics for the minimum-wave-drag body are approximately the same as those noted for the $n = 0.50$ body. This would be expected since the aspect ratios of these two bodies are approximately the same.

A rather large increase in $C_{D,min}$ occurs for each body as the Mach number is increased from approximately 0.90 up to 1.12 (fig. 11(a)). The large increases in $C_{D,min}$ which result from increasing the power-body exponent n at all Mach numbers (fig. 11(b)) are due primarily to the large increase in base area and resultant base axial force, as may be noted in figure 3. As in the case of the lift-curve slope, increasing ellipticity results in an approximately constant percentage reduction in zero-lift drag coefficient (as referenced to that of the circular body) independent of the body contour (n = variable). Generally, the minimum drag of the minimum-wave-drag body is slightly less than that of any power-law body investigated (except for $n = 0.25$ body) because of less base area and the fact that the body slope is zero at the base.

Increasing power-body exponent for a given value of ellipticity results in large reductions in $(L/D)_{max}$ at all Mach numbers. (See fig. 12.) Although increasing body exponent n for a given ellipticity results in large increases in lift and reduction in drag

due to lift due to the increased aspect ratio, the large increases in base area and base flare angle, and resultant increases in base drag which occur as n approaches 1.0 (fig. 3) more than offset the gains in lift.

The percentage increases in $(L/D)_{max}$ (as referenced to that of the circular body) due to increasing ellipticity (fig. 12(c)) are essentially independent of body contour. The values of $(L/D)_{max}$ for the minimum-wave-drag bodies of given ellipticity are generally as high as or higher than those for any of the power-law bodies investigated (except for $n = 0.25$), especially near $M = 1.00$.

Figures 13 and 14 present the effects of body shape on the longitudinal stability parameter C_{m_α} and longitudinal center-of-pressure location. The center-of-pressure locations are given in percent of body length as measured from the apex. Increasing Mach number results in slight rearward shifts in center of pressure up to $M = 1.00$ (fig. 14(a)) for each of the bodies investigated. Increasing power-body exponent n, however, results in large rearward shifts in x_{cp}/l from approximately 0.33 for $n = 0.25$ to approximately 0.66 for $n = 1.00$ (fig. 14(b)). A rearward shift due to increasing n would be expected from an observation of the longitudinal distribution of cross-sectional area for each of the bodies (fig. 1(b)). The positions of the centroid of planform area and centroid of volume for each body (fig. 14(b)) indicate that although the blunt-apex bodies (low values of n) offer advantages with respect to forward locations of center of gravity (assuming a constant density loading), a stability problem could be expected because of the extreme forward location of the center of pressure.

SUMMARY OF RESULTS

An investigation has been made in the Langley high-speed 7- by 10-foot tunnel to determine the transonic aerodynamic characteristics of a series of power-law bodies and a theoretical hypersonic minimum-wave-drag body of equal length and equal volume. Also included in the investigation are the effects of altering cross-sectional ellipticity for a given body, while maintaining a constant longitudinal distribution of cross-sectional area. The Mach number range of the investigation was from 0.50 to 1.12, and the angle of attack was varied from approximately -6° to 28° at 0° of sideslip.

Results of the investigation are summarized as follows:

1. Increasing power-body exponent for a given value of ellipticity results in increases in the lift-curve slope at low angles of attack and in the overall lift variation with angle of attack throughout the Mach number range. Large increases in minimum drag at a given Mach number also occur with increasing body exponent primarily because of the large increase in base area. The maximum lift-drag ratio for the power-law bodies was obtained with the lowest power-body exponent (smallest base area) at all

Mach numbers investigated. Increasing body exponent also resulted in large rearward shifts in longitudinal center-of-pressure location at all Mach numbers.

2. Increasing ellipticity for any given power-law body resulted in large increases in lift and maximum lift-drag ratio and only slight effects on center-of-pressure location.

3. A comparison between a theoretically determined body shape for minimized pressure drag at hypersonic speeds and the series of power-law bodies investigated indicates that the overall aerodynamic characteristics of the theoretical body are similar to those experienced with a power-law body having an exponent of 0.50. The values of maximum lift-drag ratio at transonic speeds for the theoretical body were slightly higher than those for the power-law bodies for all values of ellipticity.

Langley Research Center,
National Aeronautics and Space Administration,
Langley Station, Hampton, Va., October 25, 1965.

REFERENCES

1. Carleton, W. E.; and Matthews, R. K.: The Aerodynamic Characteristics of Three Elliptical-Cone Lifting Bodies at Transonic Speeds. AEDC-TDR-63-53, U.S. Air Force, April 1963.

2. Jorgensen, Leland H.: Elliptic Cones Alone and With Wings at Supersonic Speeds. NACA Rept. 1376, 1958. (Supersedes NACA TN 4045.)

3. Spencer, Bernard, Jr., and Phillips, W. Pelham: Effects of Cross-Section Shape on the Low-Speed Aerodynamic Characteristics of a Low-Wave-Drag Hypersonic Body. NASA TN D-1963, 1963.

4. Fuller, Dennis E.; Shaw, Davis S.; and Wassum, Donald L.: Effect of Cross-Section Shape on the Aerodynamic Characteristics of Bodies at Mach Numbers From 2.50 to 4.63. NASA TN D-1620, 1963.

5. Spencer, Bernard, Jr.; Phillips, W. Pelham; and Fournier, Roger H.: Supersonic Aerodynamic Characteristics of a Series of Bodies Having Variations in Fineness Ratio and Cross-Section Ellipticity. NASA TN D-2389, 1964.

6. Spencer, Bernard, Jr.; and Phillips, W. Pelham: Transonic Aerodynamic Characteristics of a Series of Bodies Having Variations in Fineness and Cross-Sectional Ellipticity. NASA TN D-2622, 1965.

7. Stivers, Louis S., Jr.; and Levy, Lionel L., Jr.: Longitudinal Force and Moment Data at Mach Numbers From 0.60 to 1.40 for a Family of Elliptic Cones With Various Semiapex Angles. NASA TN D-1149, 1961.

8. Fuller, Dennis E.; and Langhams, Victor E.: Effect of Afterbody Geometry and Sting Diameter on the Aerodynamic Characteristics of Slender Bodies at Mach Numbers From 1.57 to 2.86. NASA TN D-2042, 1963.

9. Miele, Angelo: Slender Shapes of Minimum Drag in Newtonian Flow. z. Flugwissenschaften, Jahrg 11, Heft 5, May 1963, pp. 203-210.

10. Miele, Angelo; Pritchard, Robert E.; and Hull, David G.: General Theory of Optimum Hypersonic Slender Bodies Including Frictional Effects. J. Astronaut. Sci., vol. X, no. 2, 1963, pp. 41-54.

11. Eggers, A. J., Jr.; Resnikoff, Meyer M.; and Dennis, David H.: Bodies of Revolution Having Minimum Drag at High Supersonic Airspeeds. NACA Rept. 1306, 1957. (Supersedes NACA TN 3666.)

12. Suddath, Jerrold H.; and Oehman, Waldo I.: Minimum Drag Bodies With Cross-Sectional Ellipticity. NASA TN D-2432, 1964.

13. Baradell, Donald L.; and McLellan, Charles H.: Lateral-Range and Hypersonic Lift-Drag-Ratio Requirements for Efficient Ferry Service From a Near-Earth Manned Space Station. 2nd Manned Space Flight Meeting (Dallas, Texas), American Inst. Aero. and Astronautics, Apr. 1963, pp. 159-166.

14. Gregory, Thomas J.; Petersen, Richard H.; and Wyss, John A.: Performance Trade-Offs and Research Problems for Hypersonic Transports. Paper No. 64-605, Am. Inst. Aeron. Astronaut., Aug., 1964.

15. Stivers, Louis S., Jr.; and Levy, Lionel L., Jr.: Effects of Sting-Support Diameter on the Base Pressures of an Elliptic Cone at Mach Numbers From 0.60 to 1.40. NASA TN D-354, 1961.

16. Cahn, Maurice S.: An Experimental Investigation of Sting-Support Effects on Drag and a Comparison With Jet Effects at Transonic Speeds. NACA Rept. 1353, 1958. (Supersedes NACA RM L56F18a.)

TABLE I.- DESIGN BODY ORDINATES

x/l	a/b = 1.0	a/b = 2.0		a/b = 3.0	
	a/l	a/l	b/l	a/l	b/l
		n = 0.425			
0	0	0	0	0	0
.0080	.0212	.0299	.0150	.0366	.0122
.0100	.0224	.0316	.0158	.0387	.0129
.0200	.0266	.0376	.0188	.0460	.0154
.0300	.0295	.0417	.0209	.0511	.0170
.0400	.0316	.0447	.0222	.0548	.0183
.0600	.0350	.0496	.0248	.0607	.0202
.1000	.0398	.0563	.0281	.0689	.0230
.1200	.0417	.0589	.0306	.0722	.0241
.2000	.0473	.0669	.0335	.0820	.0273
.2800	.0515	.0728	.0364	.0892	.0297
.3600	.0548	.0776	.0388	.0950	.0317
.5200	.0601	.0850	.0425	.1041	.0347
.6800	.0643	.0909	.0454	.1113	.0371
.8400	.0678	.0958	.0479	.1174	.0391
1.0000	.0708	.1001	.0500	.1226	.0408
		n = 0.50			
0	0	0	0	0	0
.0050	.0058	.0081	.0041	.0100	.0033
.0100	.0082	.0115	.0058	.0141	.0047
.0200	.0116	.0163	.0082	.0200	.0067
.0400	.0163	.0231	.0115	.0283	.0094
.0600	.0200	.0283	.0141	.0346	.0115
.1200	.0283	.0400	.0200	.0490	.0164
.2000	.0366	.0517	.0259	.0633	.0211
.2800	.0432	.0612	.0306	.0749	.0250
.3600	.0490	.0694	.0347	.0849	.0283
.4400	.0542	.0766	.0383	.0939	.0313
.5200	.0590	.0834	.0417	.1021	.0340
.6000	.0633	.0895	.0448	.1097	.0366
.6800	.0674	.0953	.0477	.1167	.0389
.7600	.0713	.1008	.0504	.1235	.0412
.8400	.0749	.1060	.0530	.1298	.0433
.9200	.0784	.1109	.0554	.1358	.0453
1.0000	.0818	.1156	.0578	.1416	.0472
		n = 0.66			
0	0	0	0	0	0
.0400	.0103	.0146	.0073	.0179	.0060
.1200	.0215	.0304	.0152	.0372	.0124
.2000	.0302	.0427	.0214	.0523	.0174
.2800	.0378	.0534	.0267	.0655	.0218
.3600	.0447	.0632	.0316	.0774	.0258
.4400	.0511	.0722	.0361	.0885	.0295
.5200	.0571	.0807	.0404	.0989	.0330
.6000	.0628	.0888	.0444	.1088	.0362
.6800	.0682	.0965	.0482	.1182	.0394
.7600	.0735	.1040	.0520	.1273	.0424
.8400	.0786	.1111	.0556	.1273	.0454
.9200	.0835	.1181	.0590	.1447	.0482
1.0000	.0883	.1248	.0624	.1529	.0510

TABLE I.- DESIGN BODY ORDINATES – Concluded

x/l	a/b = 1.0	a/b = 2.0		a/b = 3.0	
	a/l	a/l	b/l	a/l	b/l
			n = 0.75		
0	0	0	0	0	0
.0400	.0082	.0115	.0058	.0141	.0047
.1200	.0186	.0264	.0132	.0323	.0108
.2000	.0273	.0386	.0193	.0473	.0158
.2800	.0352	.0497	.0249	.0609	.0203
.3600	.0425	.0601	.0300	.0736	.0245
.4400	.0494	.0698	.0349	.0855	.0285
.5200	.0560	.0791	.0396	.0969	.0323
.6000	.0623	.0881	.0441	.1079	.0360
.6800	.0684	.0968	.0484	.1185	.0395
.7600	.0744	.1052	.0526	.1289	.0430
.8400	.0802	.1134	.0567	.1389	.0463
.9200	.0858	.1214	.0607	.1487	.0496
1.0000	.0914	.1292	.0646	.1583	.0528
			n = 1.00		
0	0	0	0	0	0
.0400	.0040	.0057	.0028	.0069	.0023
.1200	.0120	.0170	.0085	.0208	.0069
.2000	.0200	.0283	.0141	.0346	.0115
.2800	.0280	.0396	.0198	.0485	.0162
.3600	.0360	.0513	.0254	.0624	.0208
.4400	.0440	.0622	.0311	.0762	.0254
.5200	.0520	.0735	.0368	.0901	.0300
.6000	.0600	.0848	.0424	.1039	.0346
.6800	.0680	.0962	.0481	.1178	.0393
.7600	.0760	.1075	.0537	.1316	.0439
.8400	.0840	.1188	.0594	.1455	.0485
.9200	.0920	.1301	.0650	.1593	.0531
1.0000	.1000	.1414	.0707	.1732	.0577
			Minimum-drag body		
0	0	0	0	0	0
.0400	.0098	.0139	.0070	.0170	.0057
.0800	.0161	.0228	.0114	.0279	.0093
.1200	.0216	.0305	.0153	.0373	.0124
.2000	.0312	.0441	.0221	.0540	.0180
.2800	.0396	.0560	.0280	.0686	.0229
.3600	.0469	.0663	.0332	.0813	.0271
.4400	.0534	.0775	.0388	.0924	.0308
.5200	.0592	.0837	.0419	.1025	.0342
.6000	.0646	.0913	.0457	.1119	.0373
.6800	.0695	.0982	.0491	.1203	.0401
.7600	.0738	.1043	.0521	.1278	.0426
.8400	.0773	.1093	.0542	.1338	.0446
.9200	.0800	.1131	.0565	.1385	.0462
1.0000	.0814	.1151	.0575	.1410	.0470

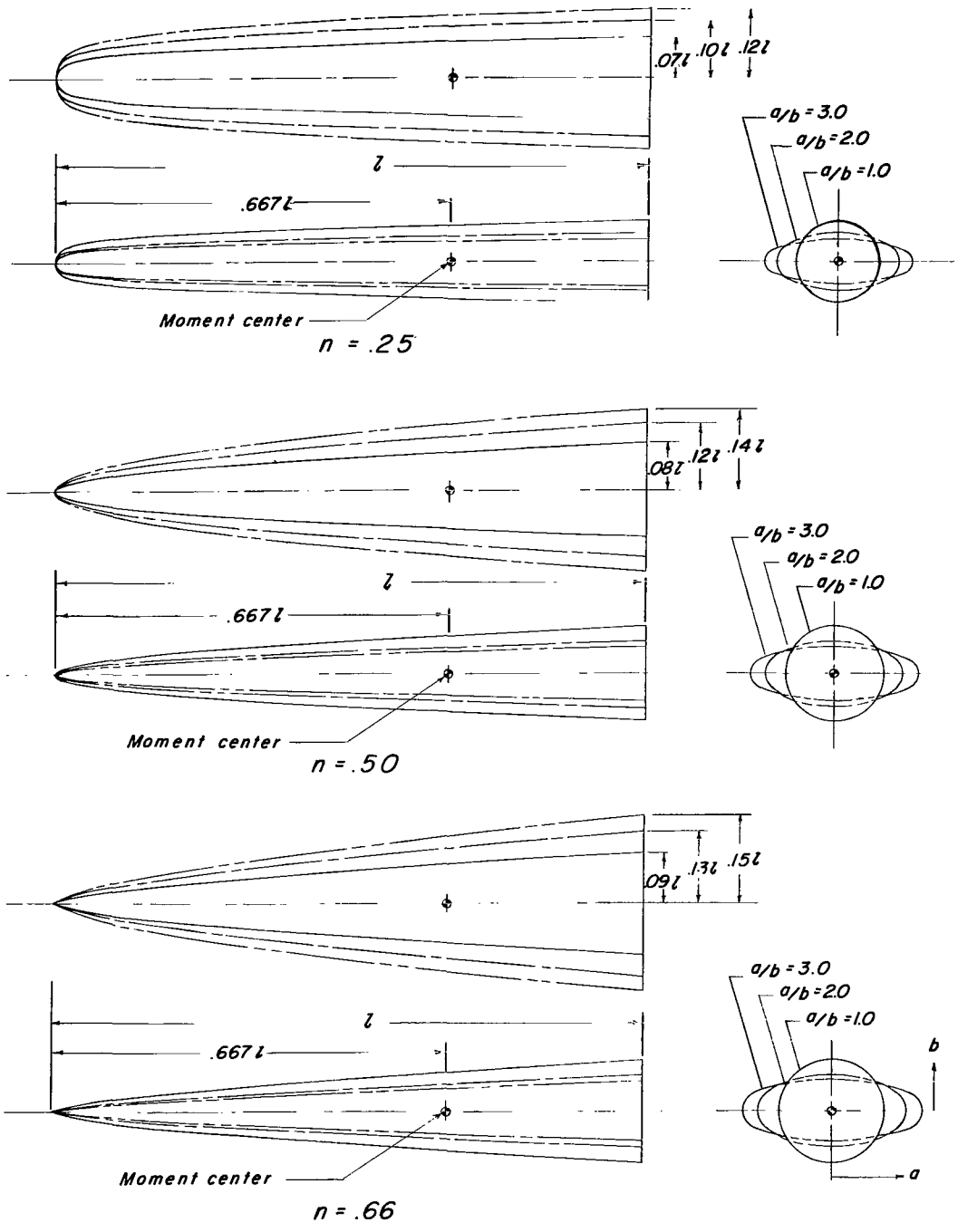

(a) Details of bodies.

Figure 1.- Drawings and pertinent geometric characteristics of the various models investigated.

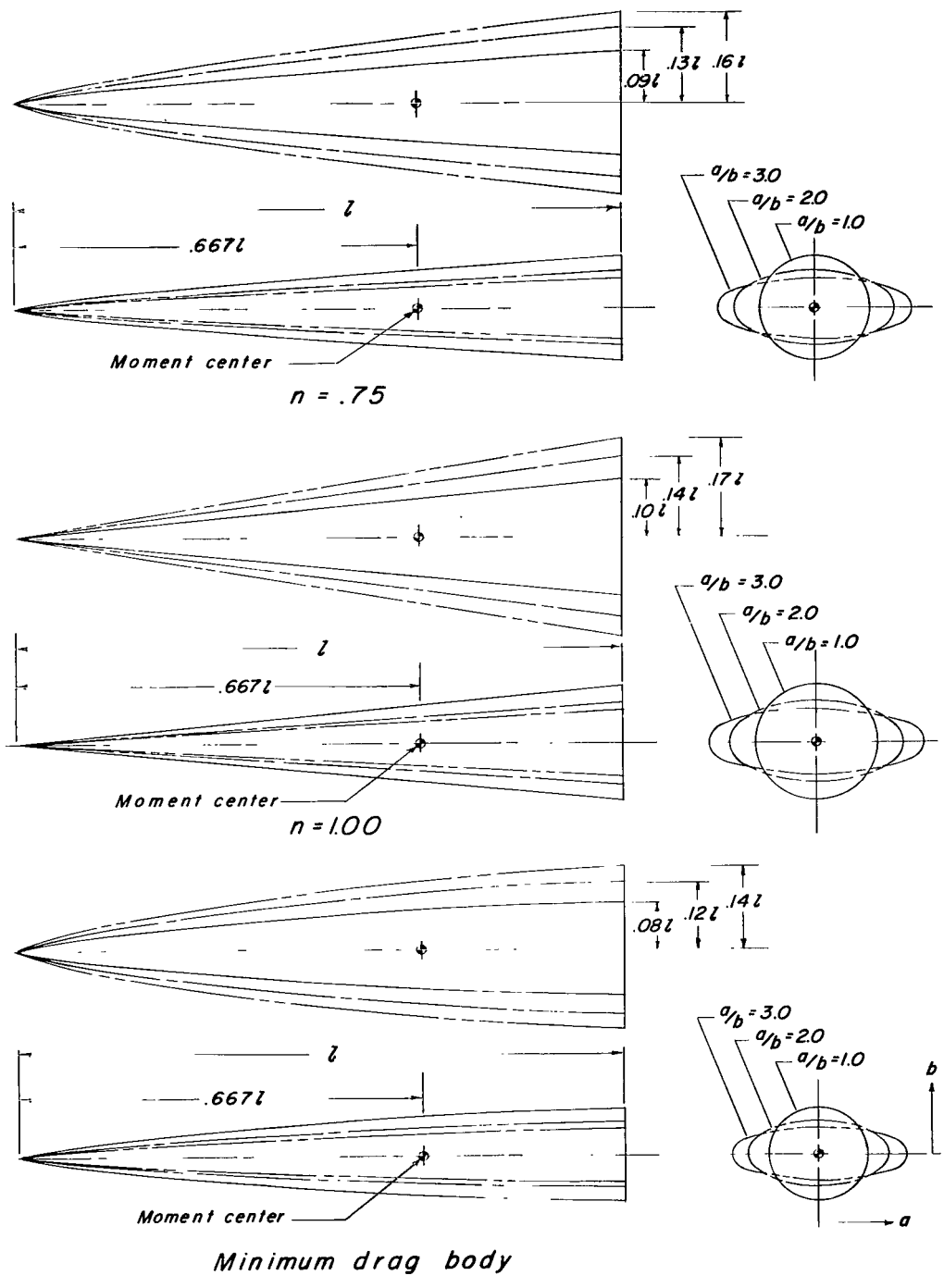

(a) Concluded.

Figure 1.- Continued.

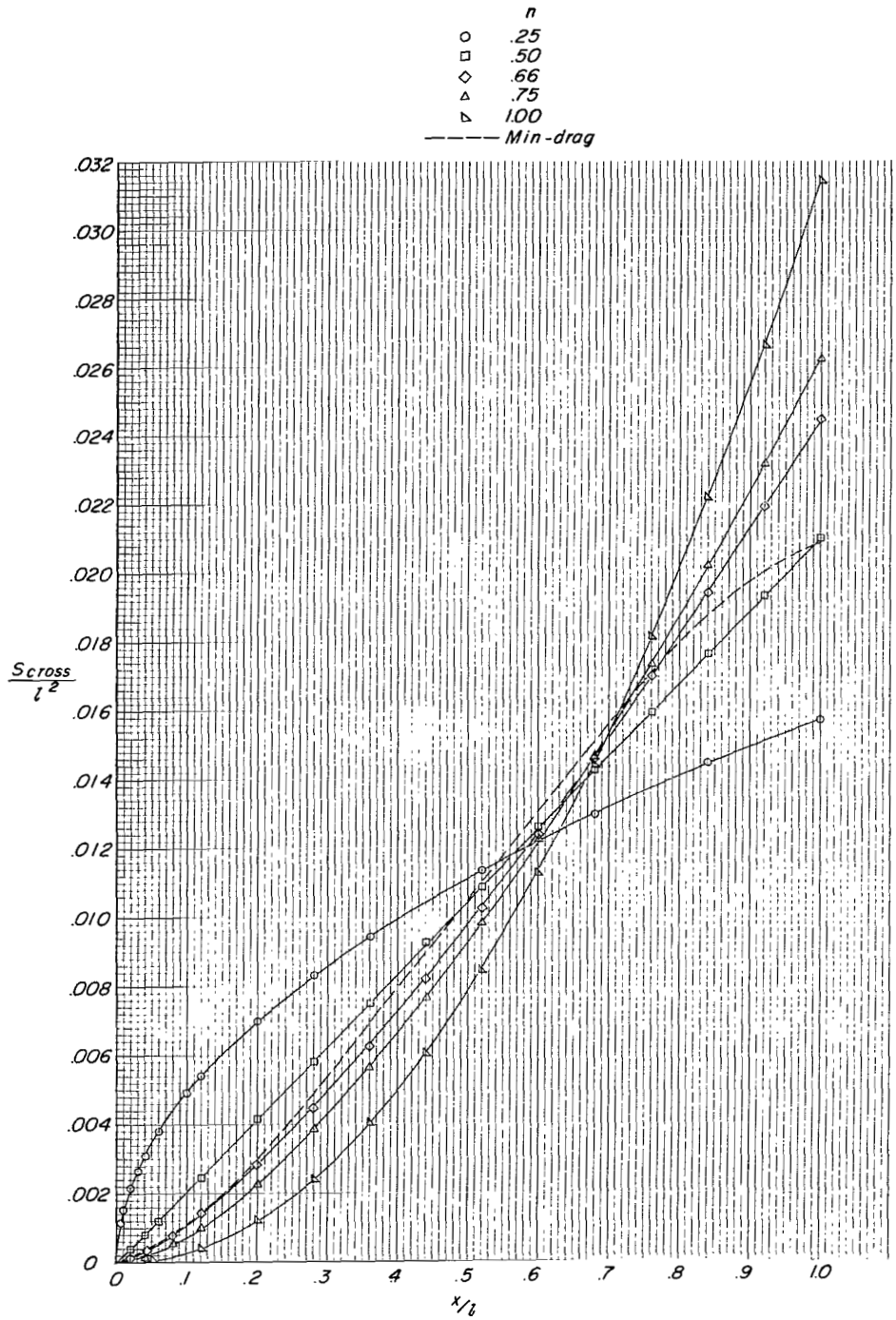

(b) Variation of S_{cross}/l^2 with x/l.

Figure 1.- Continued.

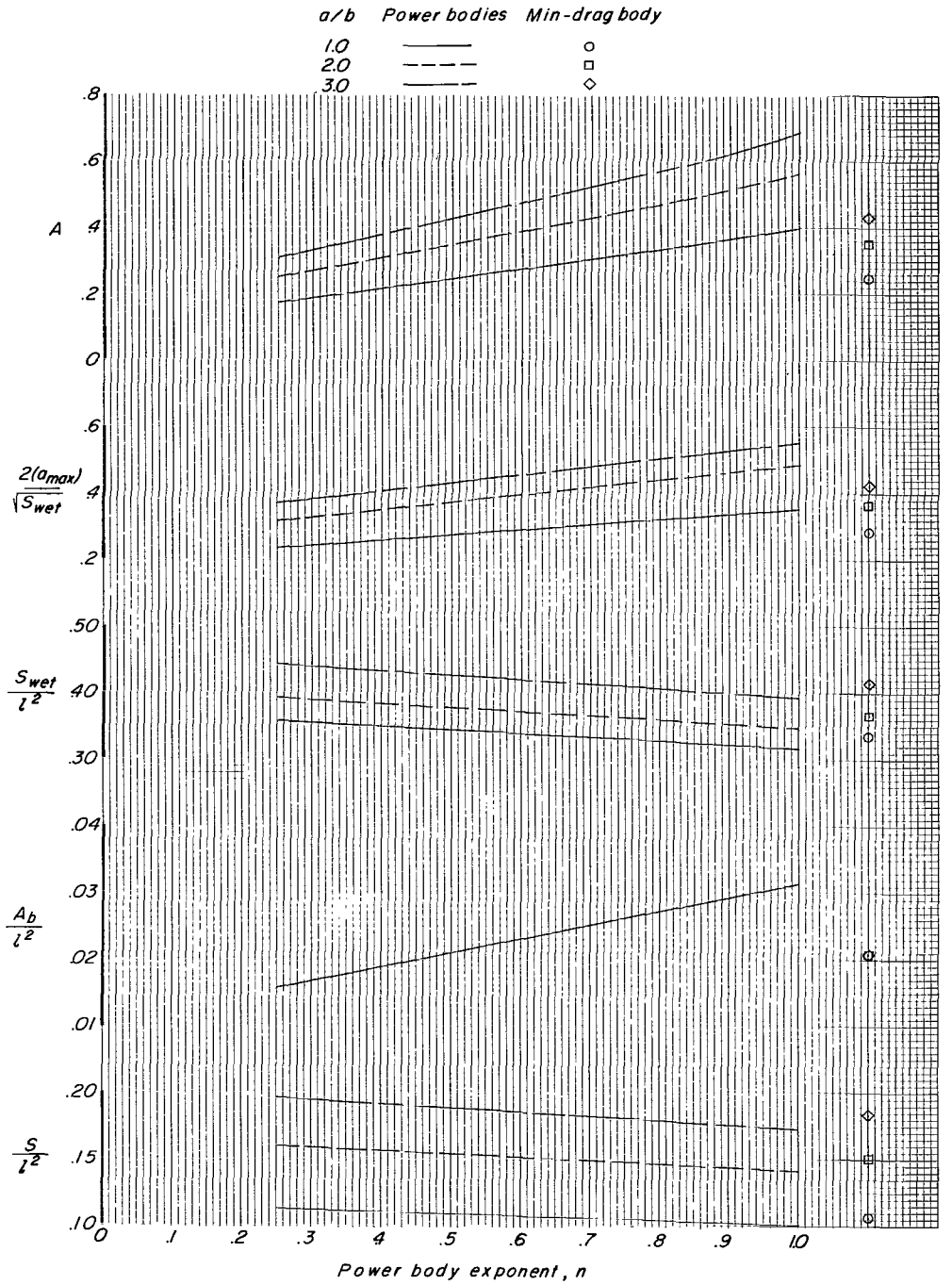

(c) Variation of various geometric parameters with power-body exponent.

Figure 1.- Continued.

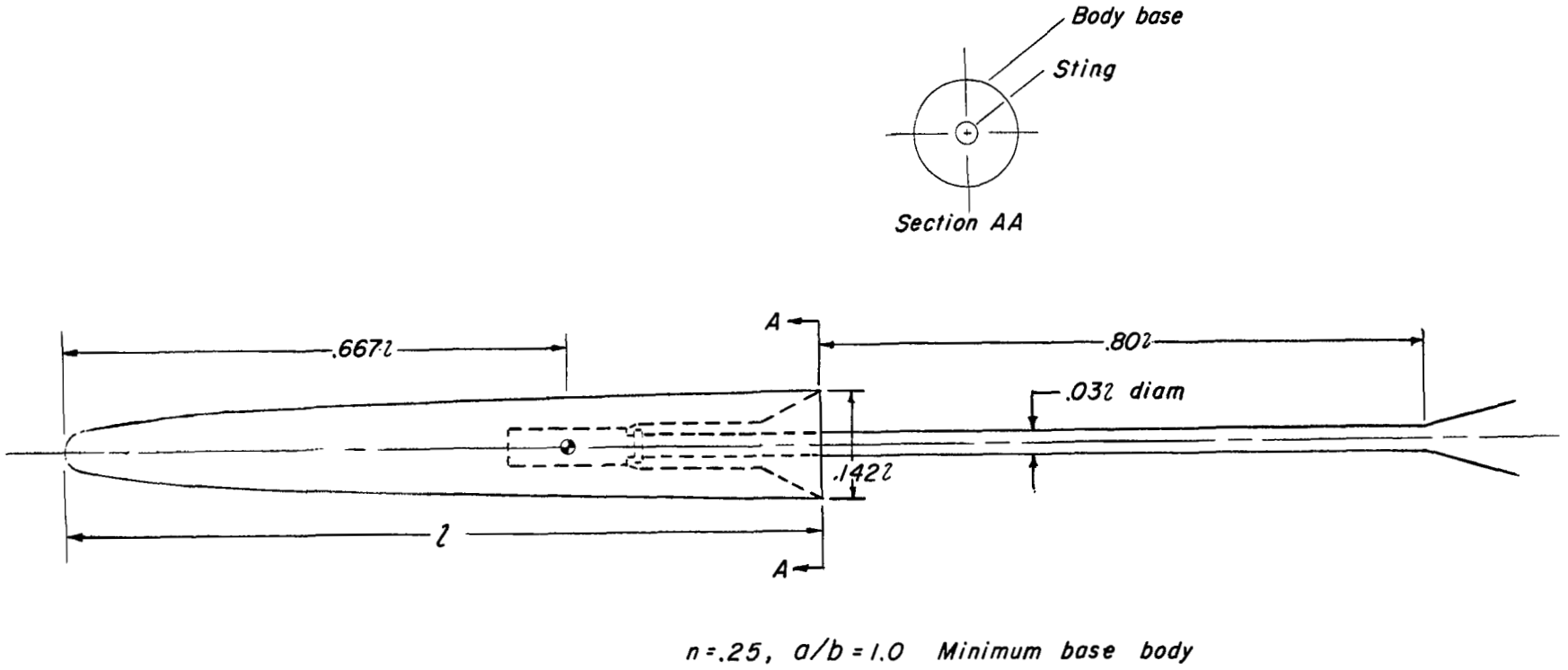

(d) Sting mounting arrangement.

Figure 1.- Concluded.

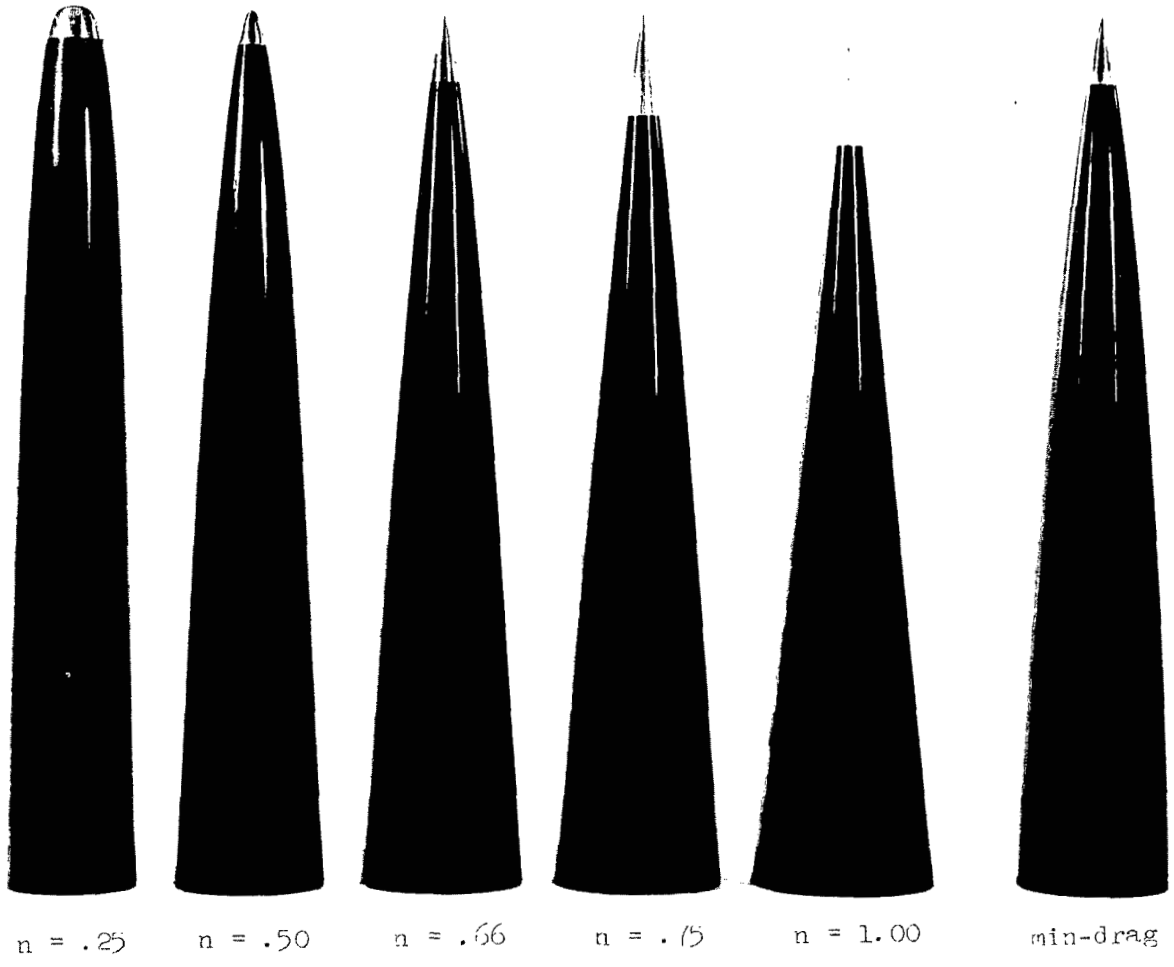

(a) a/b = 1.0.

L-65-2660.1

Figure 2.- Photographs of the models.

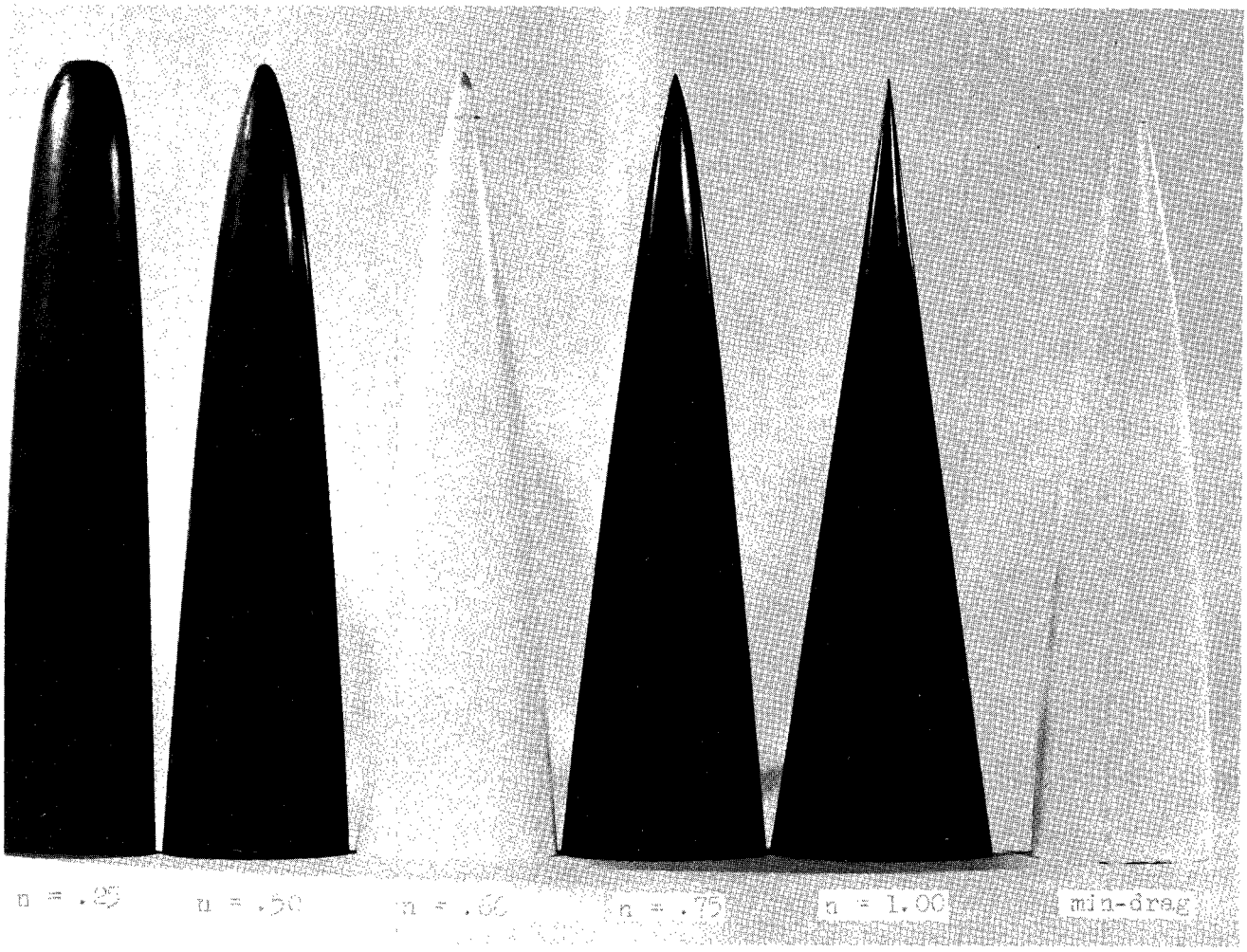

(b) a/b = 2.0.

L-65-2658.1

Figure 2.- Continued.

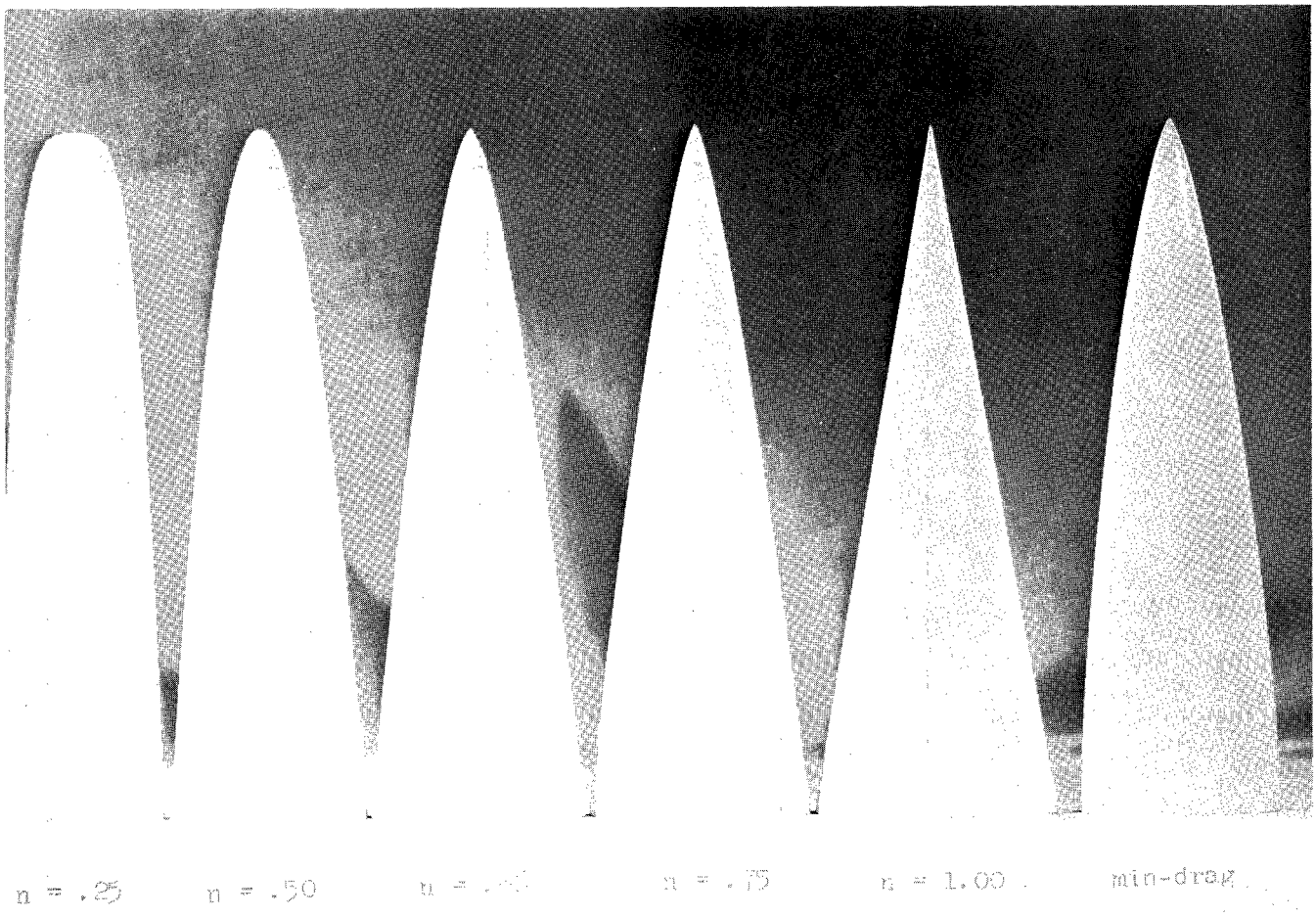

(c) a/b = 3.0.

L-65-2659.1

Figure 2.- Concluded.

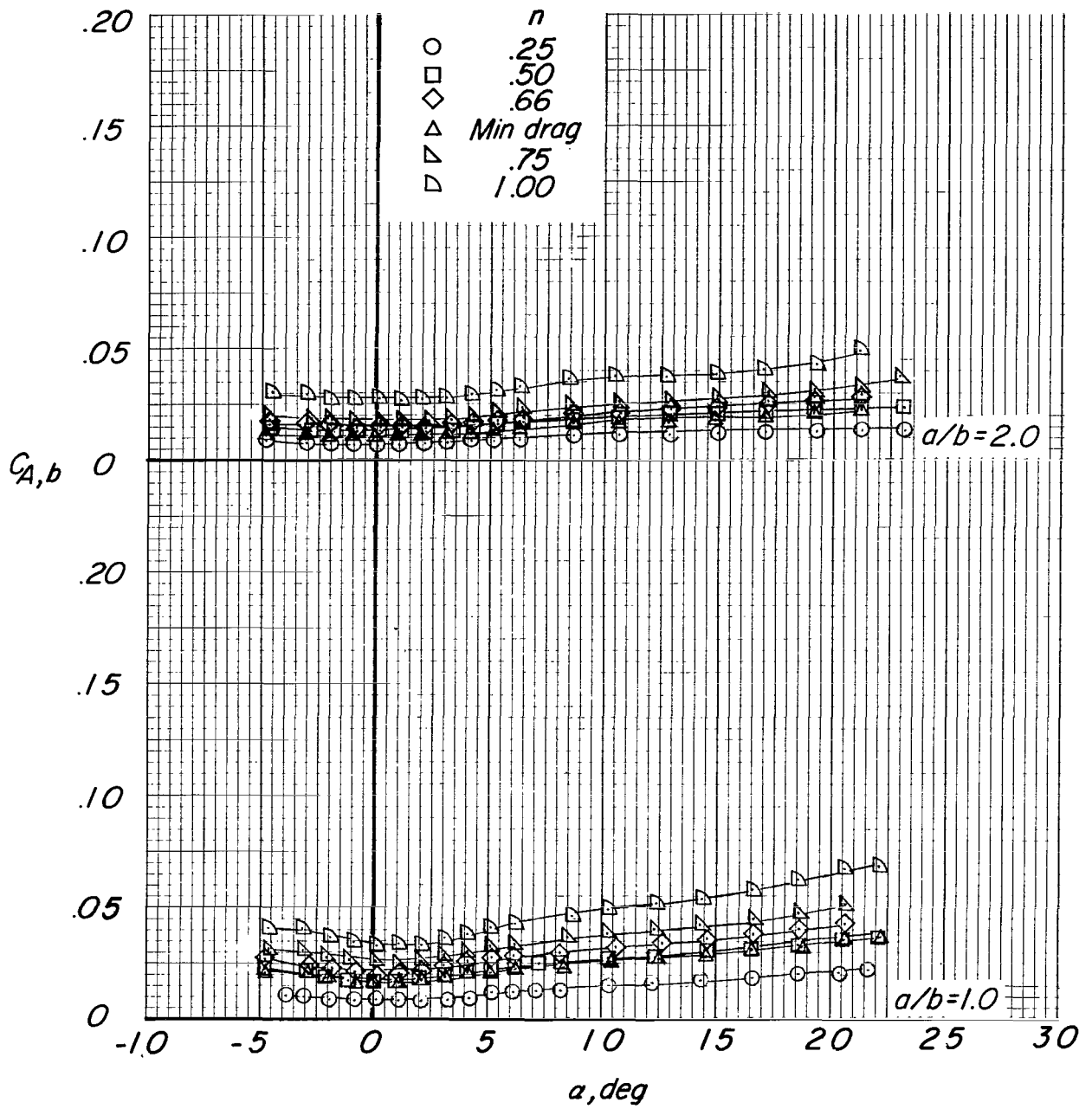

(a) M = 0.50.

Figure 3.- Variation of base-axial-force coefficient with angle of attack.

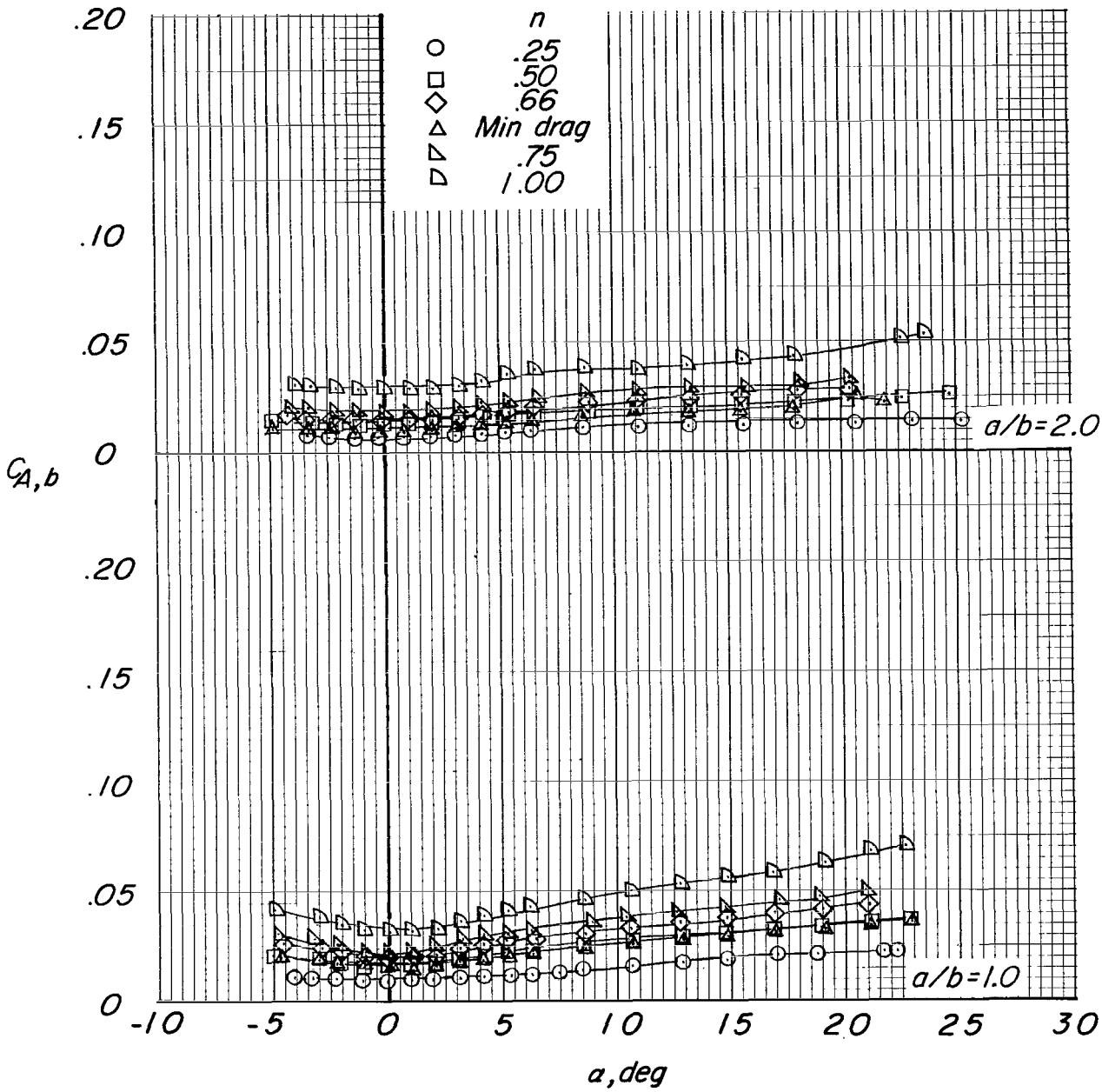

(b) M = 0.78.

Figure 3.- Continued.

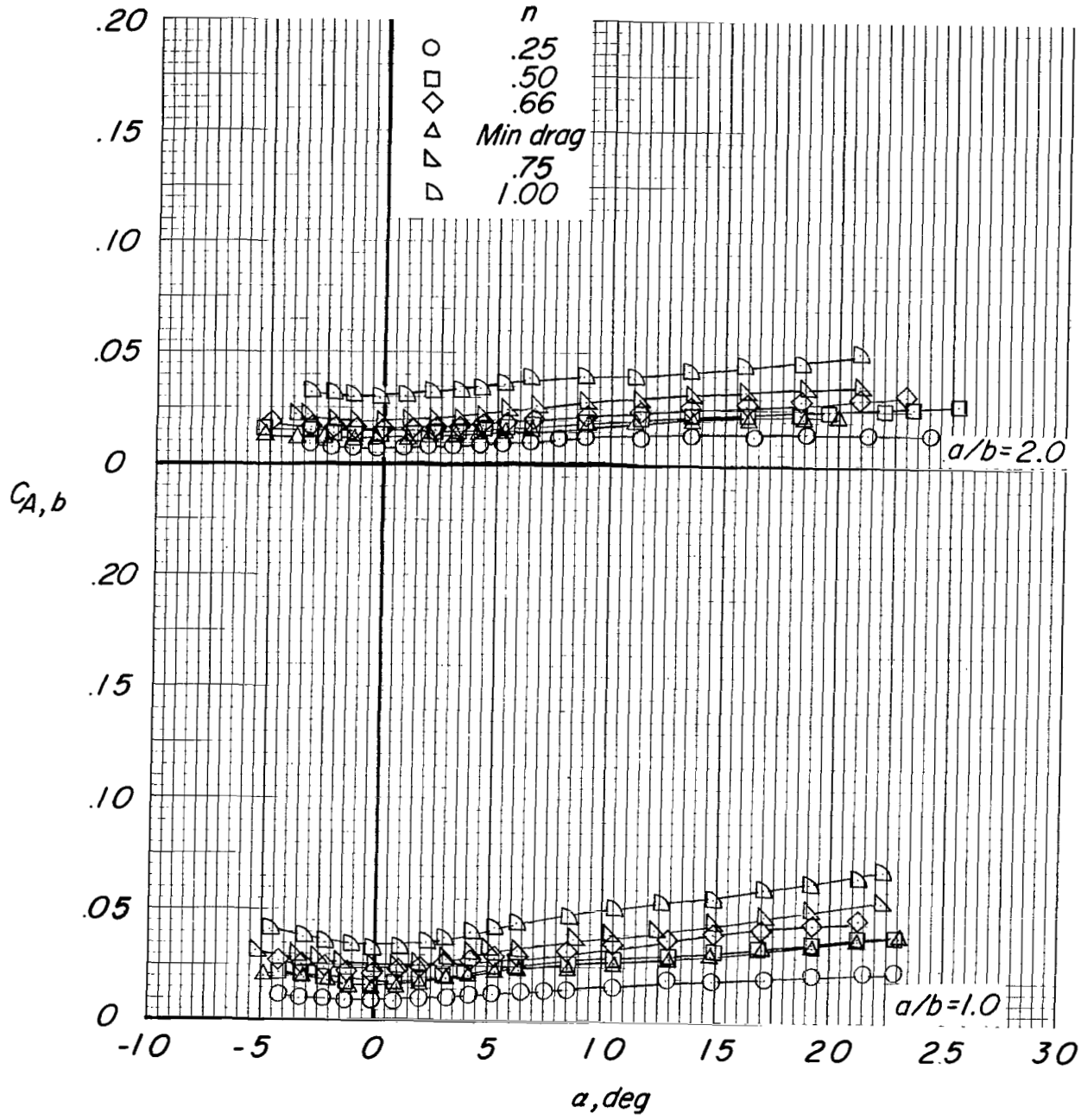

(c) M = 0.87.

Figure 3.- Continued.

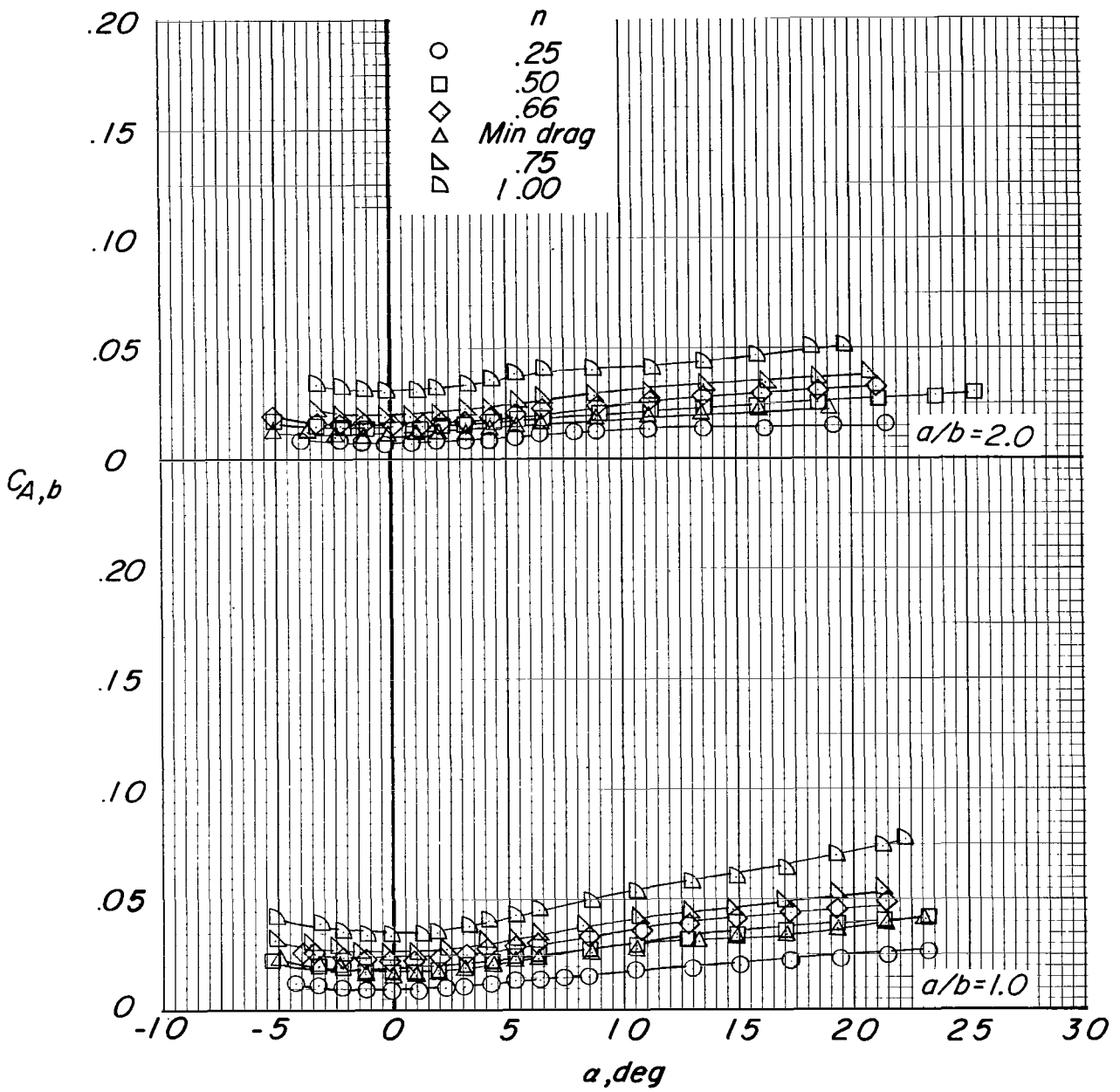

(d) M = 0.92.

Figure 3.- Continued.

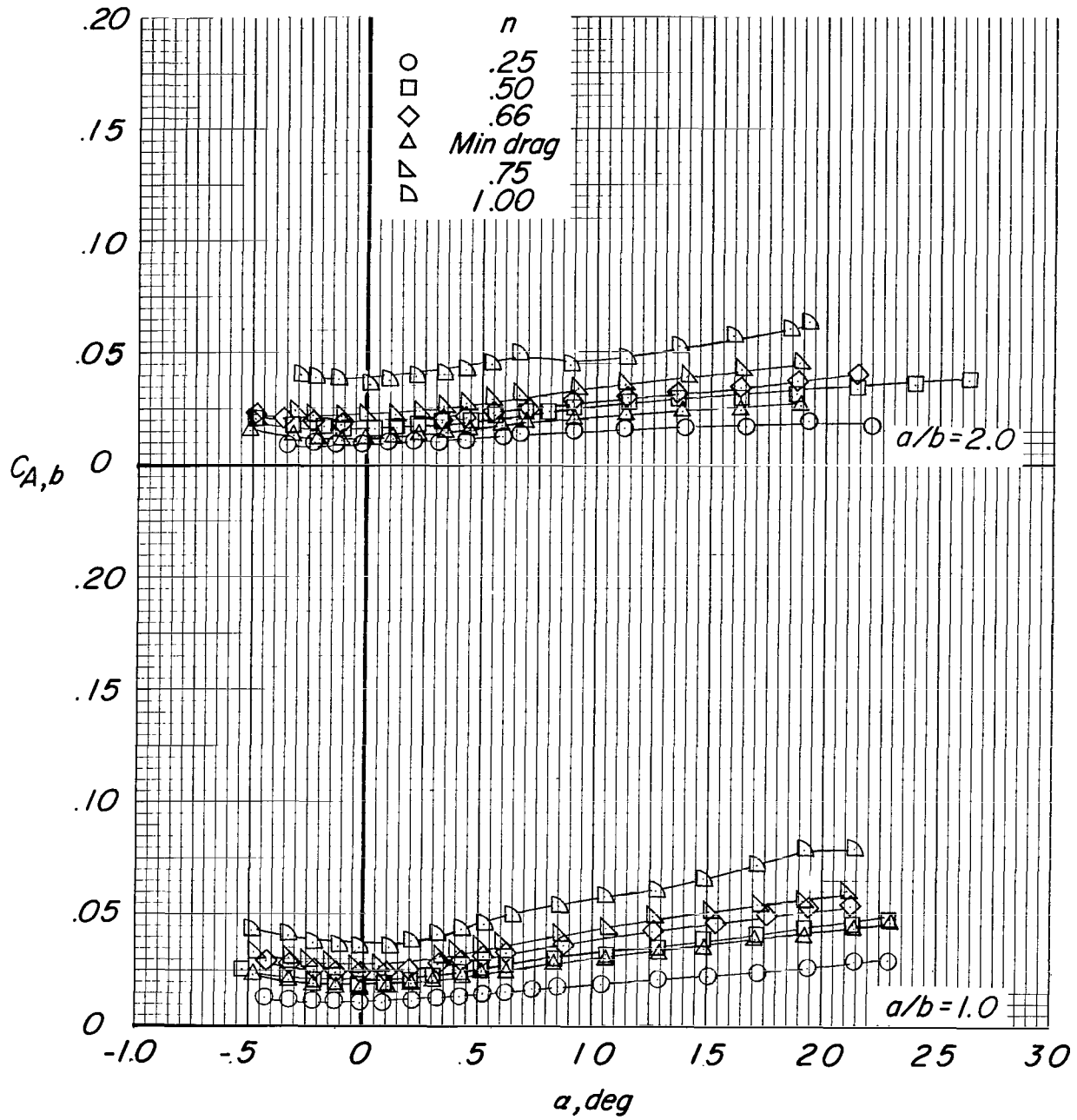

(e) M = 0.97.

Figure 3.- Continued.

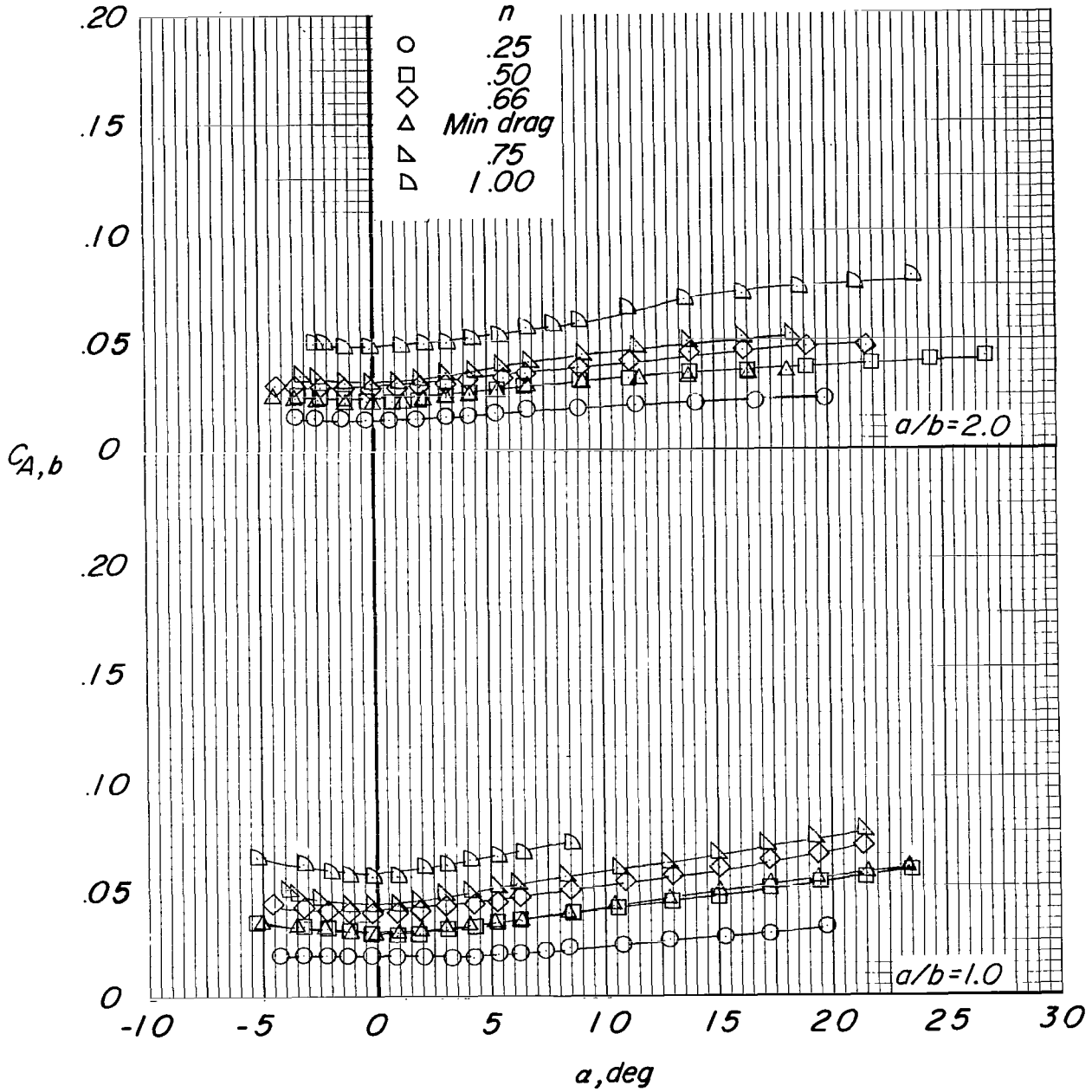

(f) M = 1.12.

Figure 3.- Concluded.

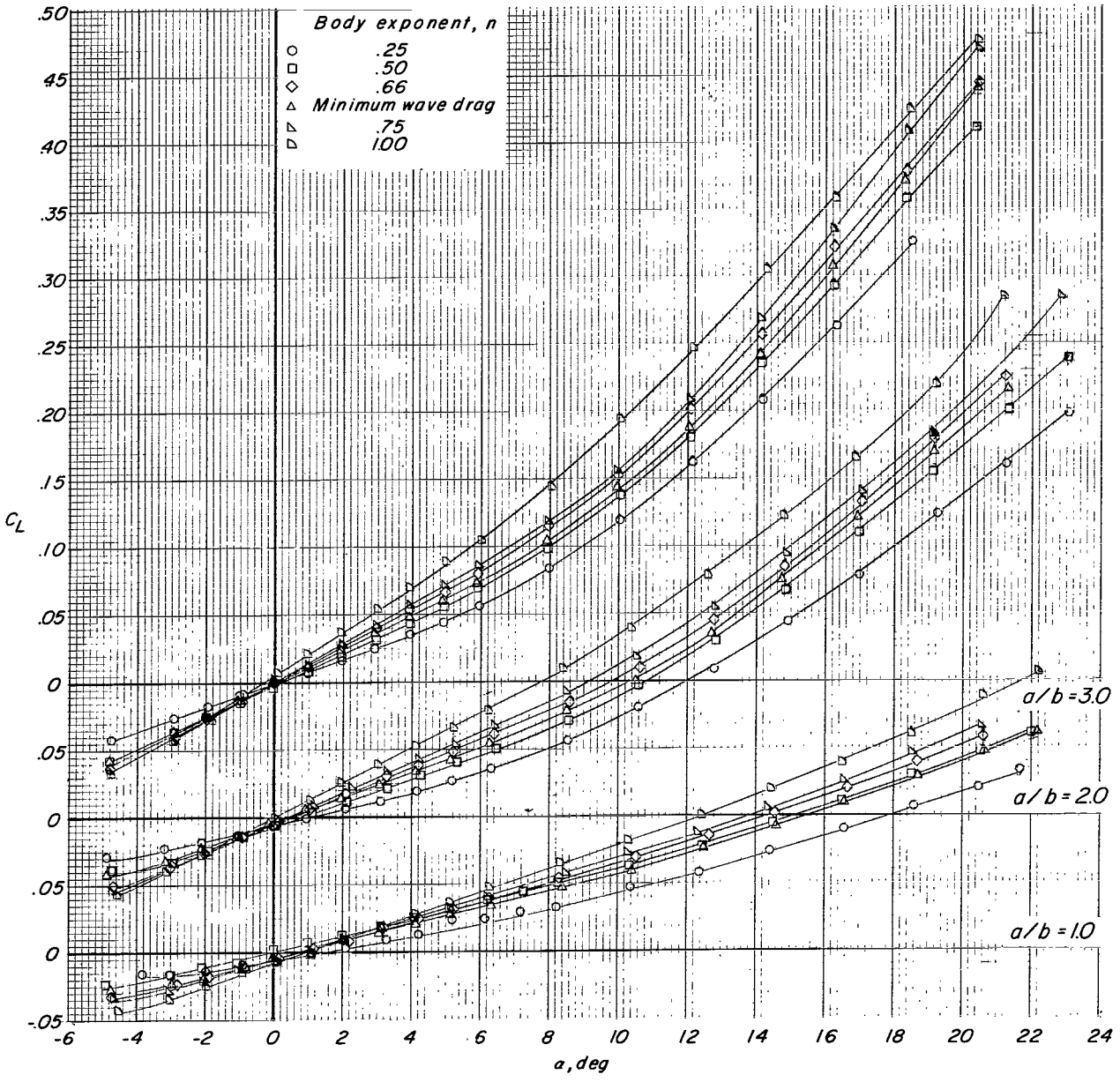

(a) C_L as a function of α.

Figure 4.- Longitudinal aerodynamic characteristics associated with the power-law bodies and minimum-wave-drag body. M = 0.50.

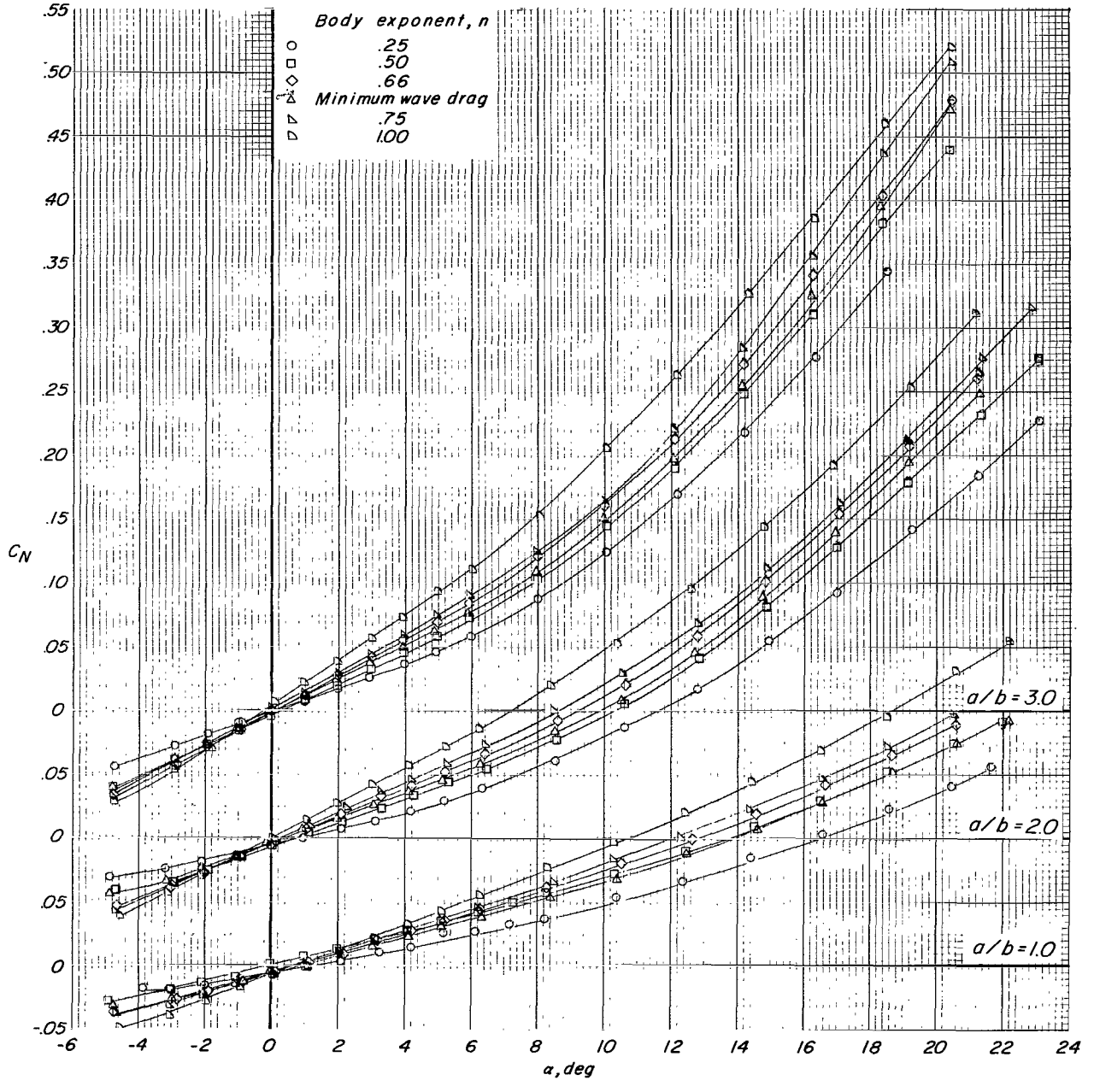

(b) C_N as a function of α.

Figure 4.- Continued.

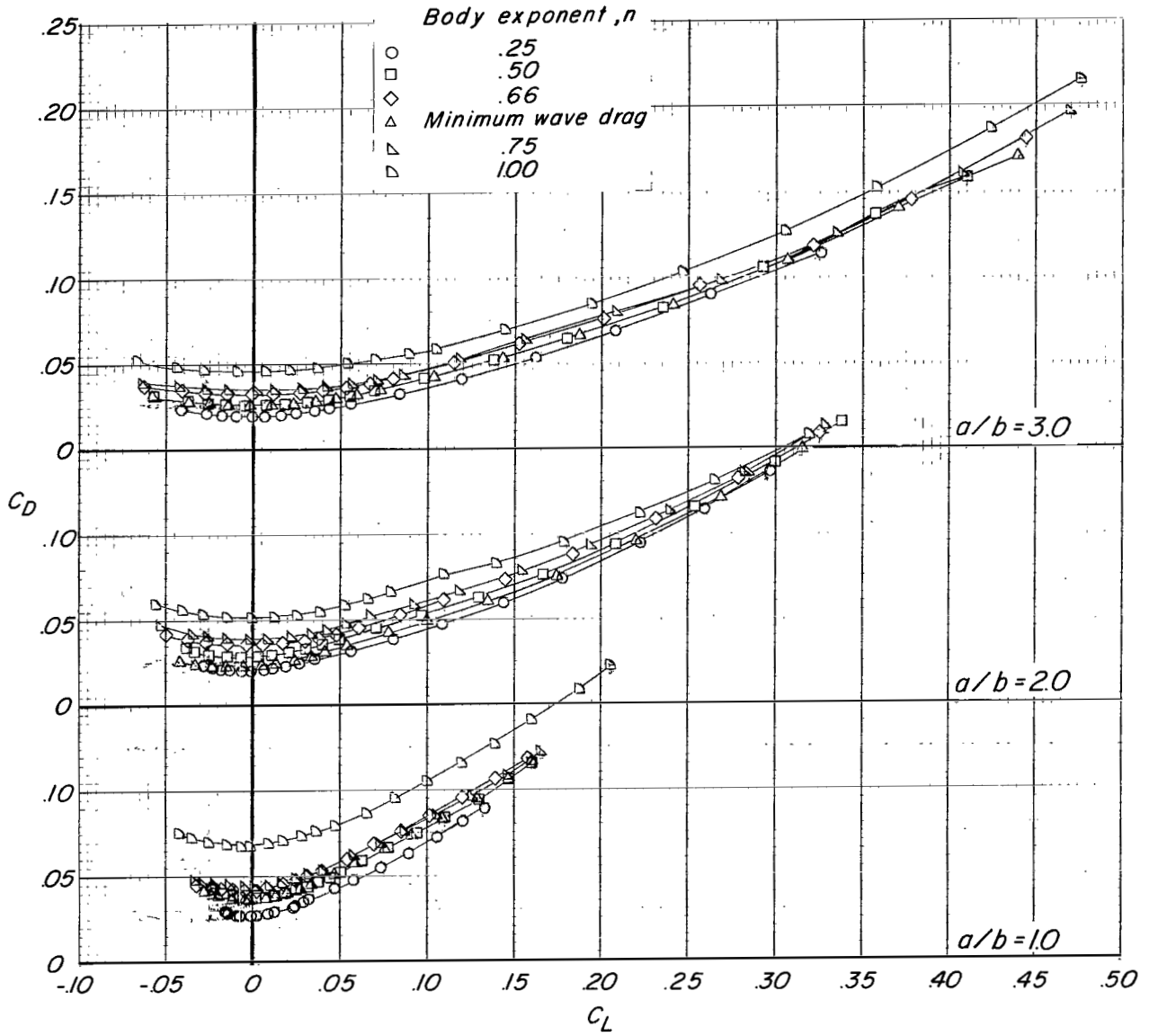

(c) C_D as a function of C_L.

Figure 4.- Continued.

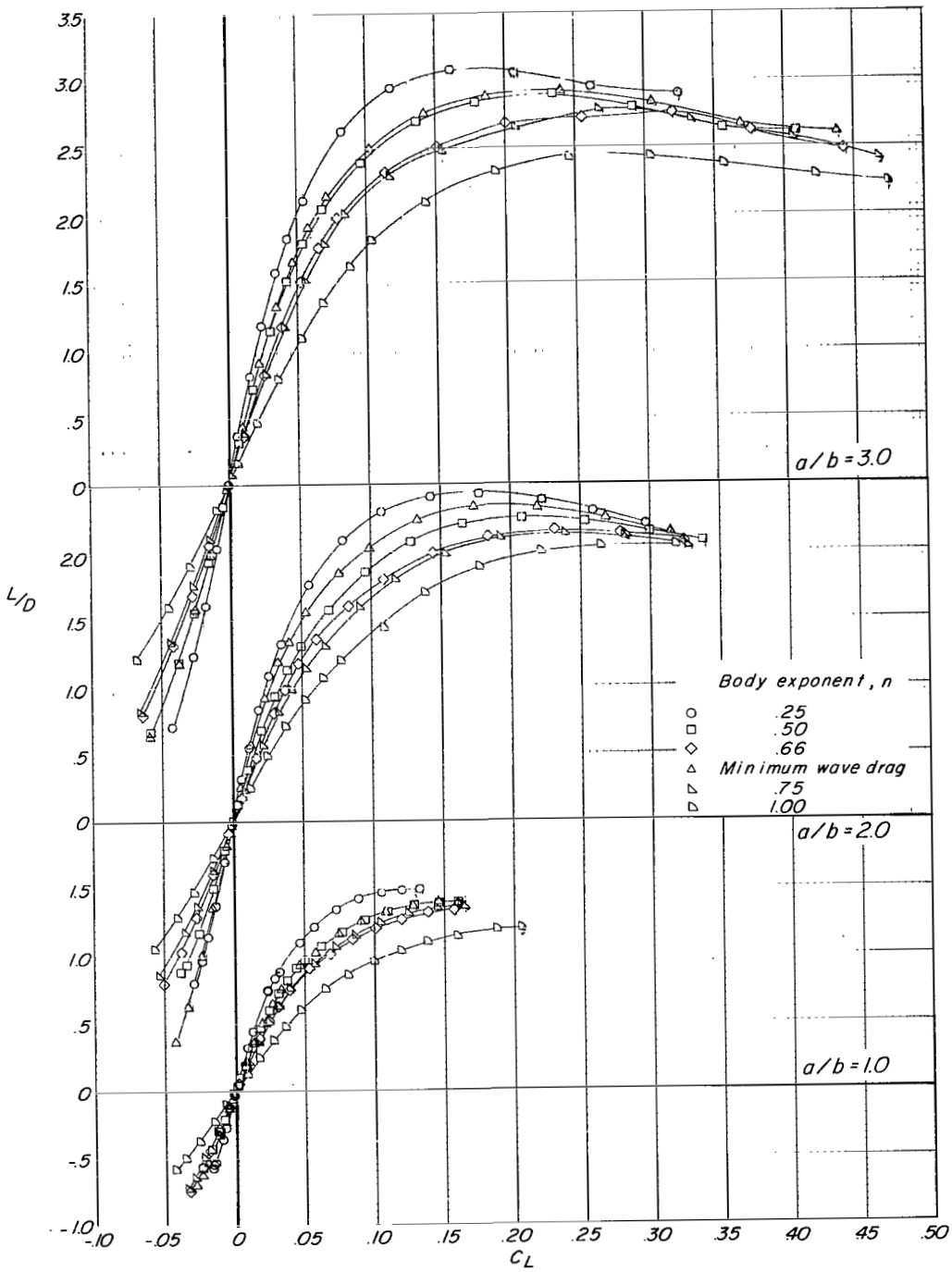

(d) L/D as a function of C_L.

Figure 4.- Continued.

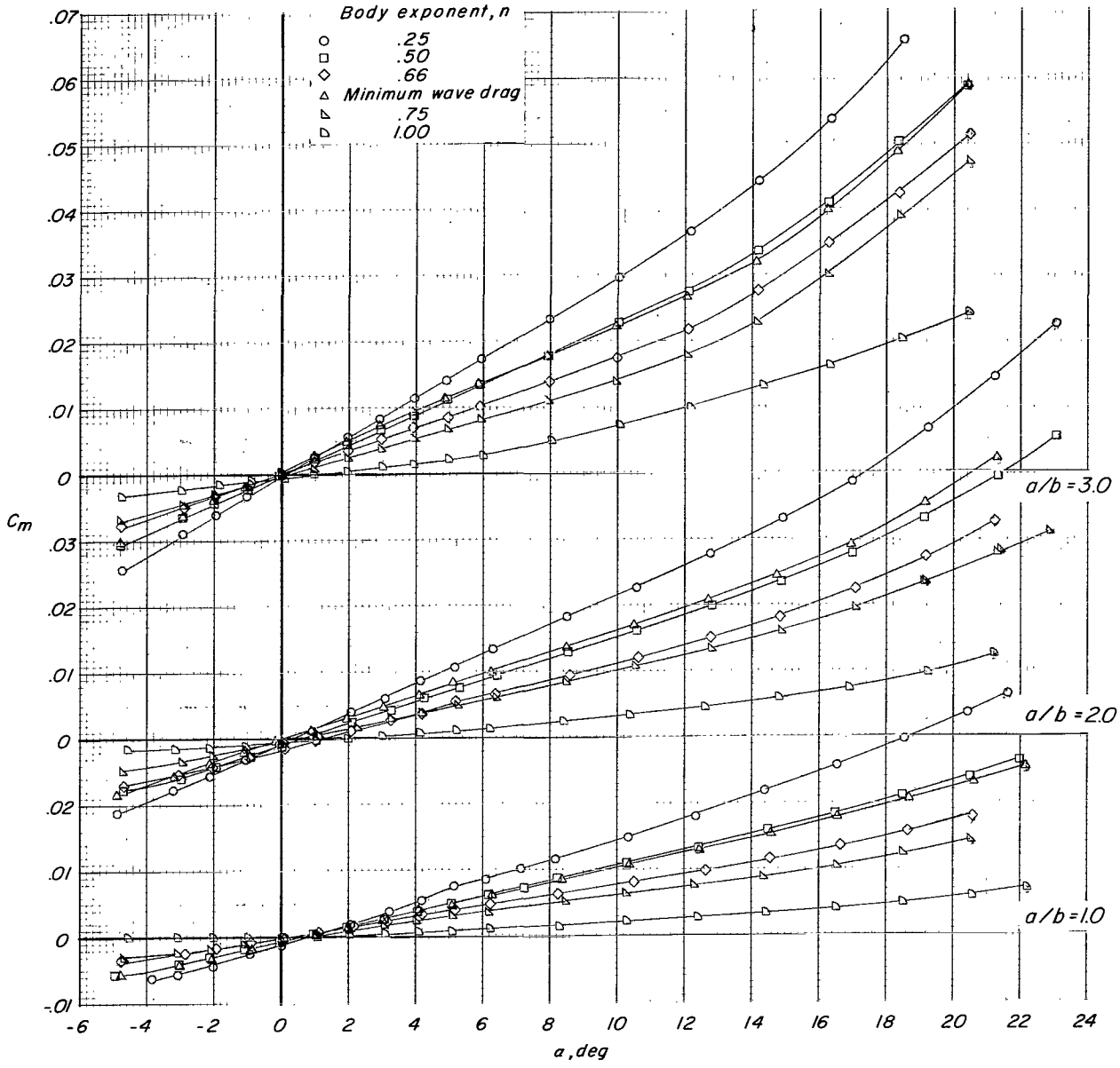

(e) C_m as a function of α.

Figure 4.- Continued.

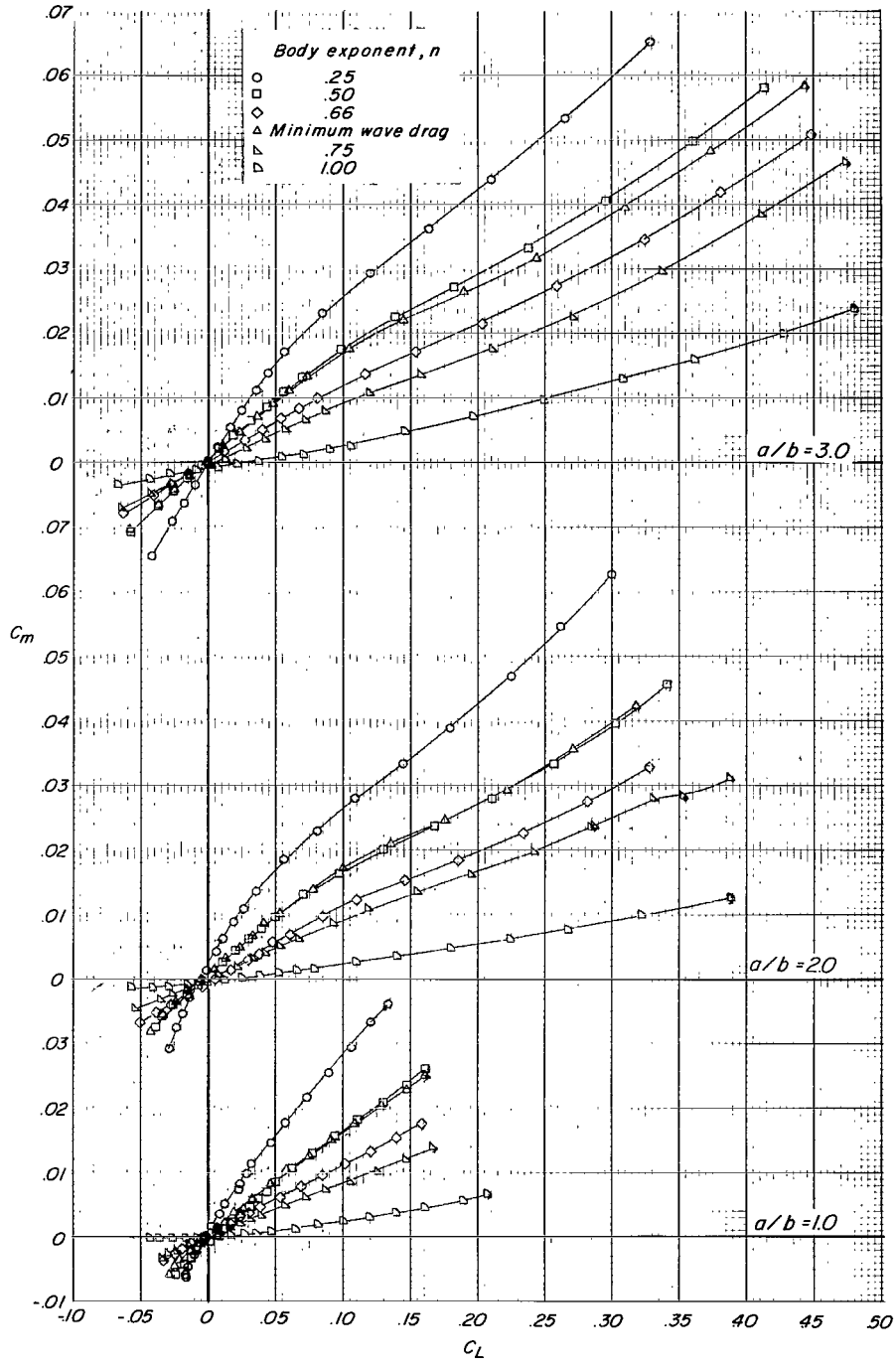

(f) C_m as a function of C_L.

Figure 4.- Concluded.

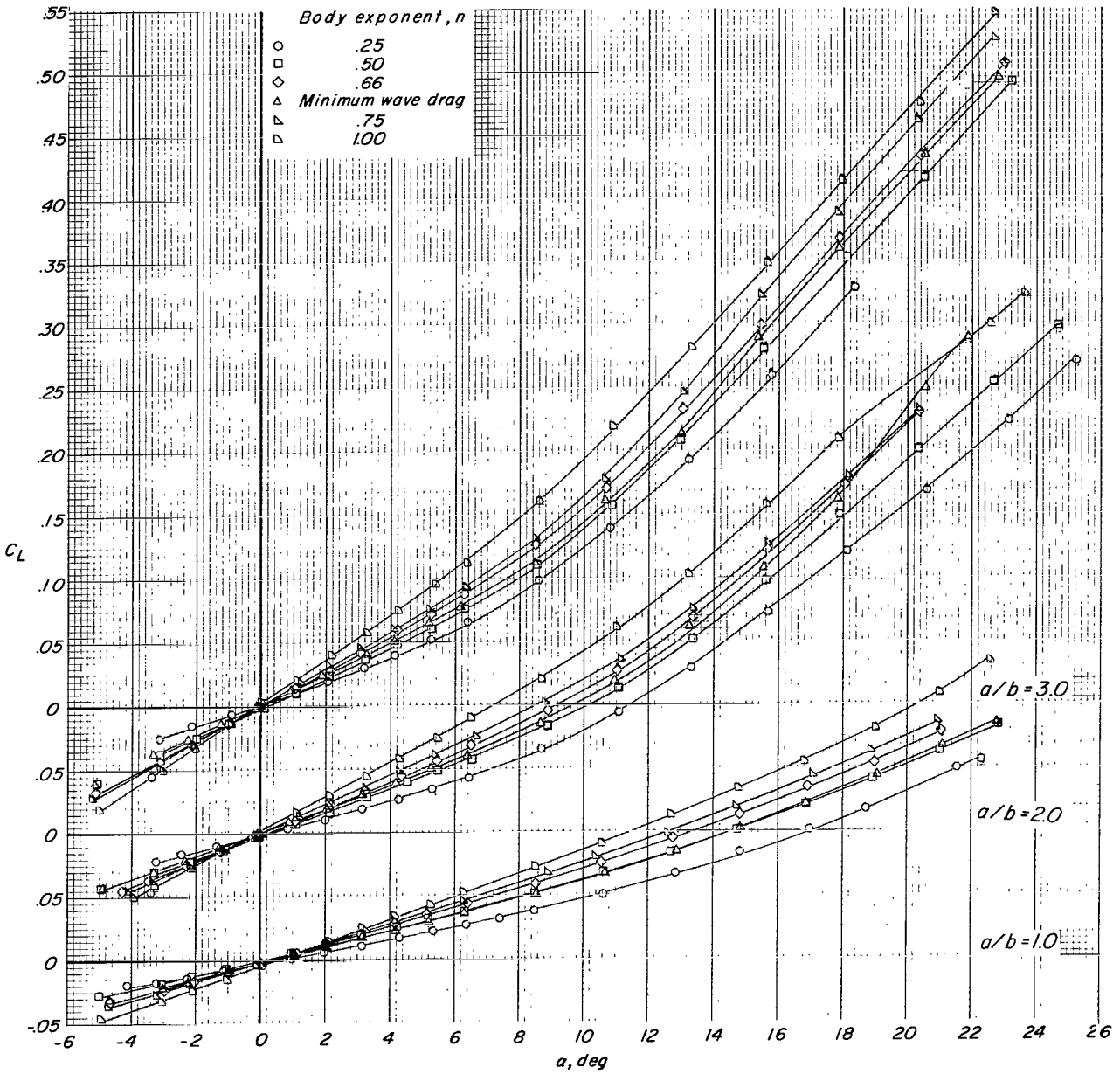

(a) C_L as a function of α.

Figure 5.- Longitudinal aerodynamic characteristics associated with the power-law bodies and minimum-wave-drag body. M = 0.80.

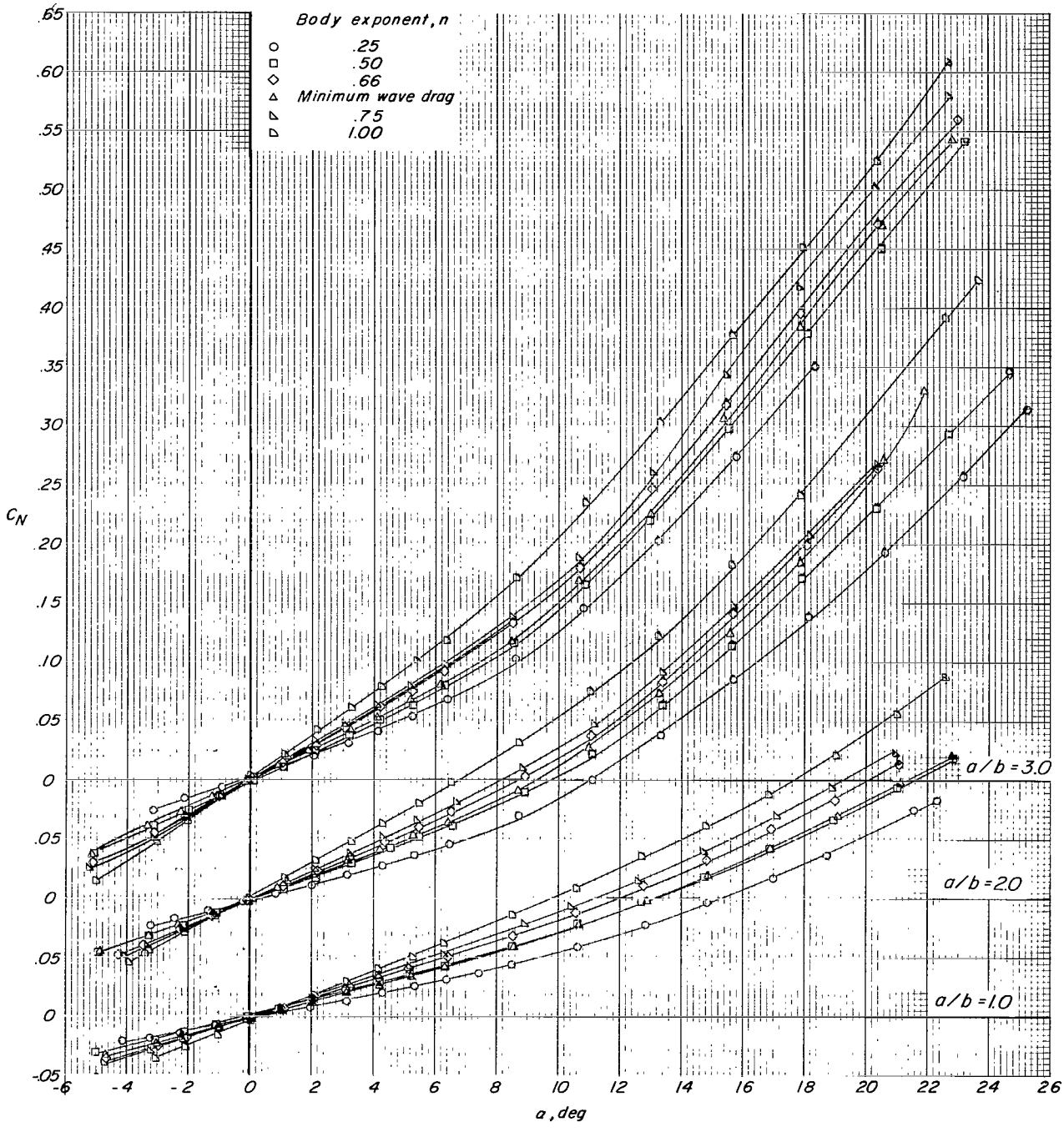

(b) C_N as a function of α.

Figure 5.- Continued.

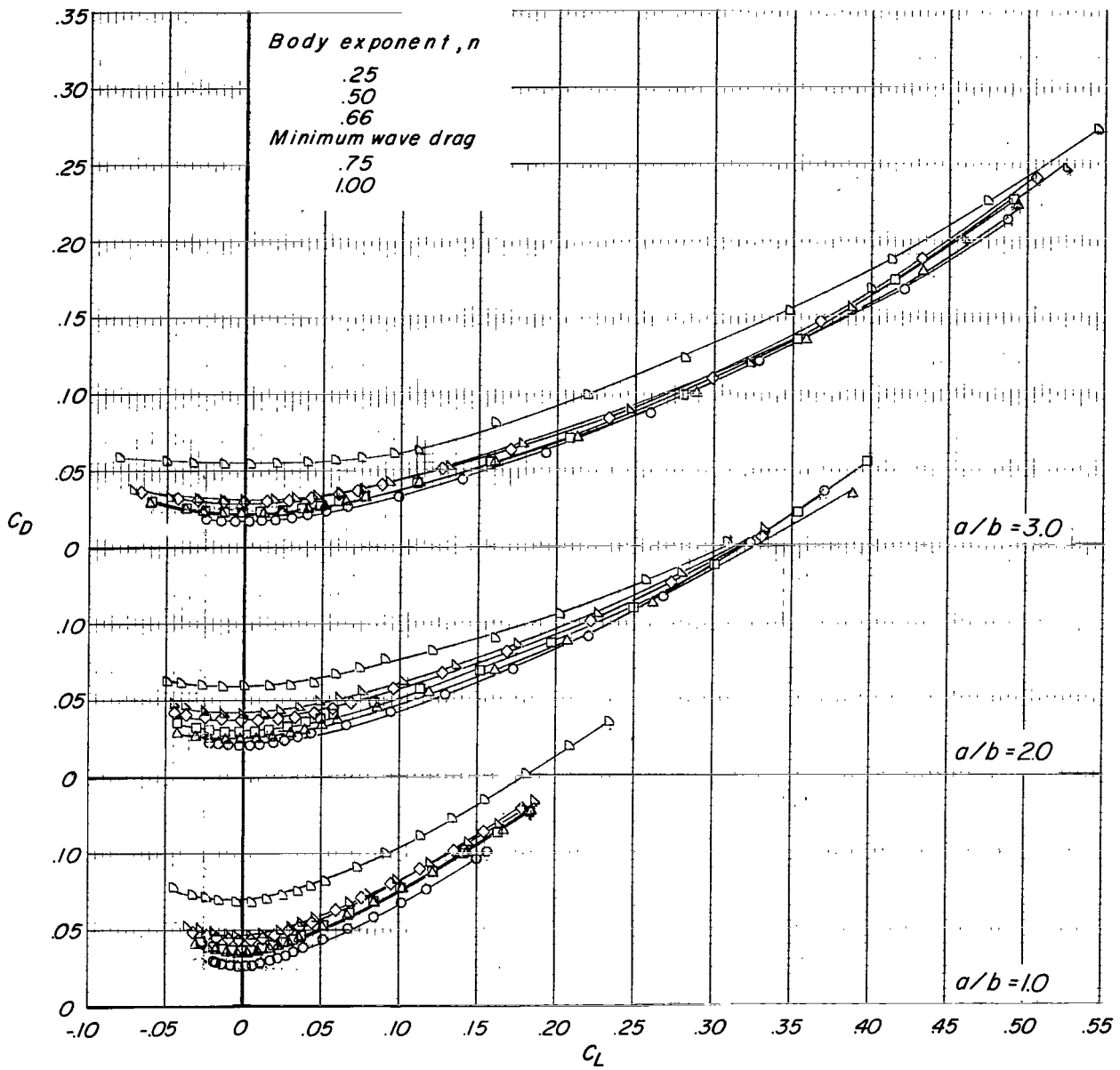

(c) C_D as a function of C_L.

Figure 5.- Continued.

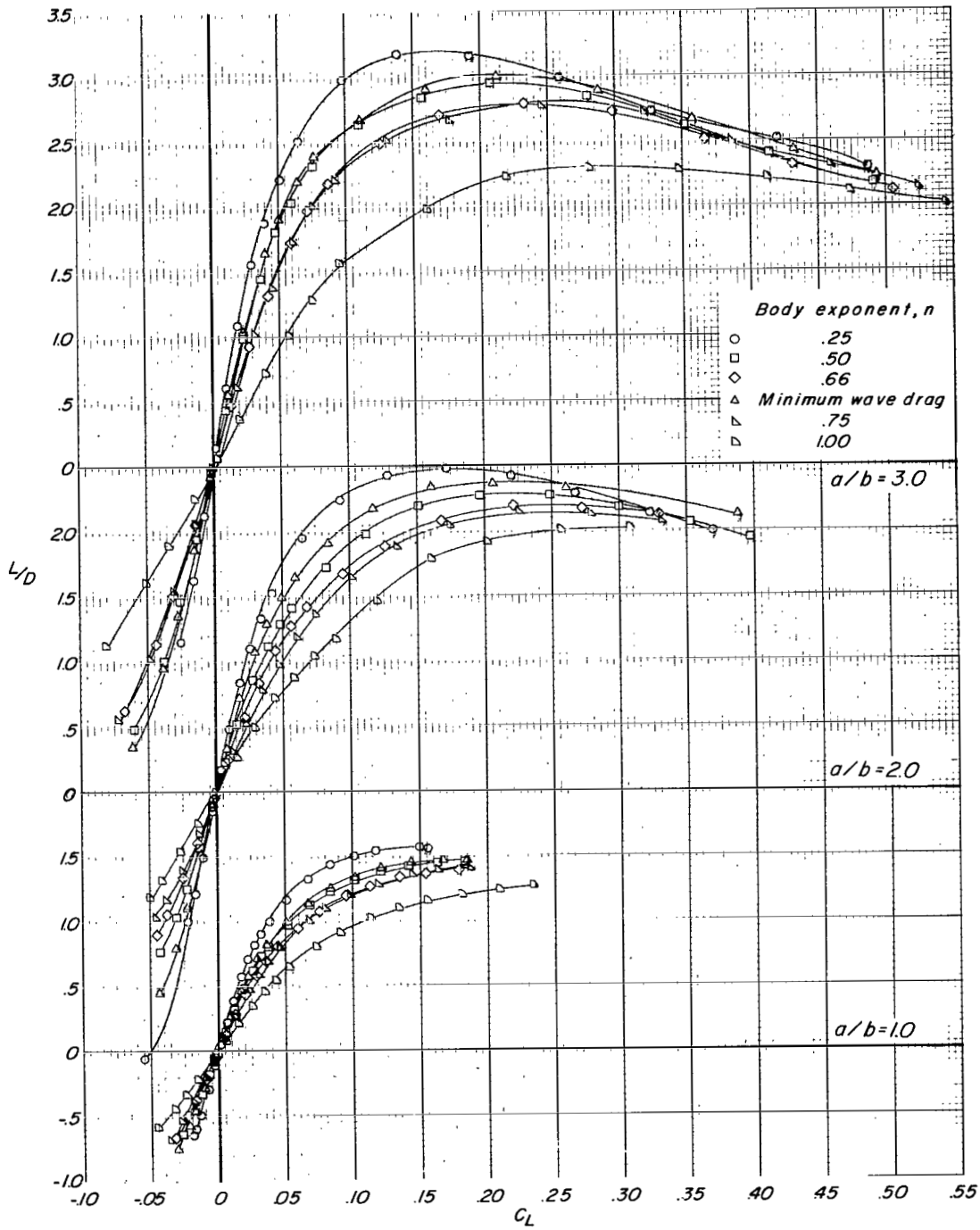

(d) L/D as a function of C_L.

Figure 5.- Continued.

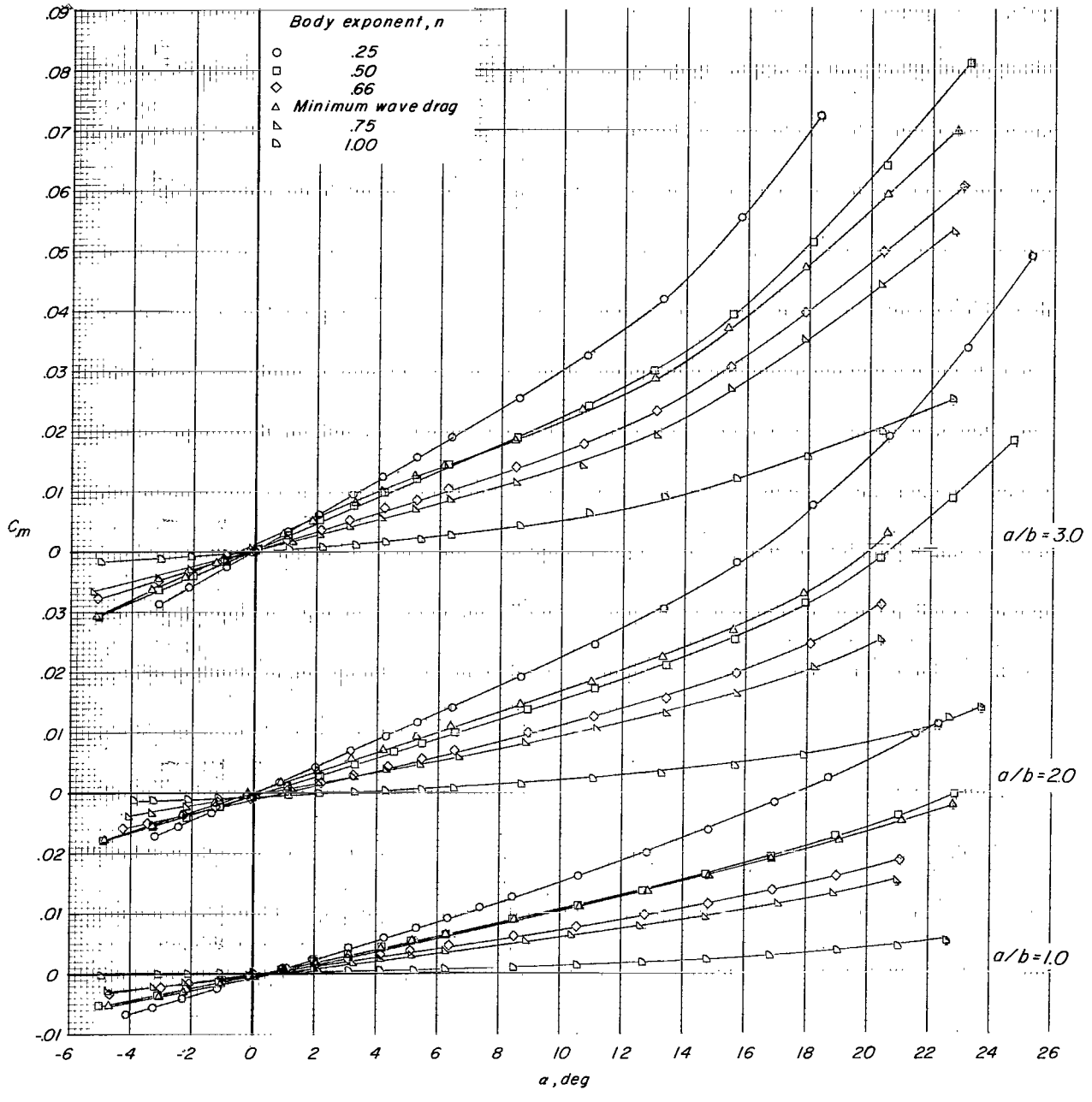

(e) C_m as a function of α.

Figure 5.- Continued.

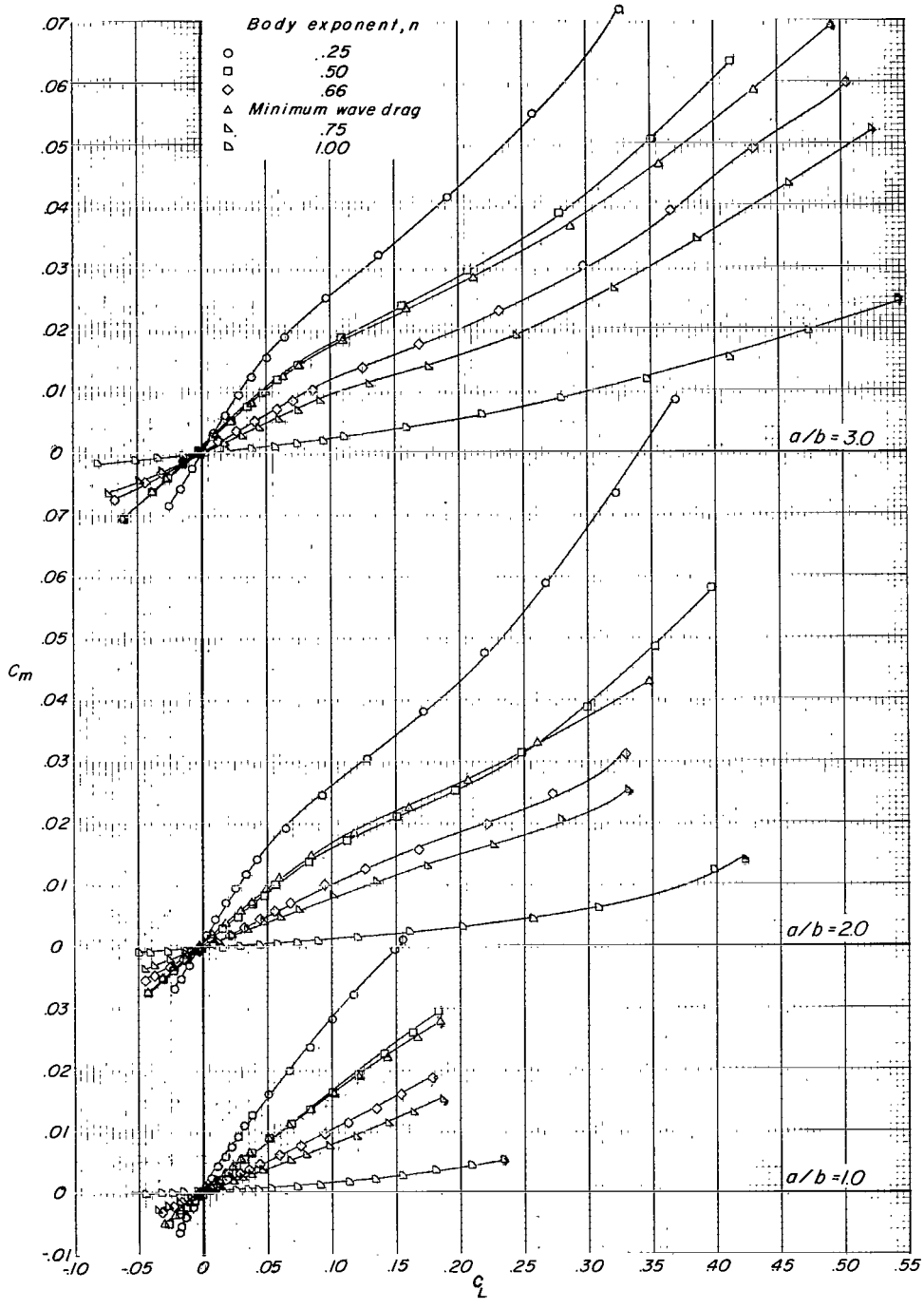

(f) C_m as a function of C_L.

Figure 5.- Concluded.

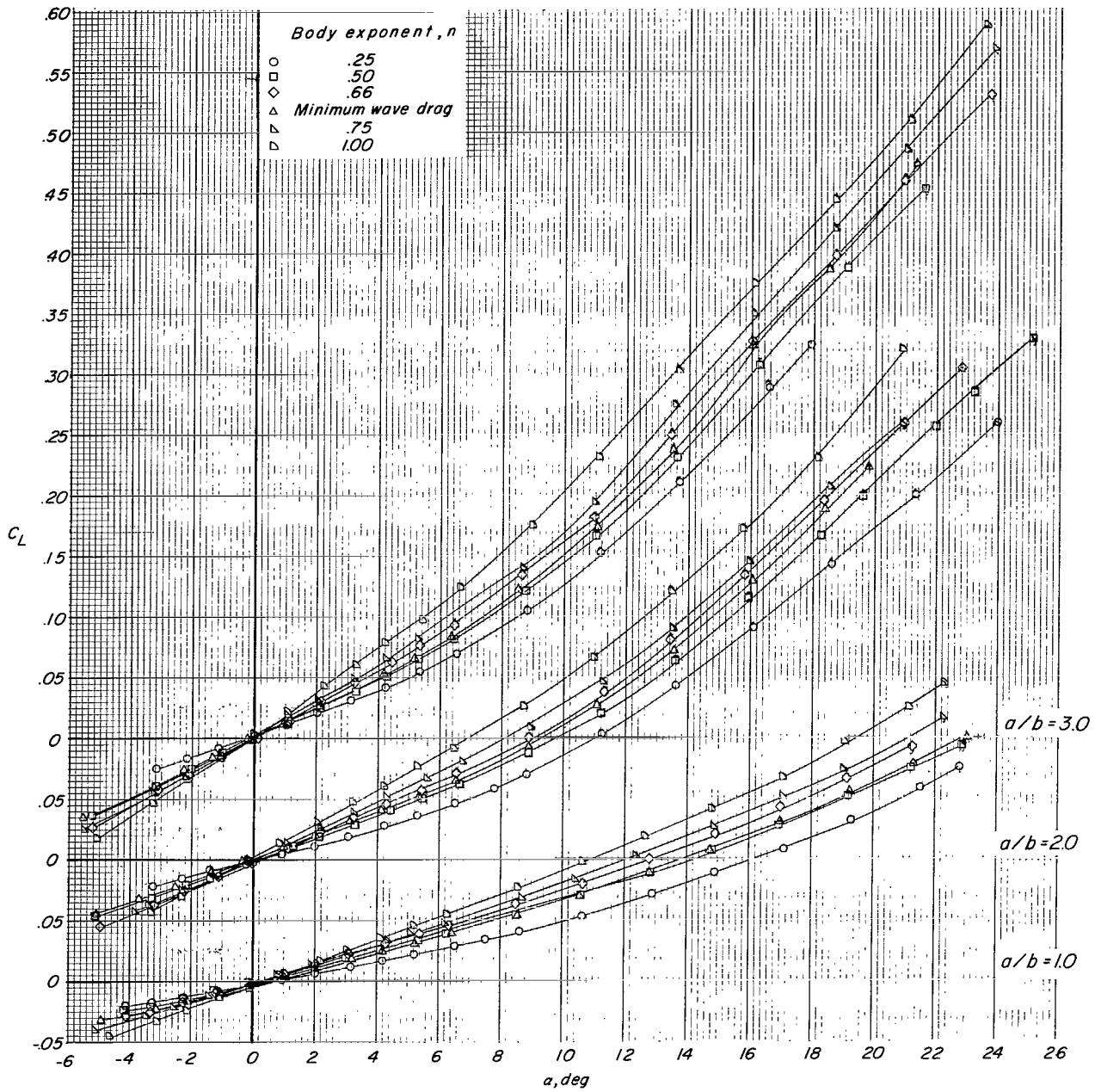

(a) C_L as a function of α.

Figure 6.- Longitudinal aerodynamic characteristics associated with the power-law bodies and minimum-wave-drag body. M = 0.90.

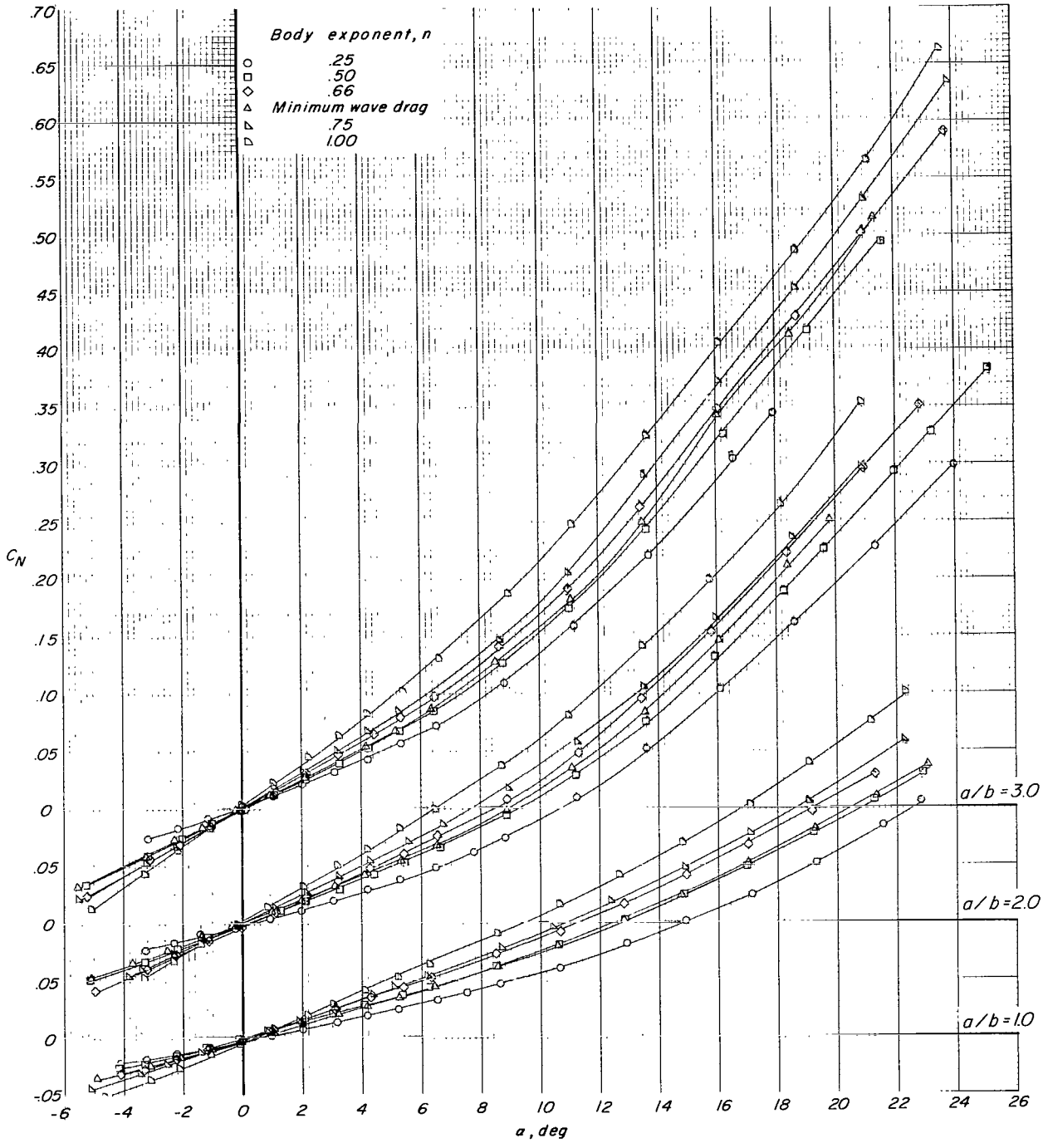

(b) C_N as a function of α.

Figure 6.- Continued.

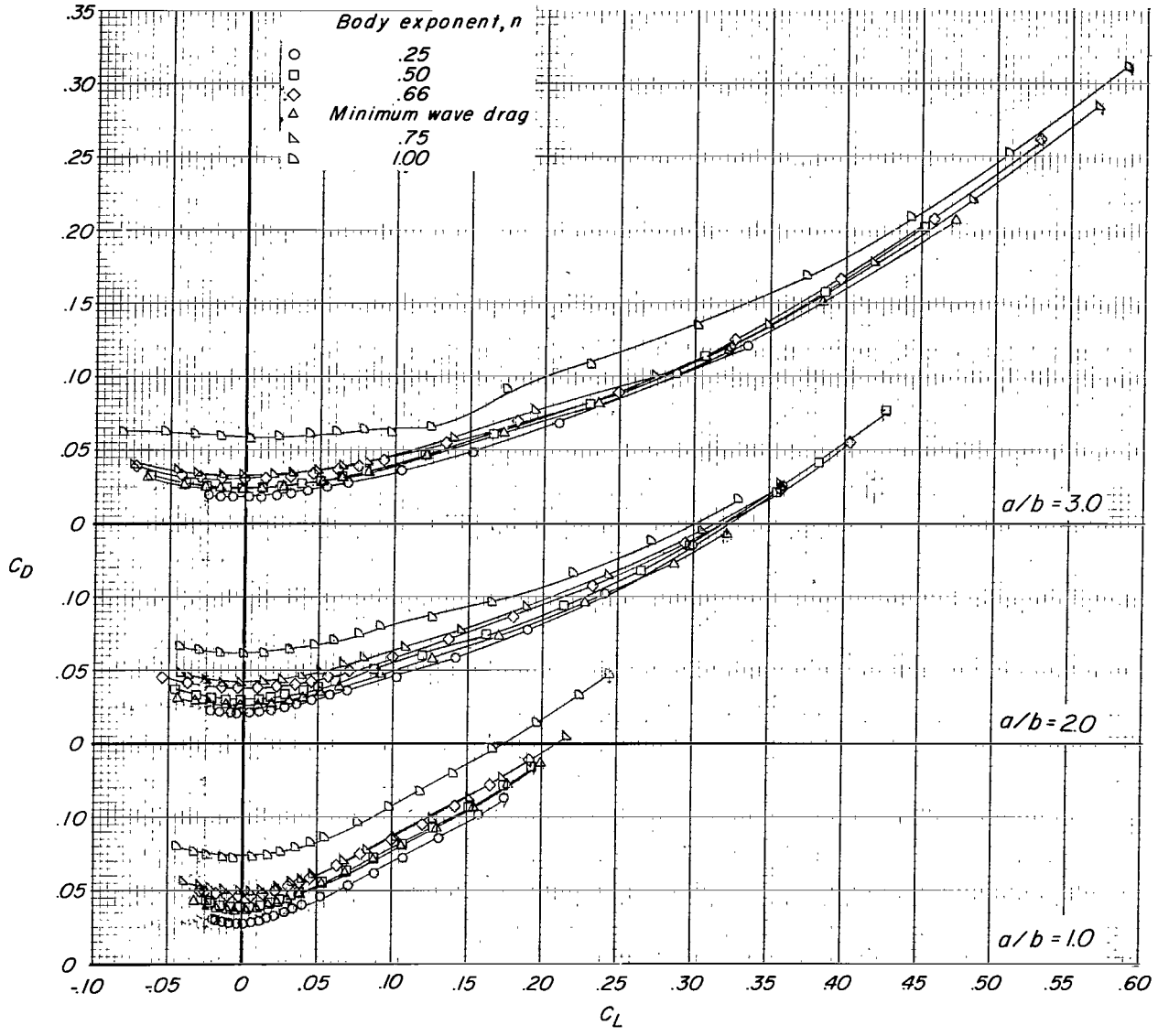

(c) C_D as a function of C_L.

Figure 6.- Continued.

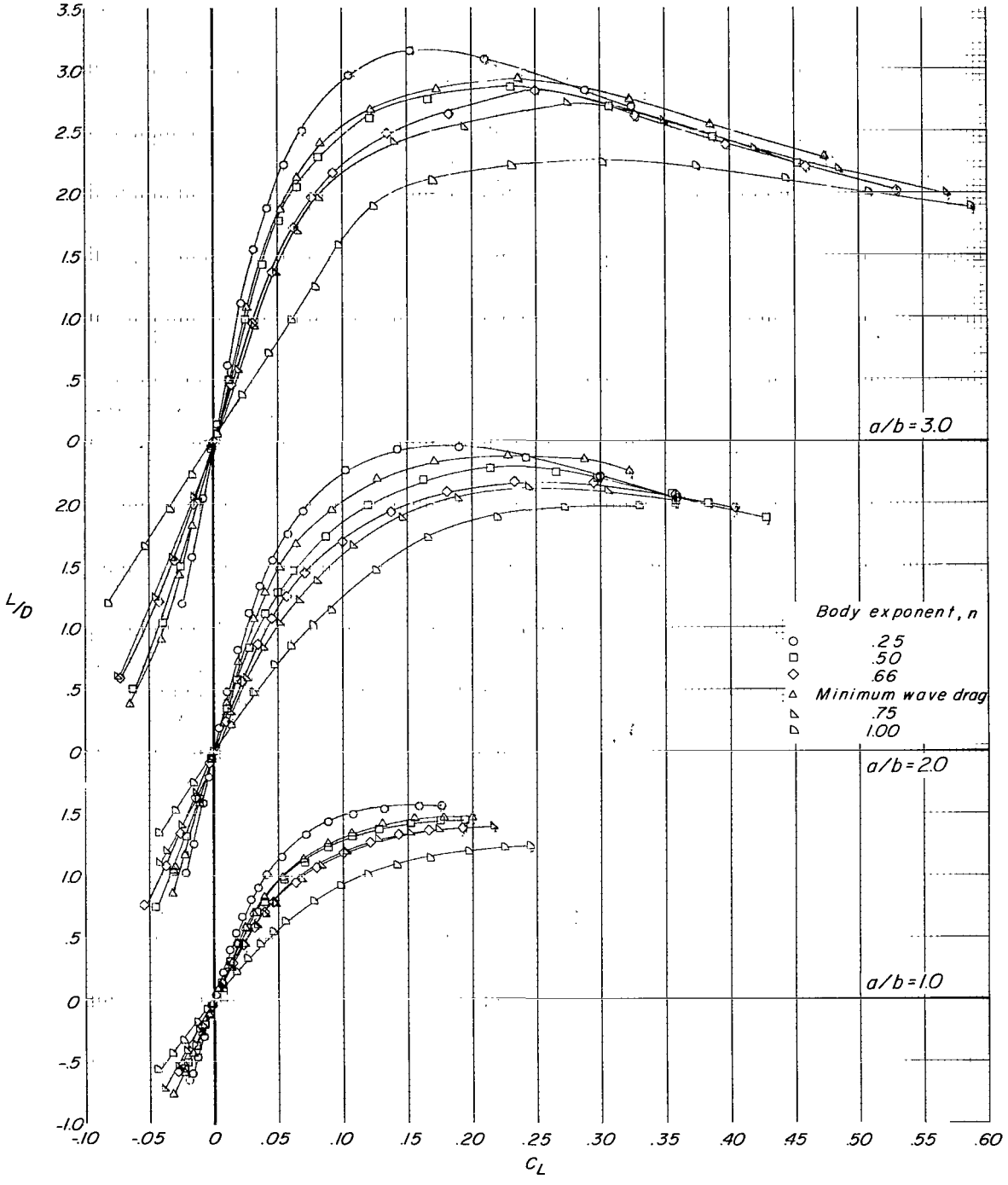

(d) L/D as a function of C_L.

Figure 6.- Continued.

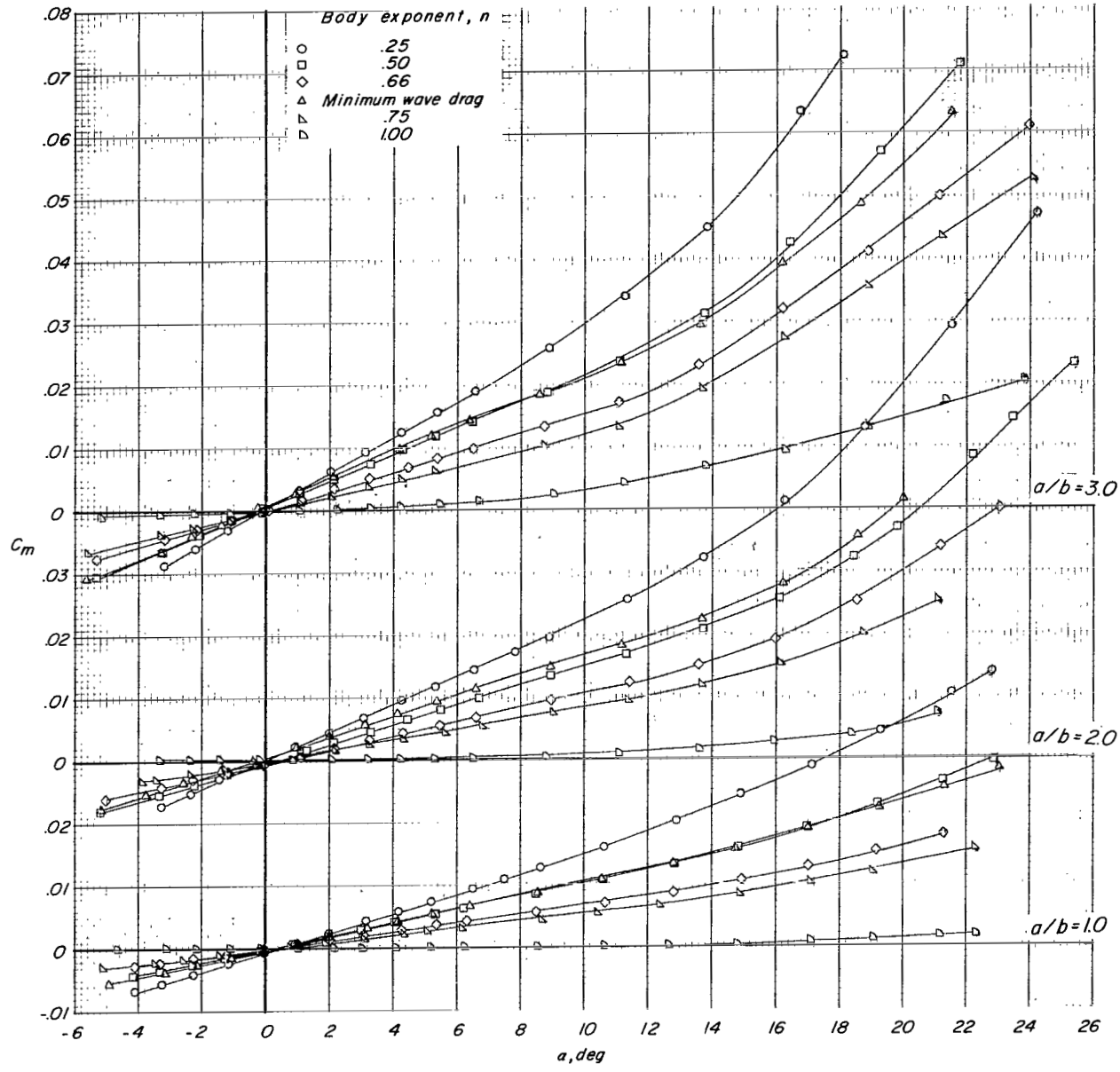

(e) C_m as a function of α.

Figure 6.- Continued.

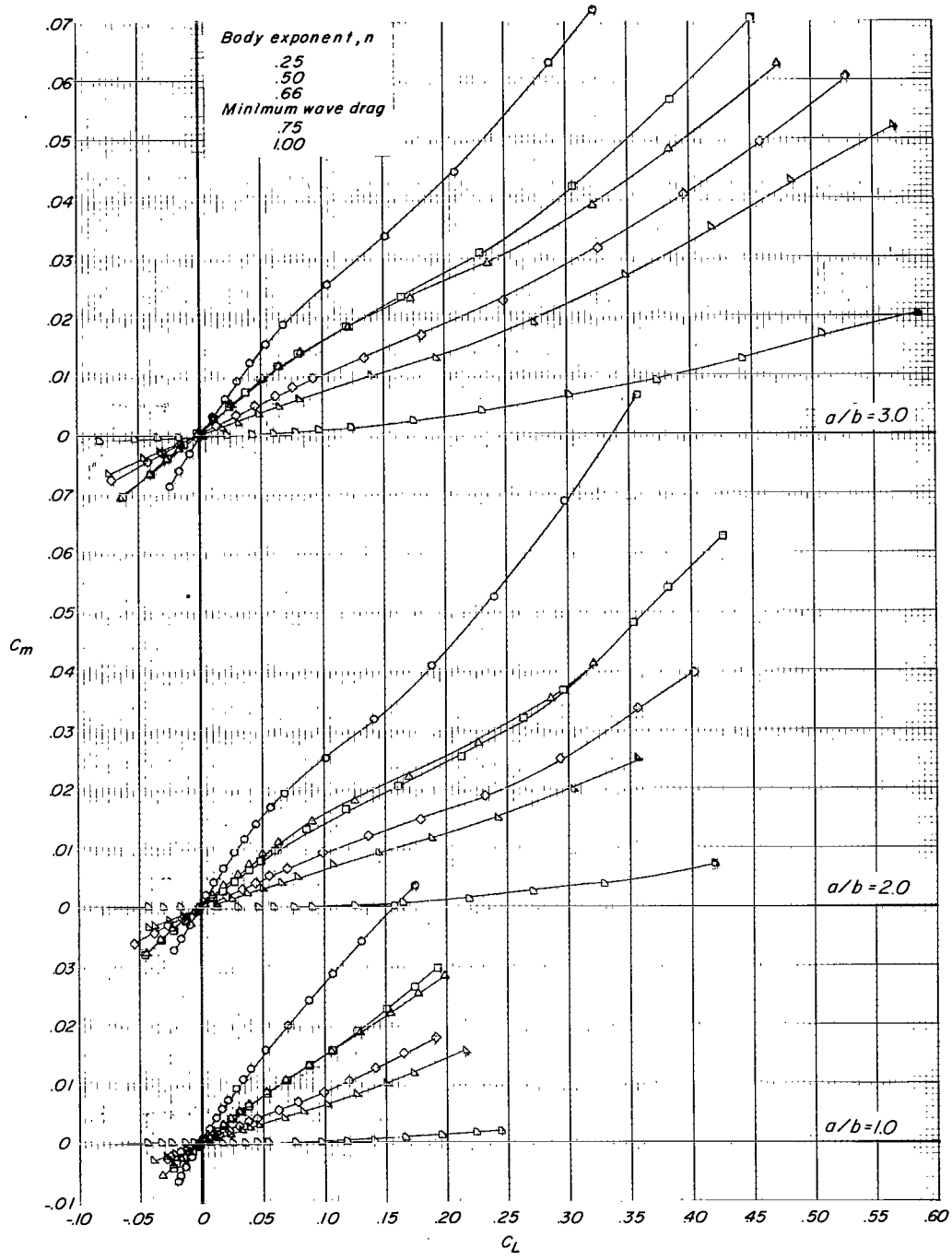

(f) C_m as a function of C_L.

Figure 6.- Concluded.

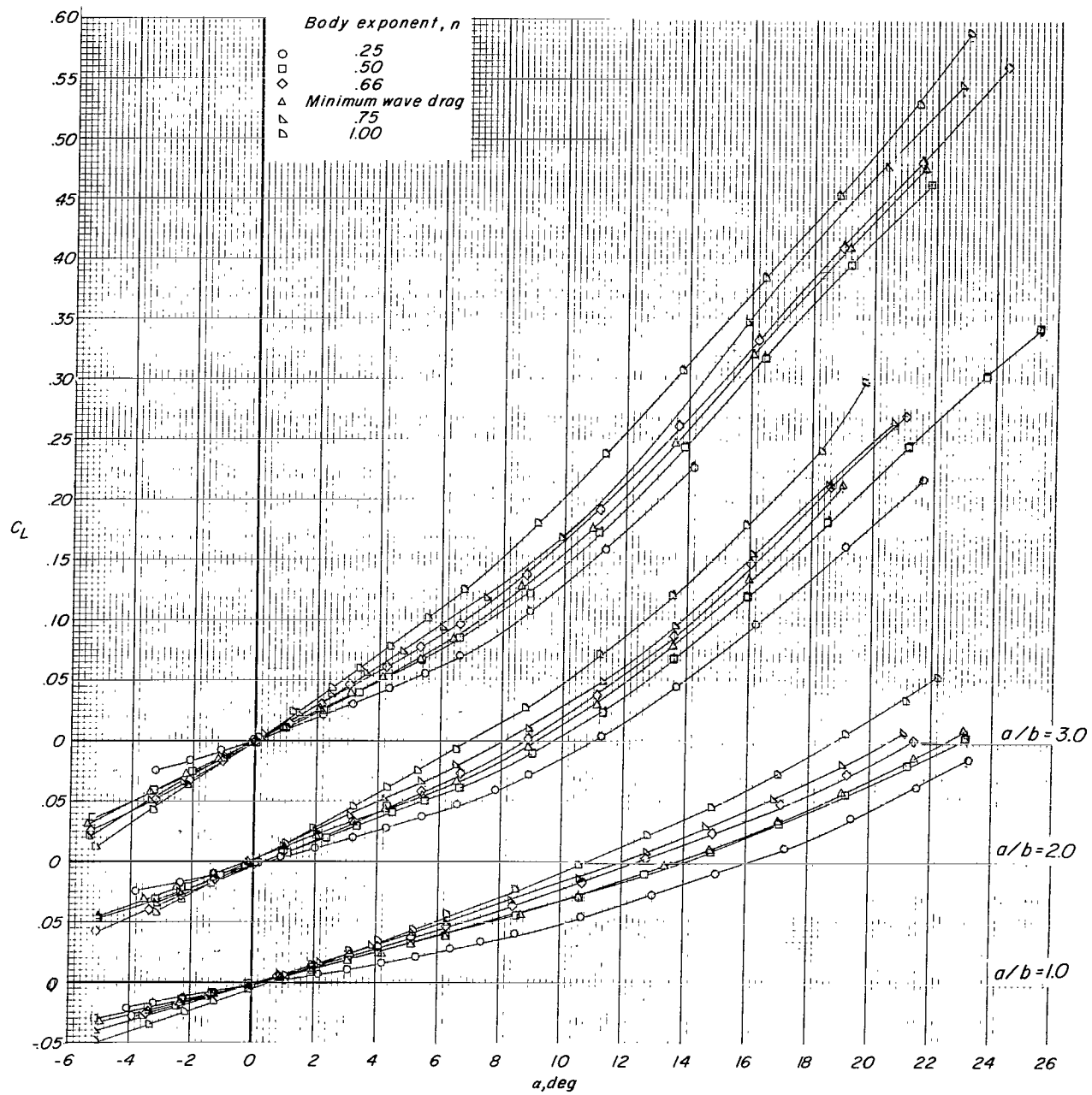

(a) C_L as a function of α.

Figure 7.- Longitudinal aerodynamic characteristics associated with the power-law bodies and minimum-wave-drag body. M = 0.95.

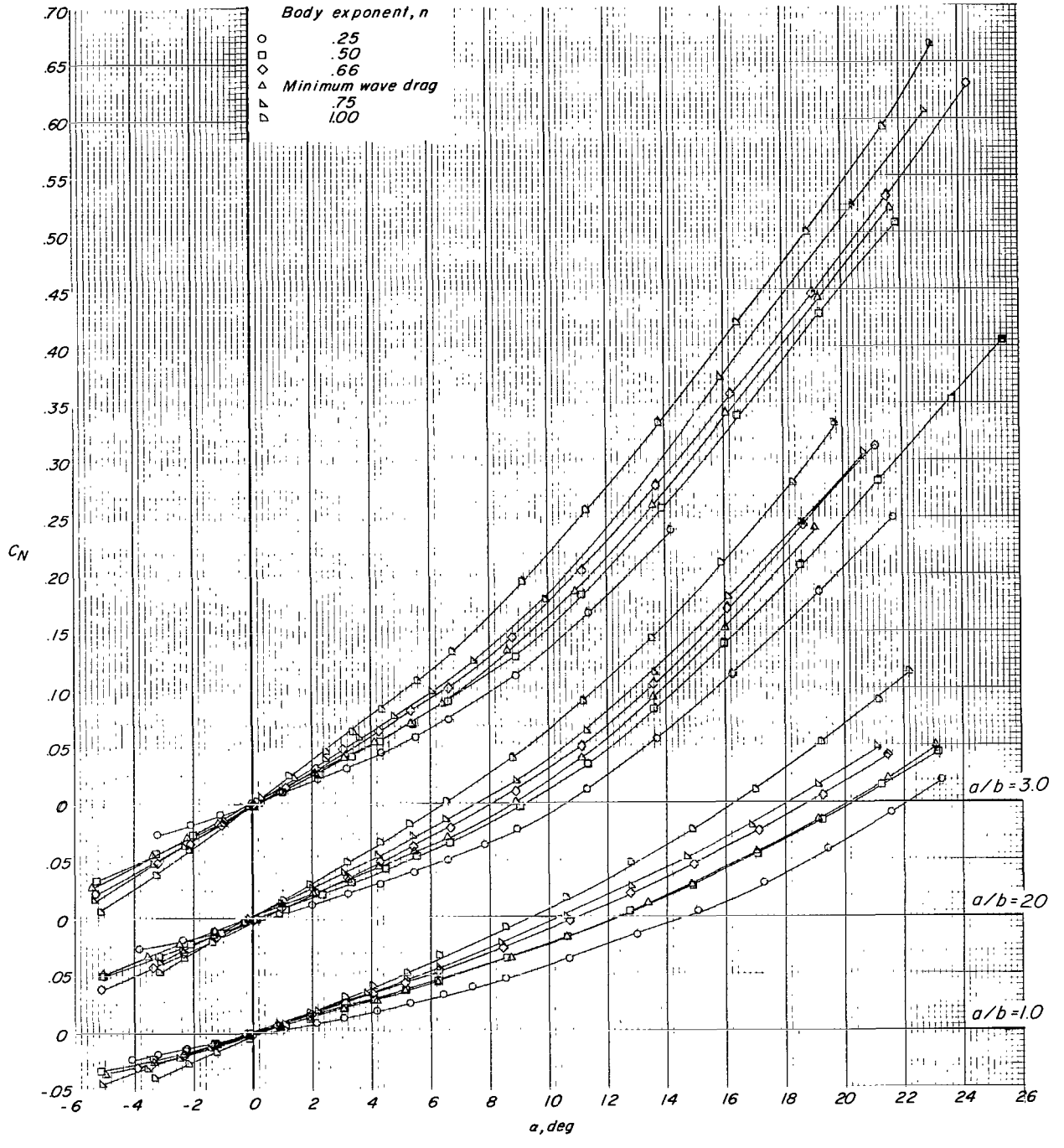

(b) C_N as a function of α.

Figure 7.- Continued.

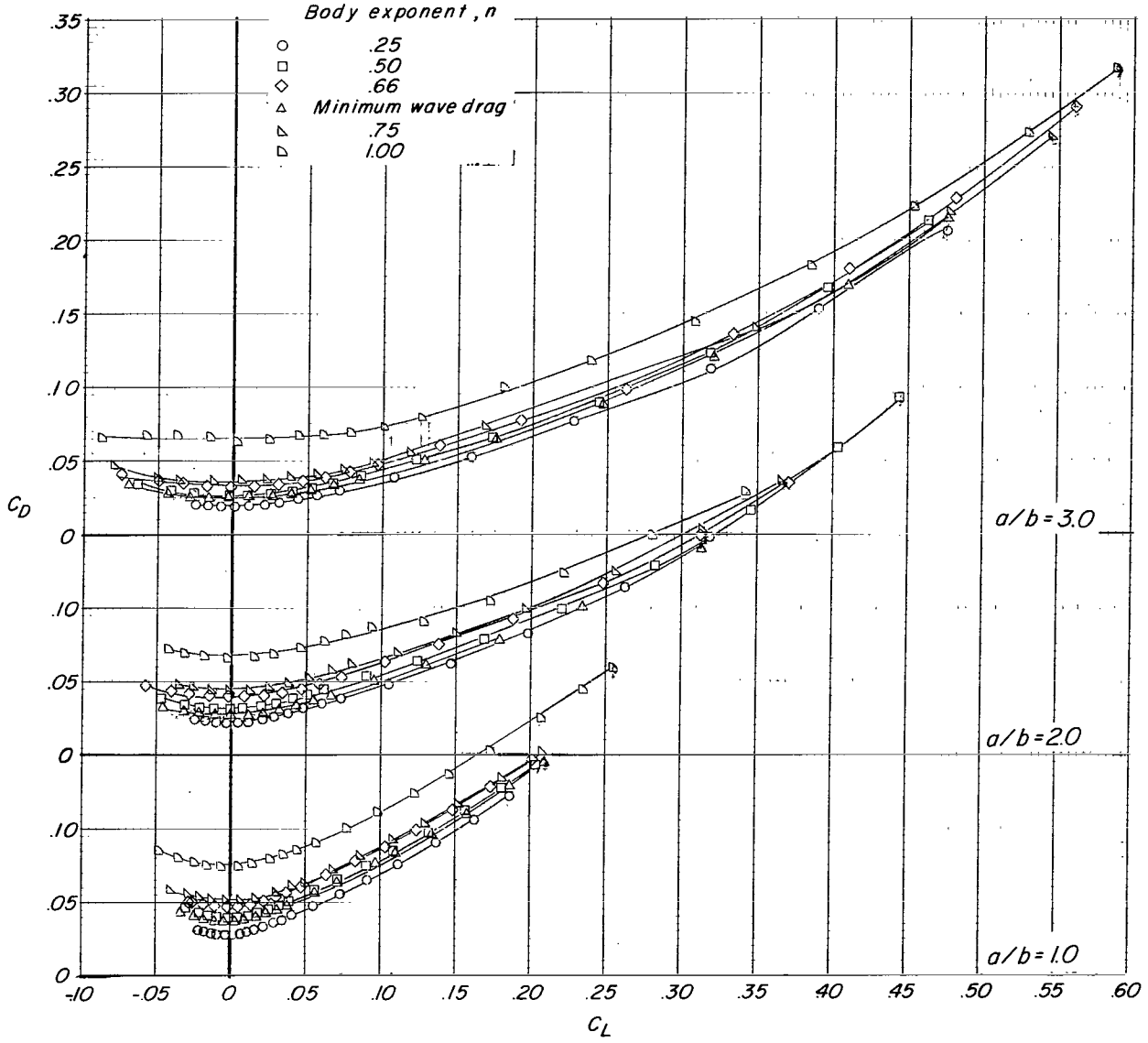

(c) C_D as a function of C_L.

Figure 7.- Continued.

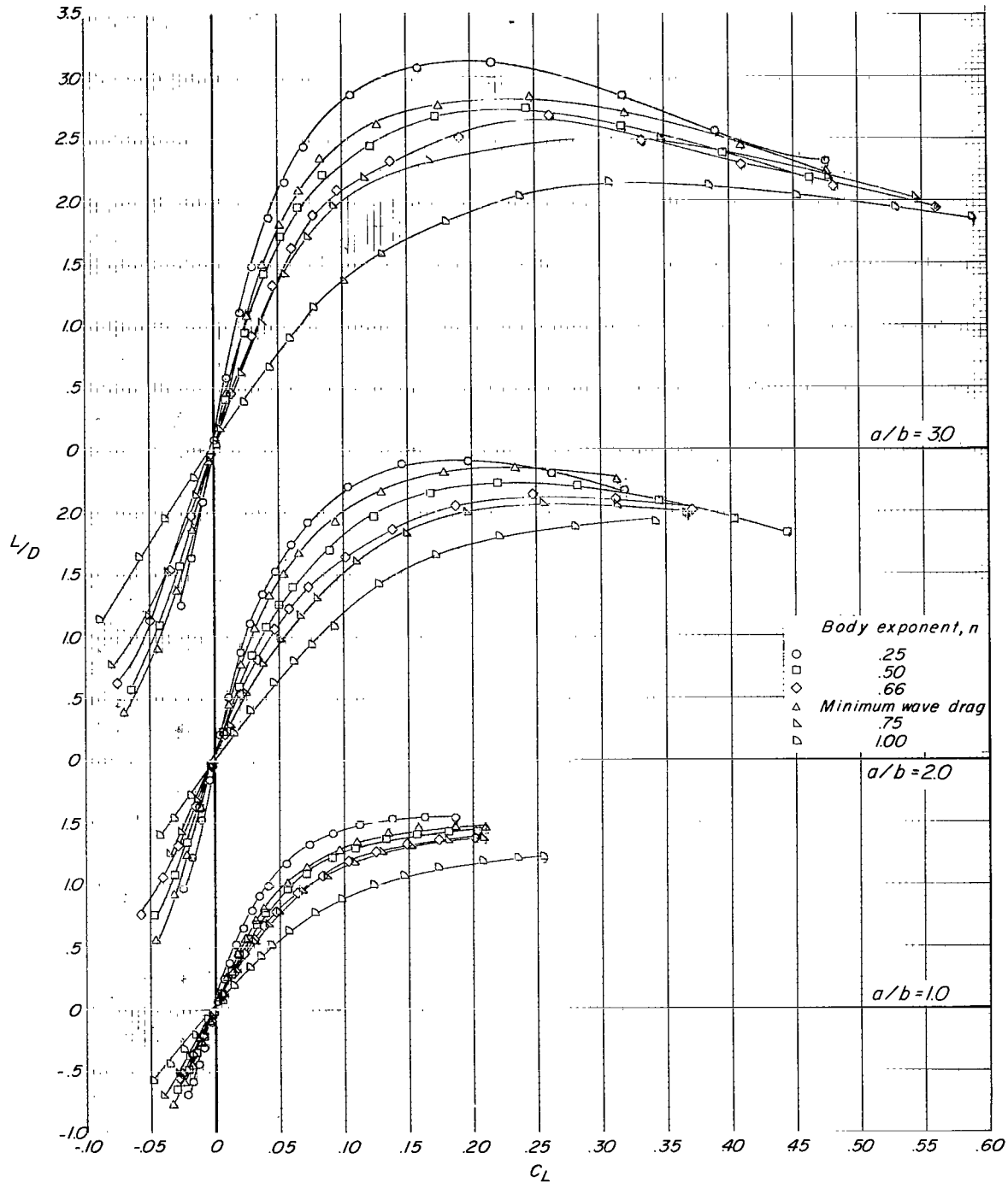

(d) L/D as a function of C_L.

Figure 7.- Continued.

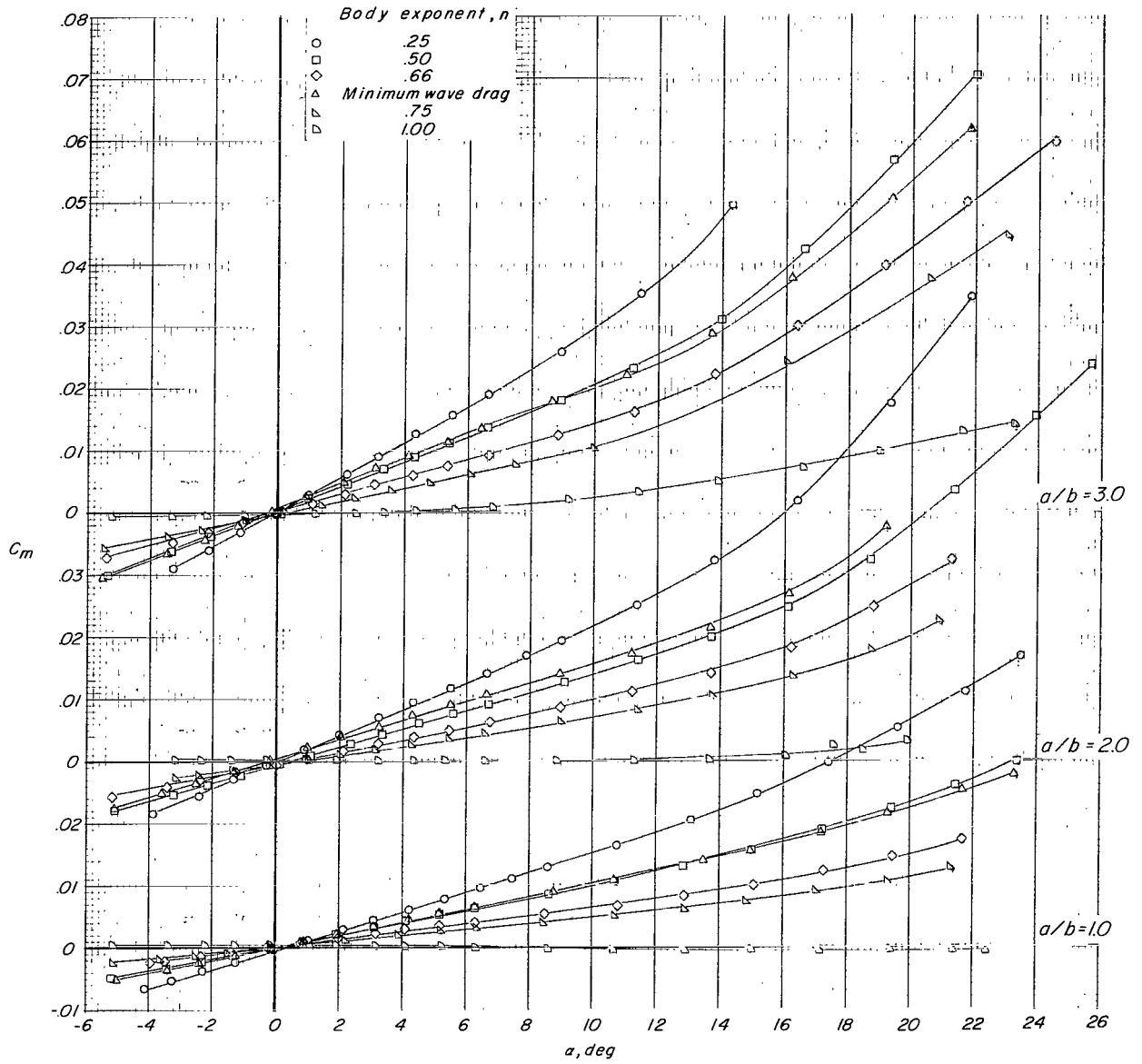

(e) C_m as a function of α.

Figure 7.- Continued.

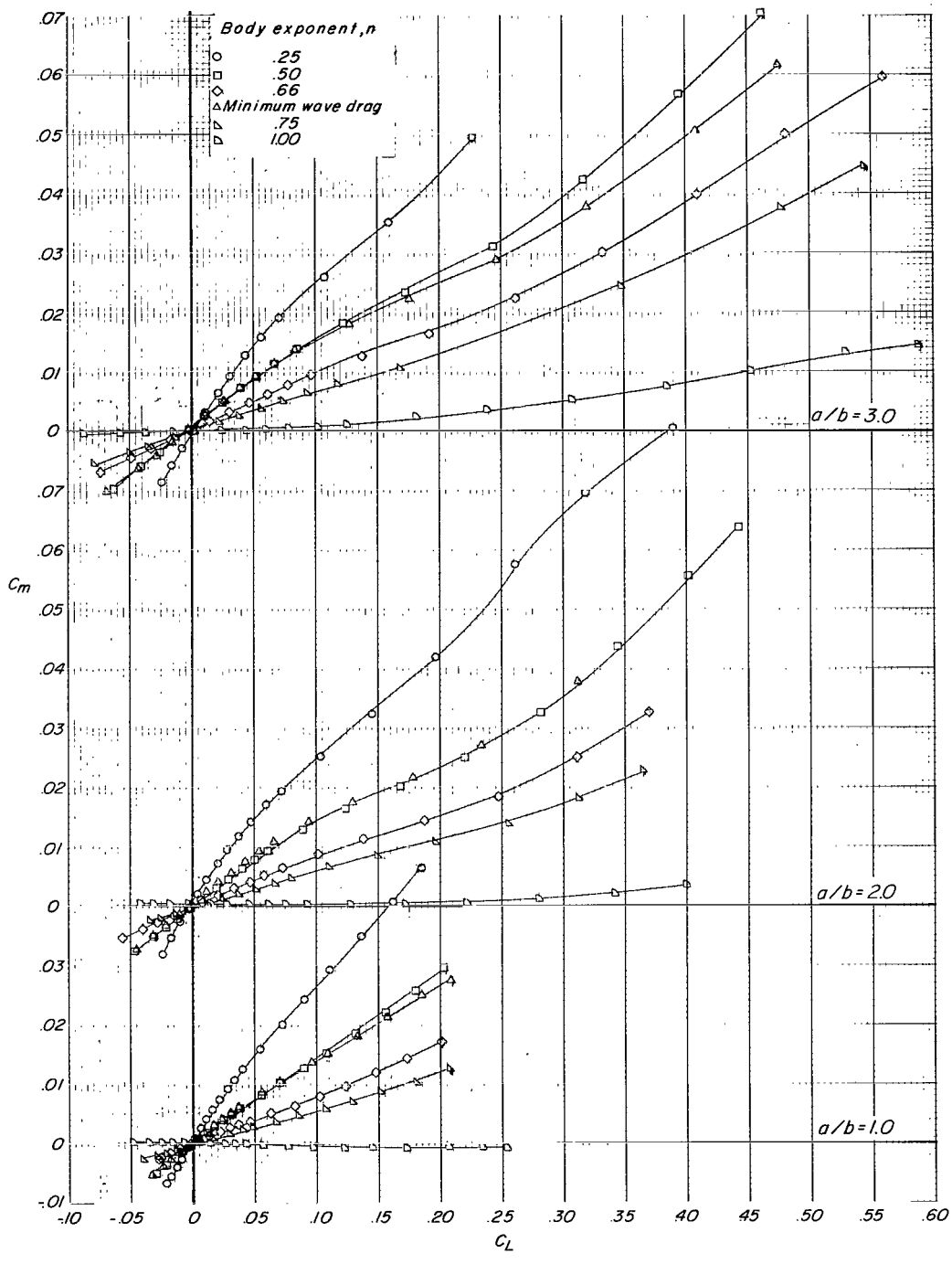

(f) C_m as a function of C_L.

Figure 7.- Concluded.

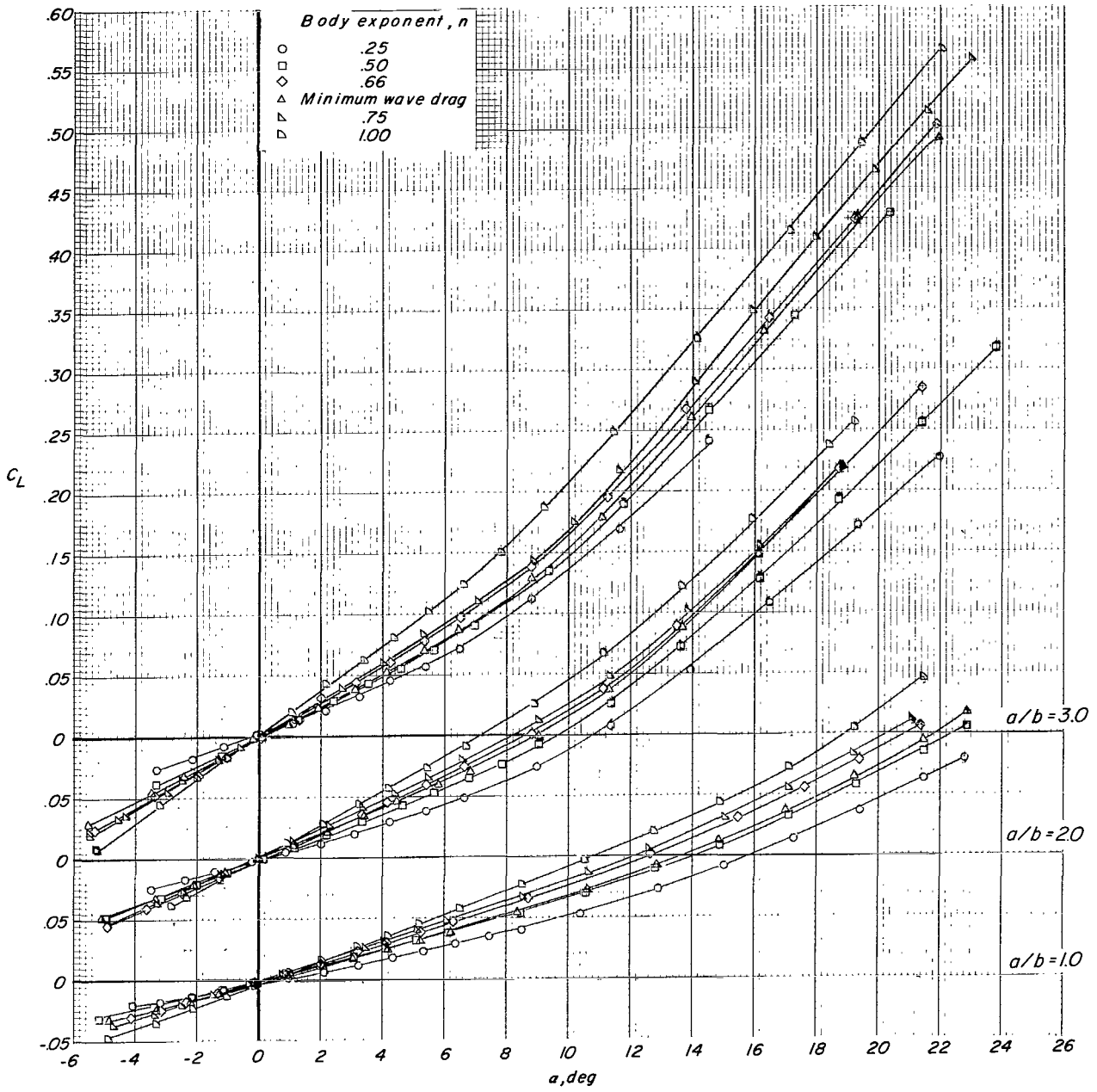

(a) C_L as a function of α.

Figure 8.- Longitudinal aerodynamic characteristics associated with the power-law bodies and minimum-wave-drag body. M = 1.00.

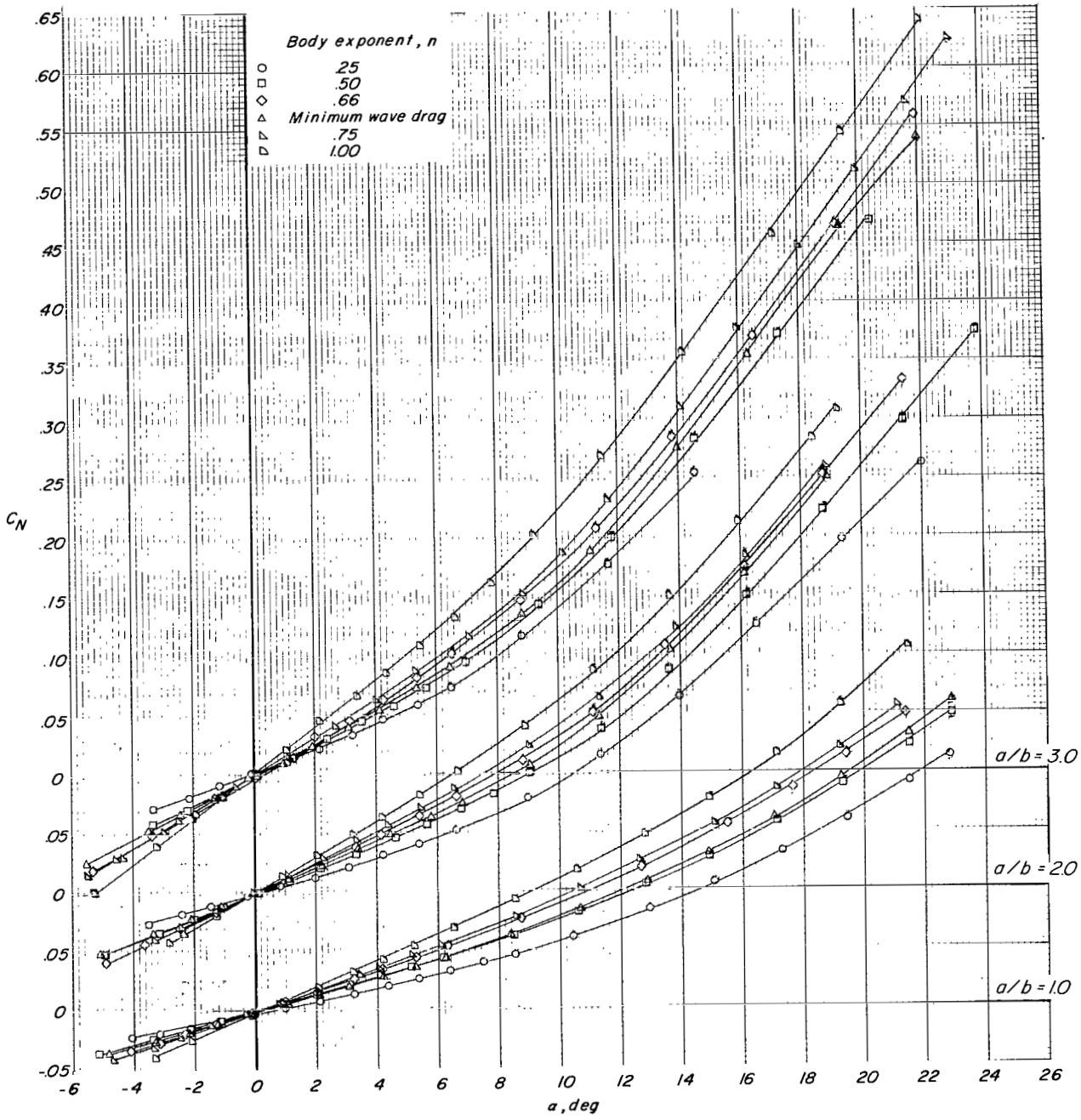

(b) C_N as a function of α.

Figure 8.- Continued.

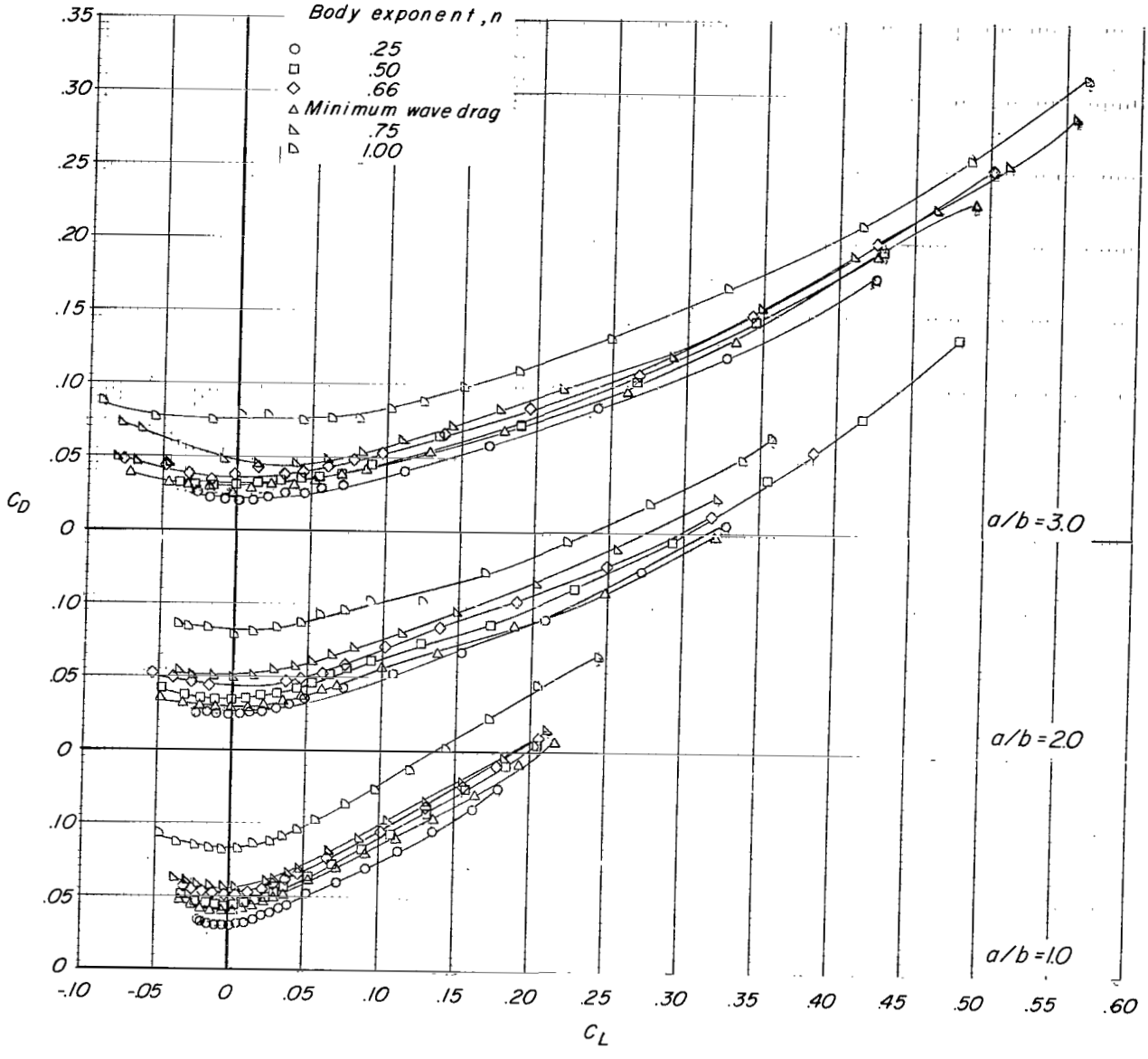

(c) C_D as a function of C_L.

Figure 8.- Continued.

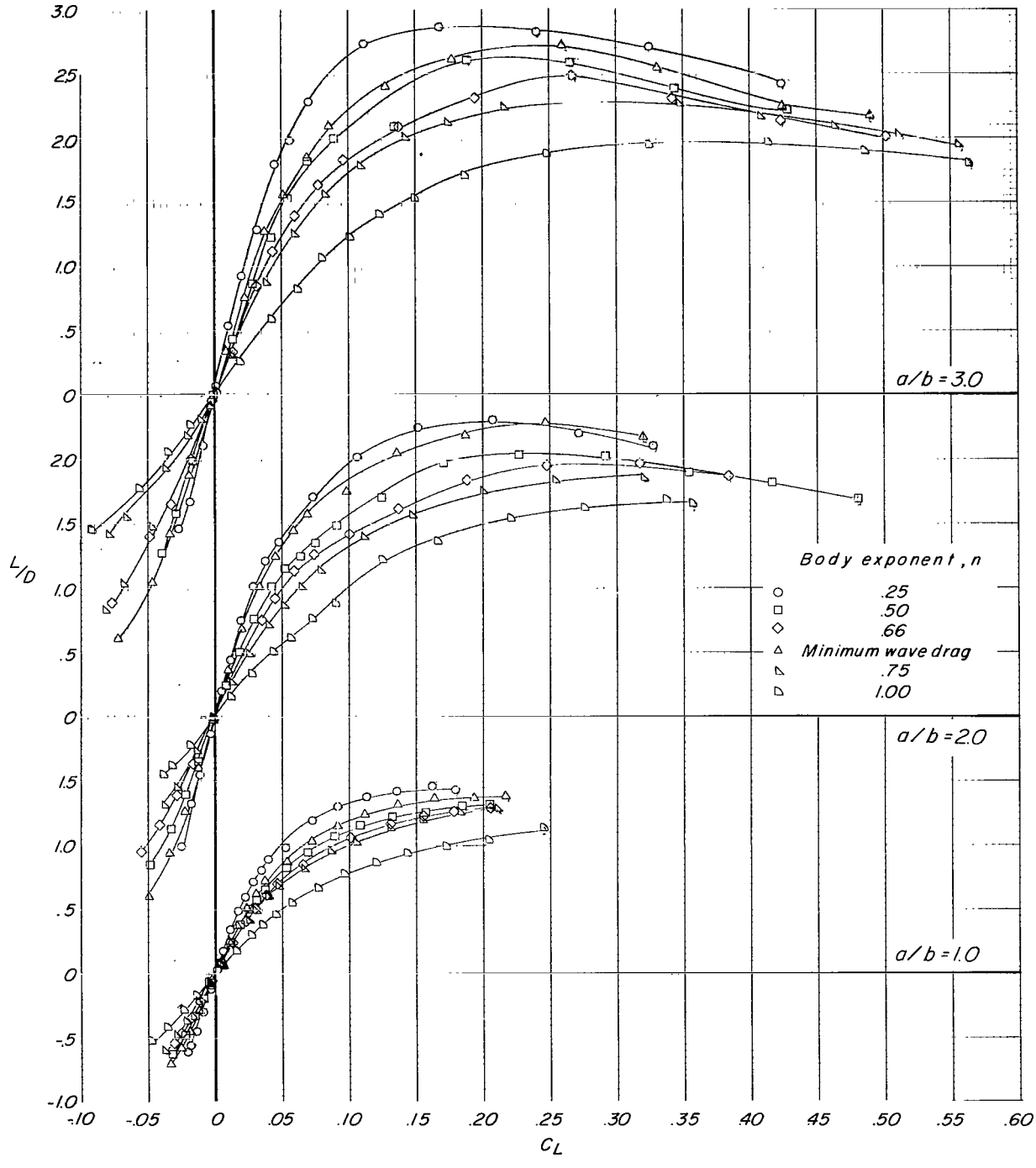

(d) L/D as a function of C_L.

Figure 8.- Continued.

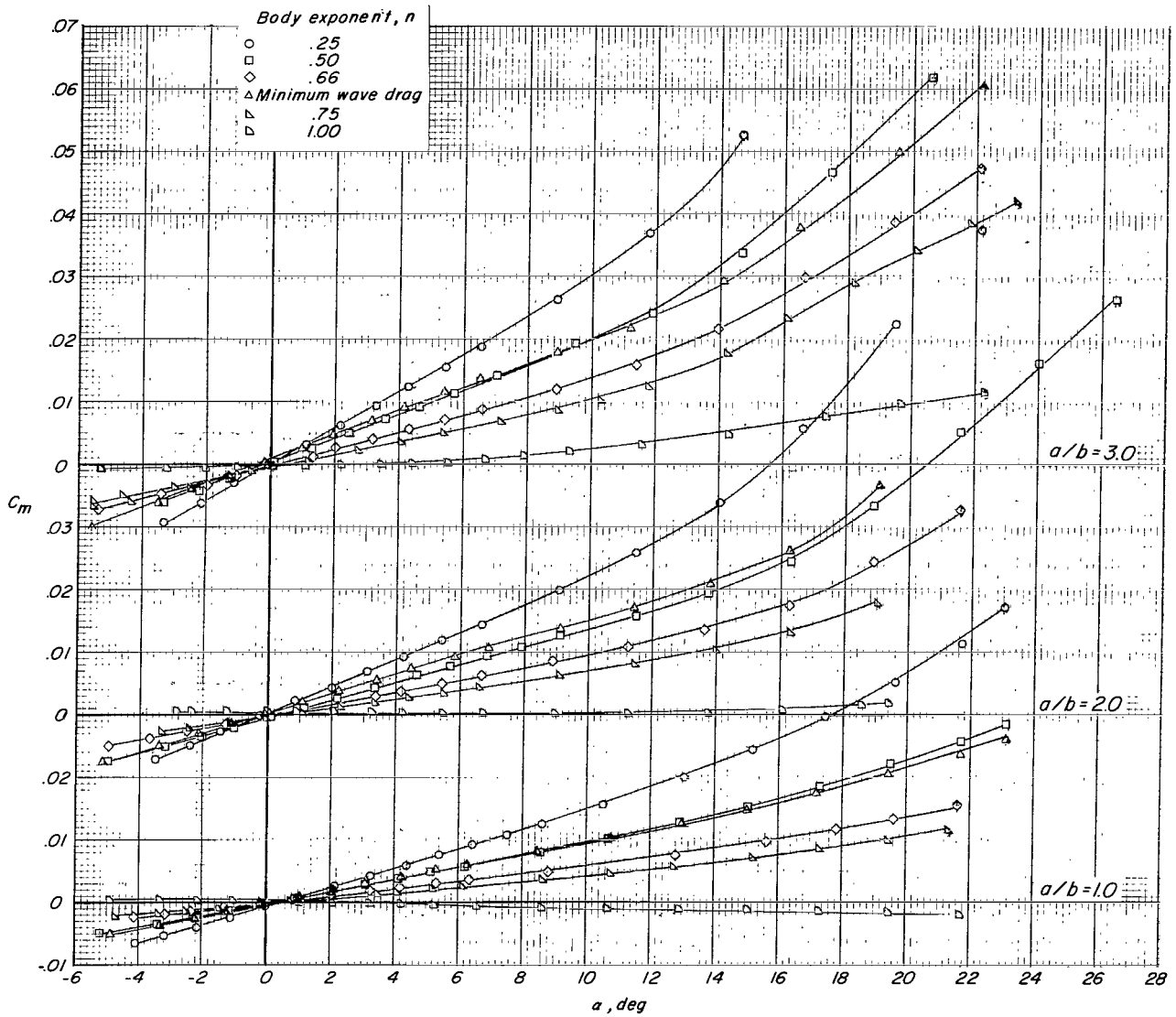

(e) C_m as a function of α.

Figure 8.- Continued.

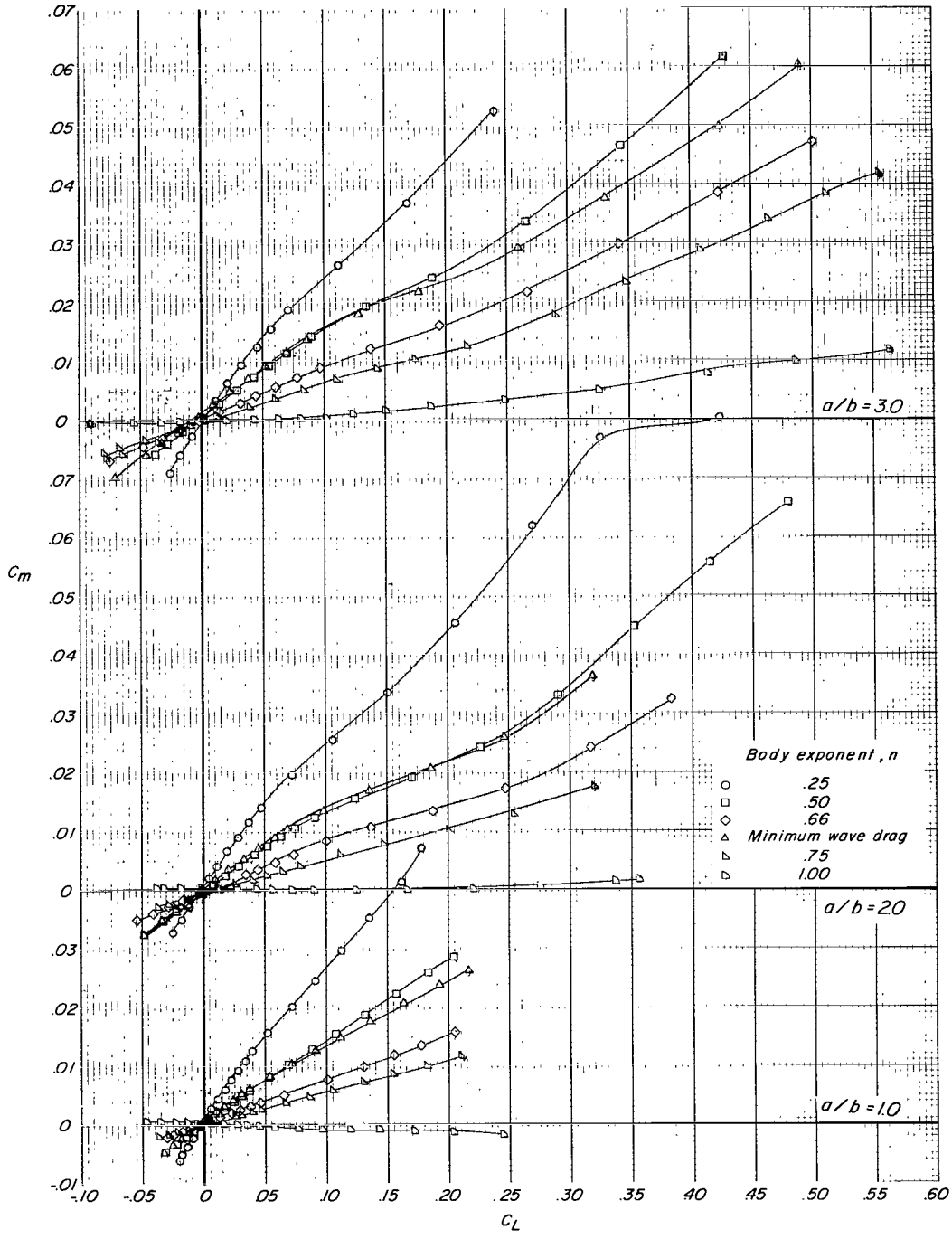

(f) C_m as a function of C_L.

Figure 8.- Concluded.

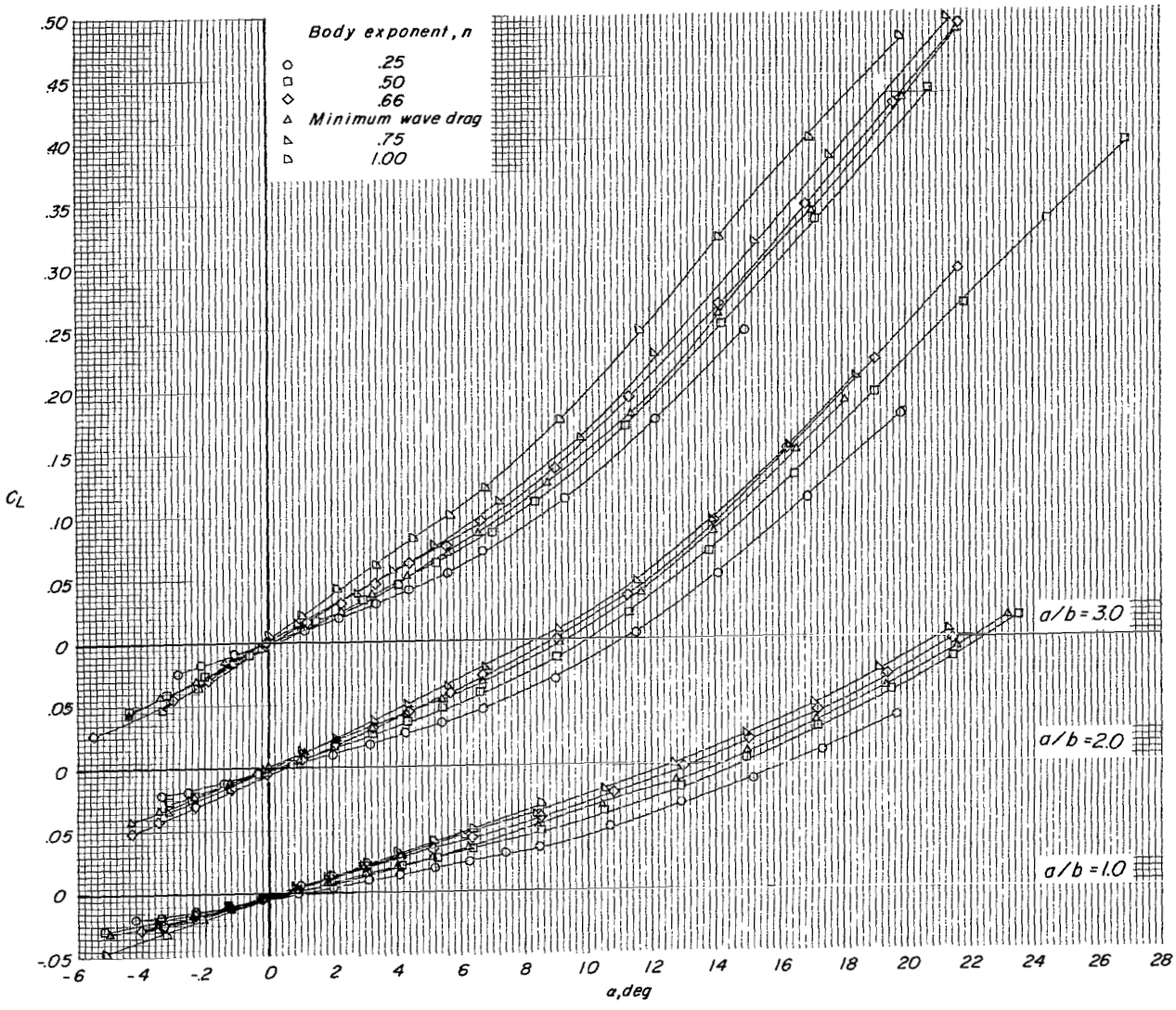

(a) C_L as a function of α.

Figure 9.- Longitudinal aerodynamic characteristics associated with the power-law bodies and minimum-wave-drag body. M = 1.12.

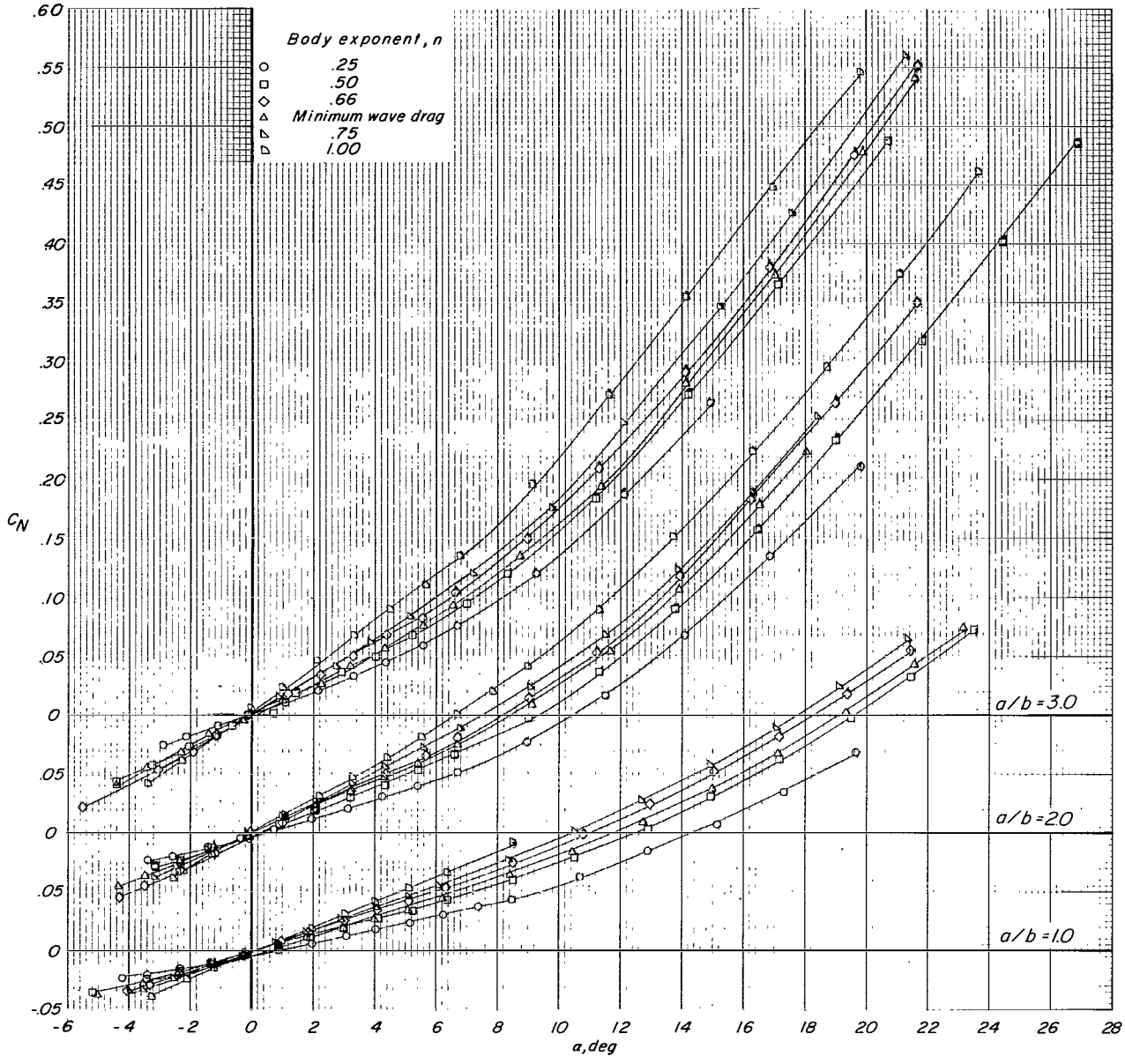

(b) C_N as a function of α.

Figure 9.- Continued.

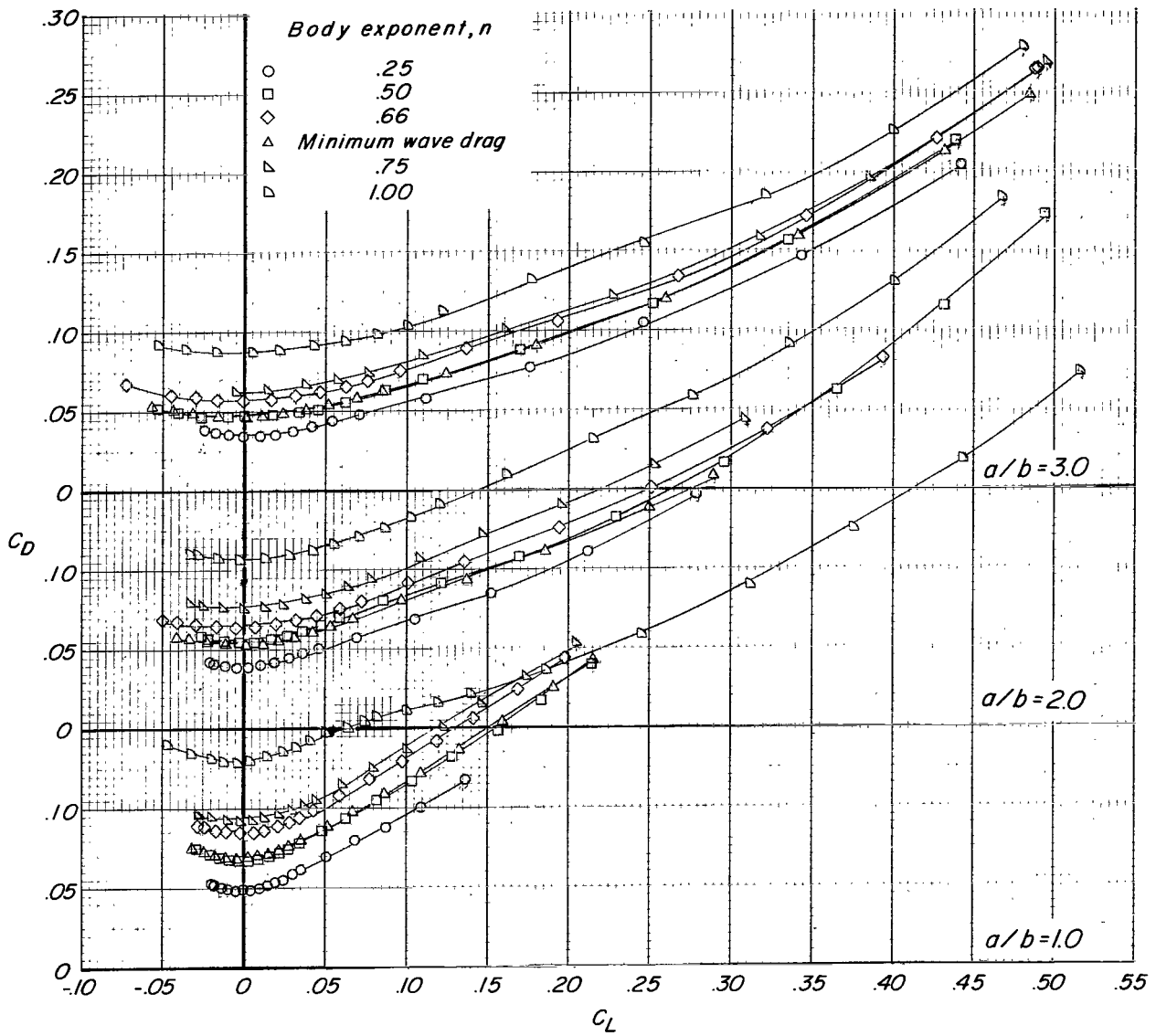

(c) C_D as a function of C_L.

Figure 9.- Continued.

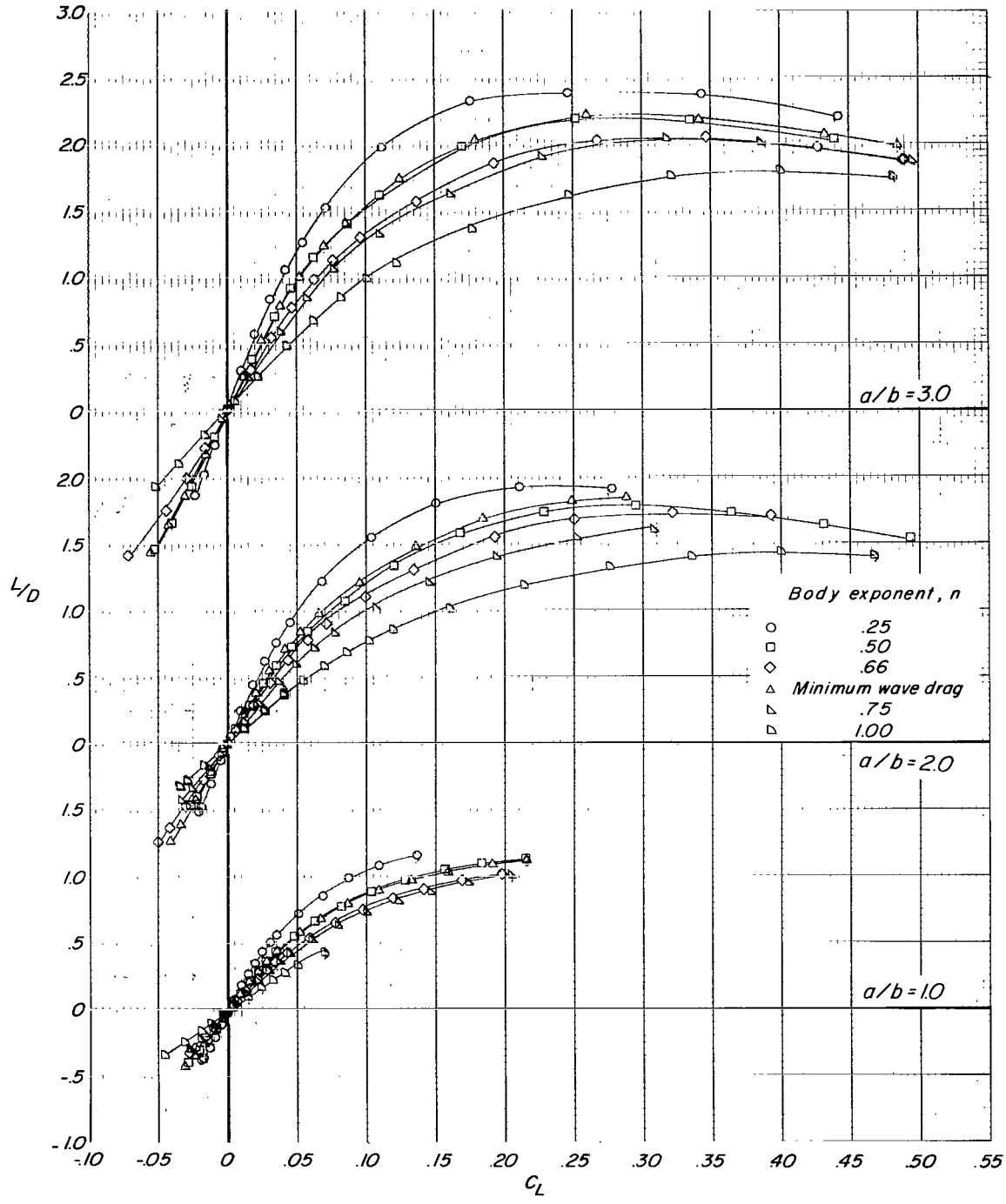

(d) L/D as a function of C_L.

Figure 9.- Continued.

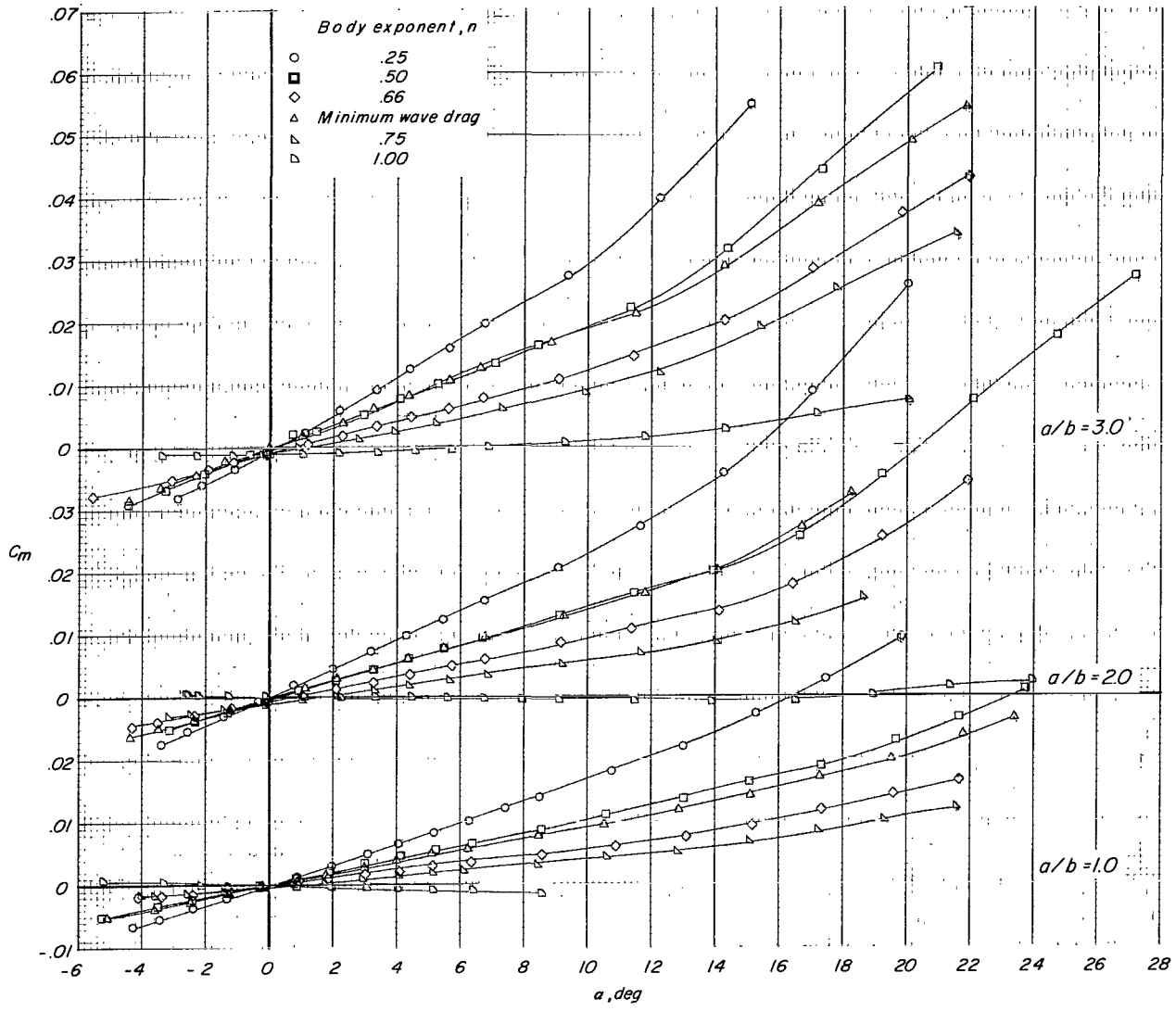

(e) C_m as a function of α.

Figure 9.- Continued.

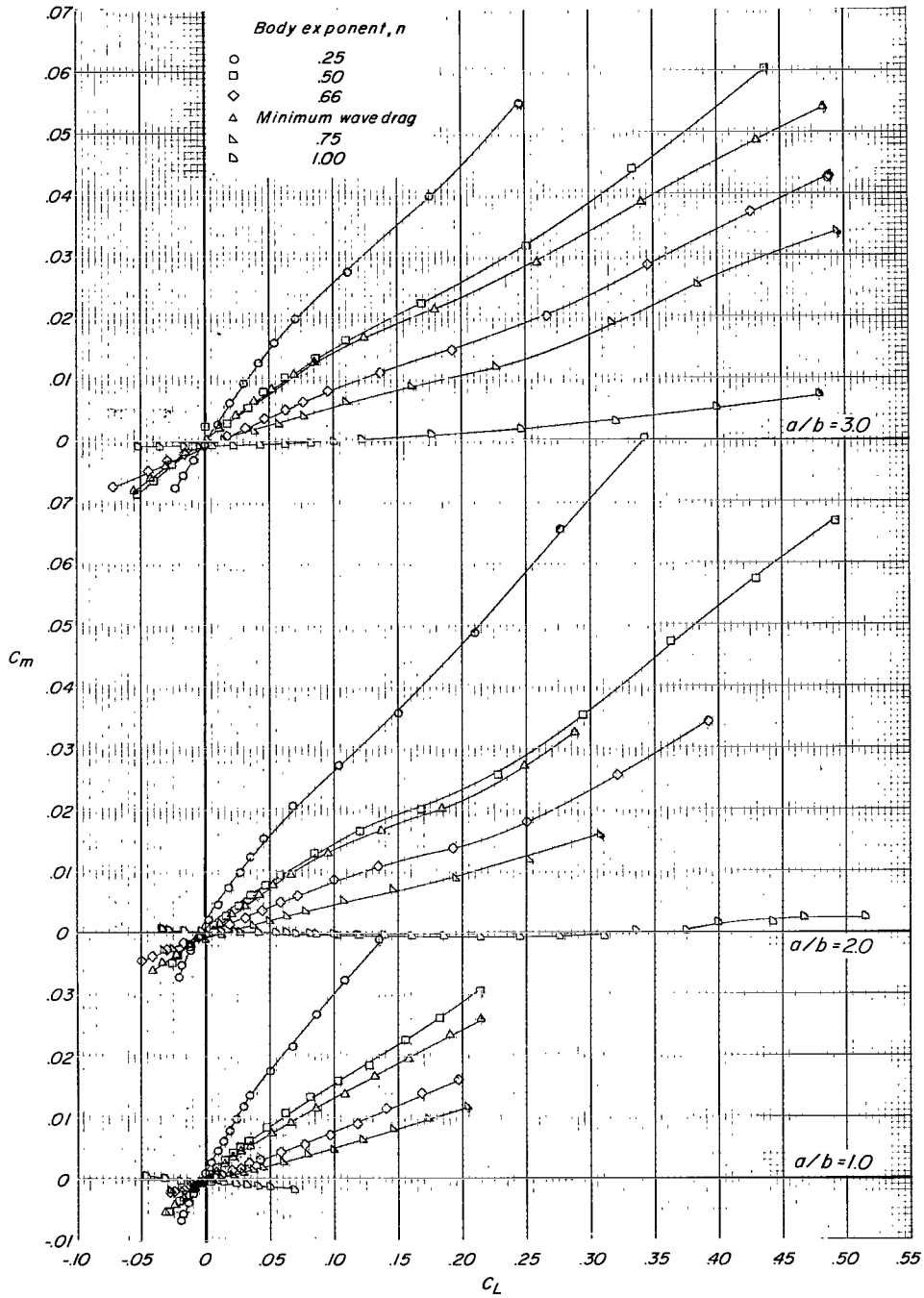

(f) C_m as a function of C_L.

Figure 9.- Concluded.

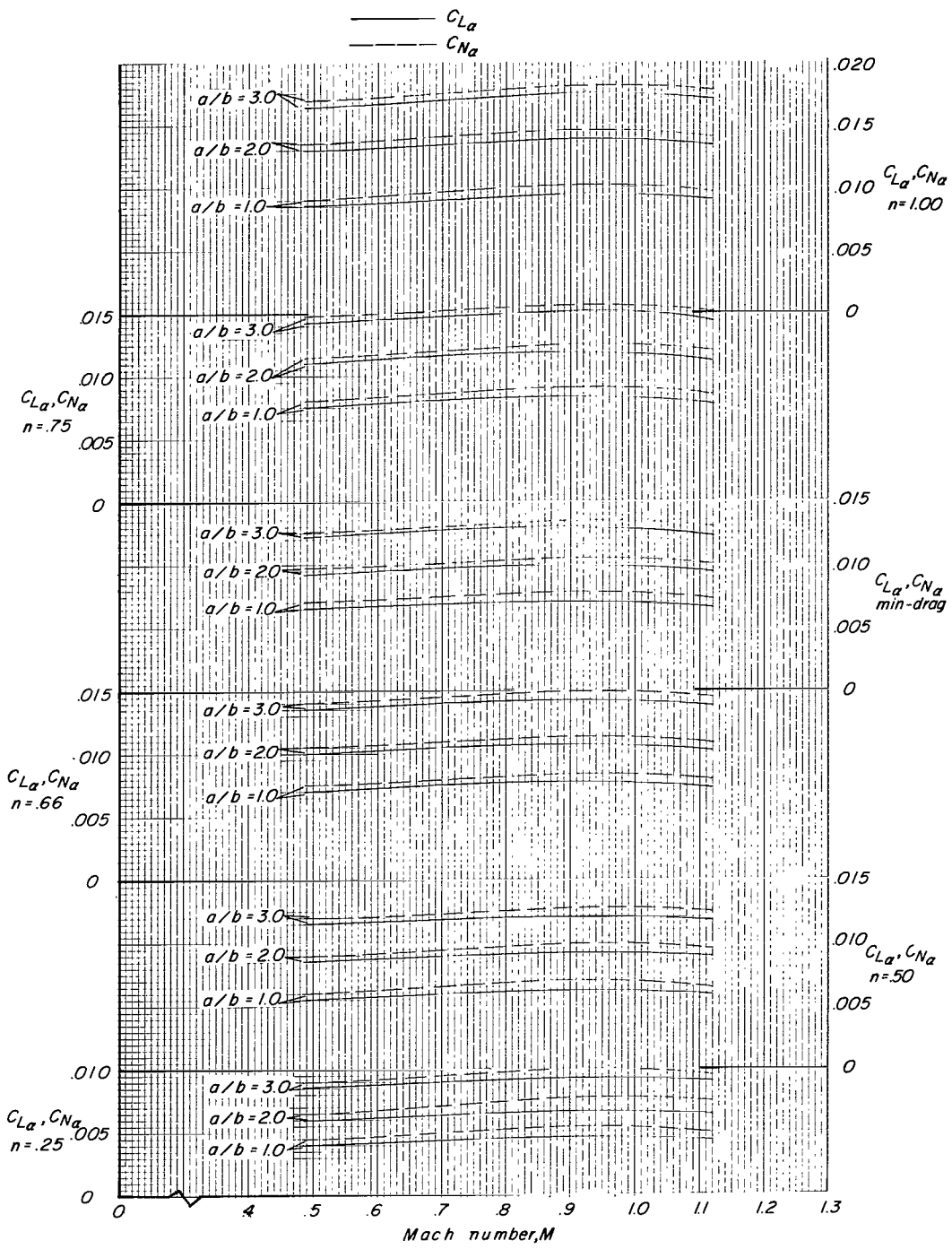

(a) Effects of Mach number on C_{L_α} and C_{N_α}.

Figure 10.- Summary of C_{L_α} and C_{N_α} parameters.

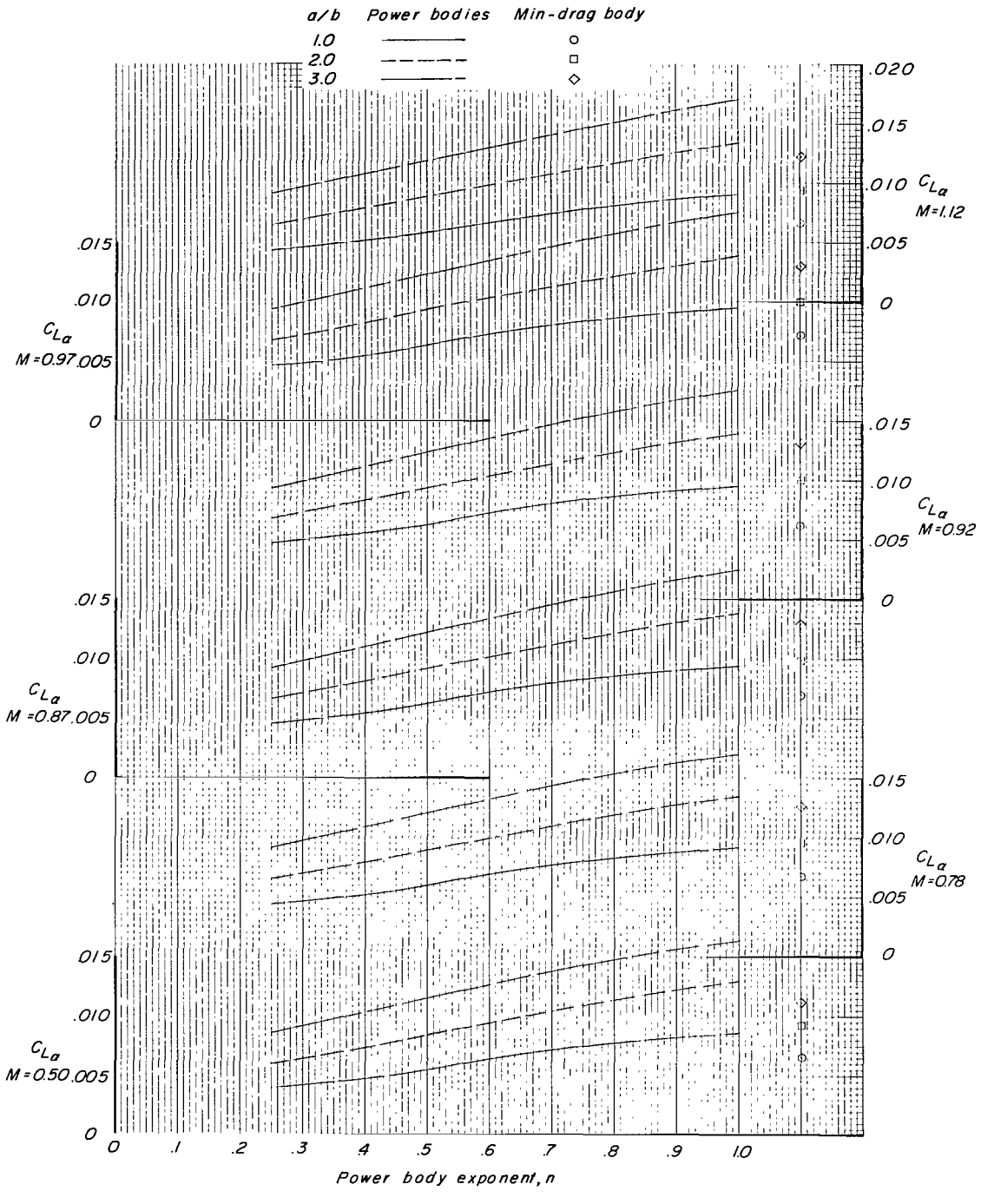

(b) Effects of power-body exponent on C_{L_α}.

Figure 10.- Continued.

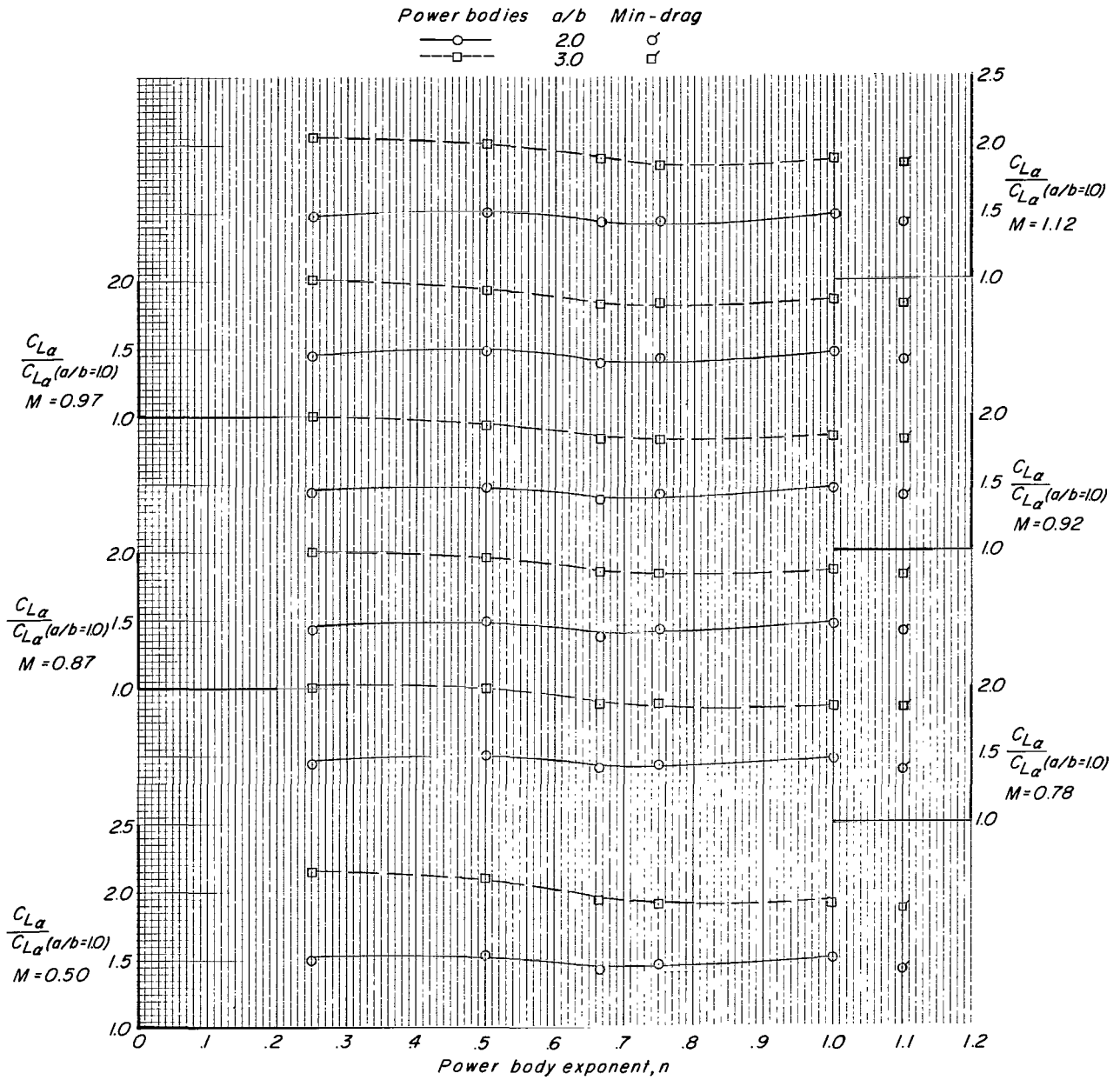

(c) Effects of power-body exponent on $\frac{C_{L_\alpha}}{C_{L_\alpha}(a/b = 1.0)}$.

Figure 10.- Concluded.

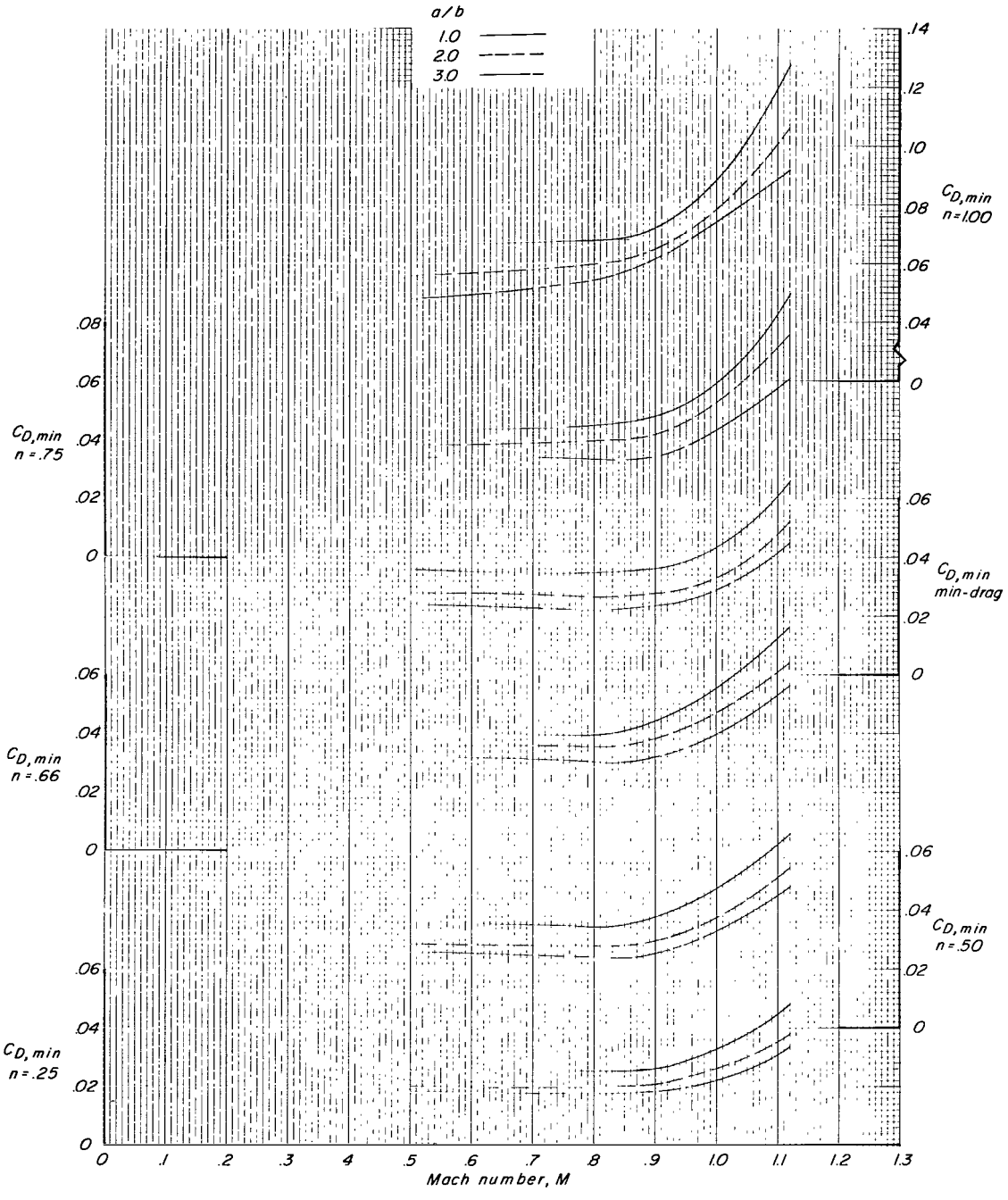

(a) Effects of Mach number on $C_{D,min}$.

Figure 11.- Summary of $C_{D,min}$ parameter.

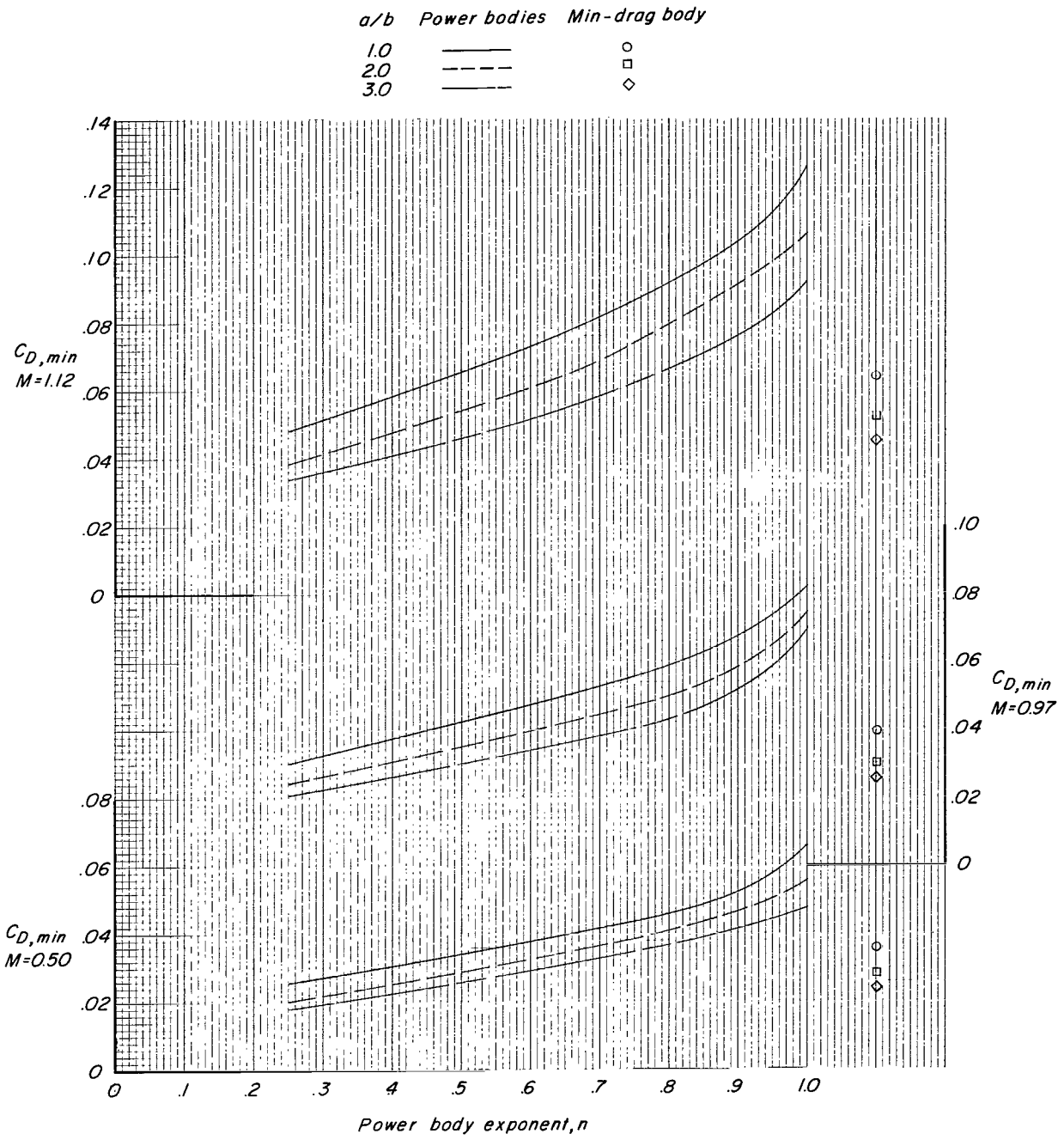

(b) Effects of power-body exponent on $C_{D,min}$.

Figure 11.- Continued.

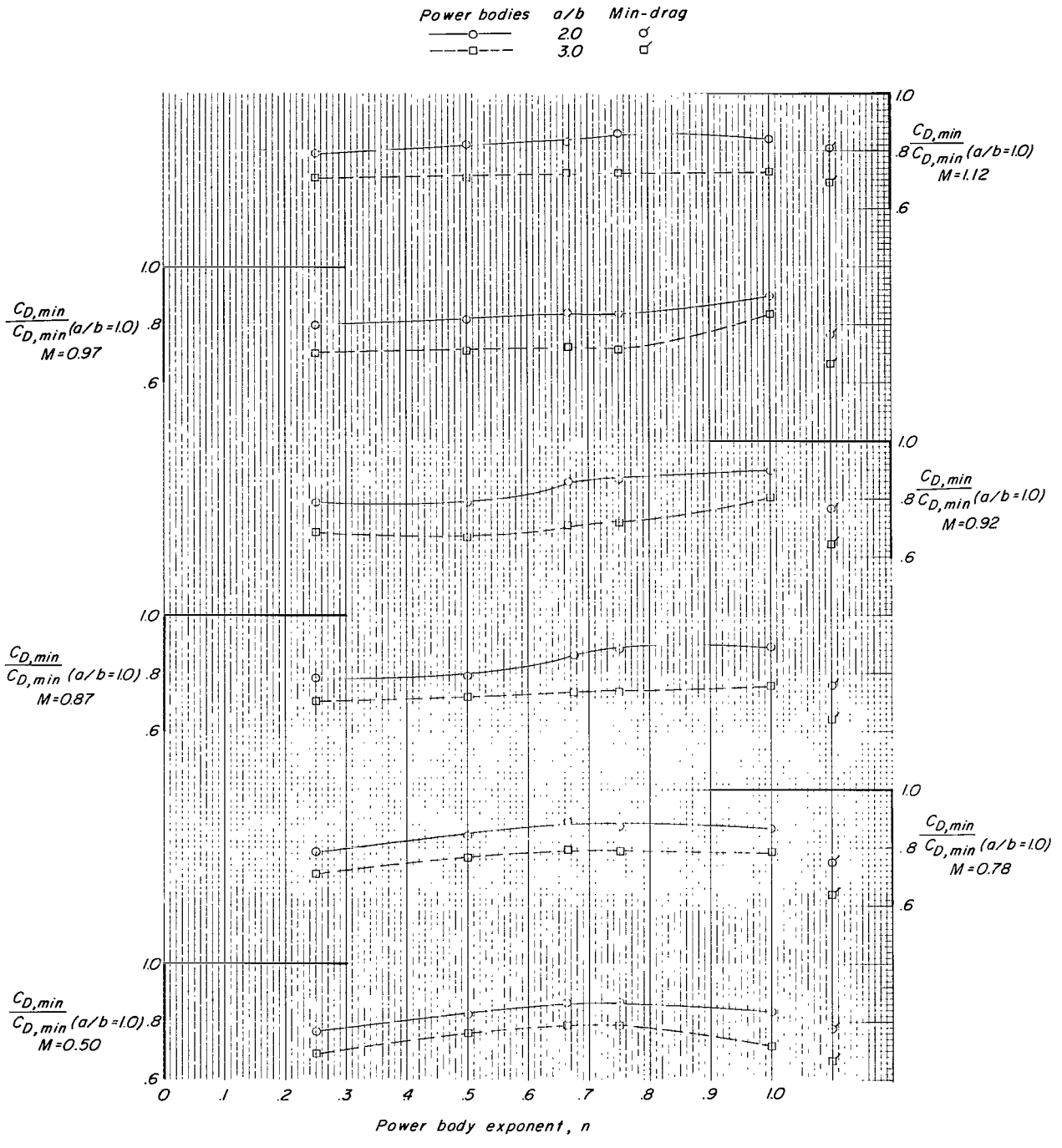

(c) Effects of power-body exponent on $\frac{C_{D,min}}{C_{D,min}(a/b = 1.0)}$.

Figure 11.- Concluded.

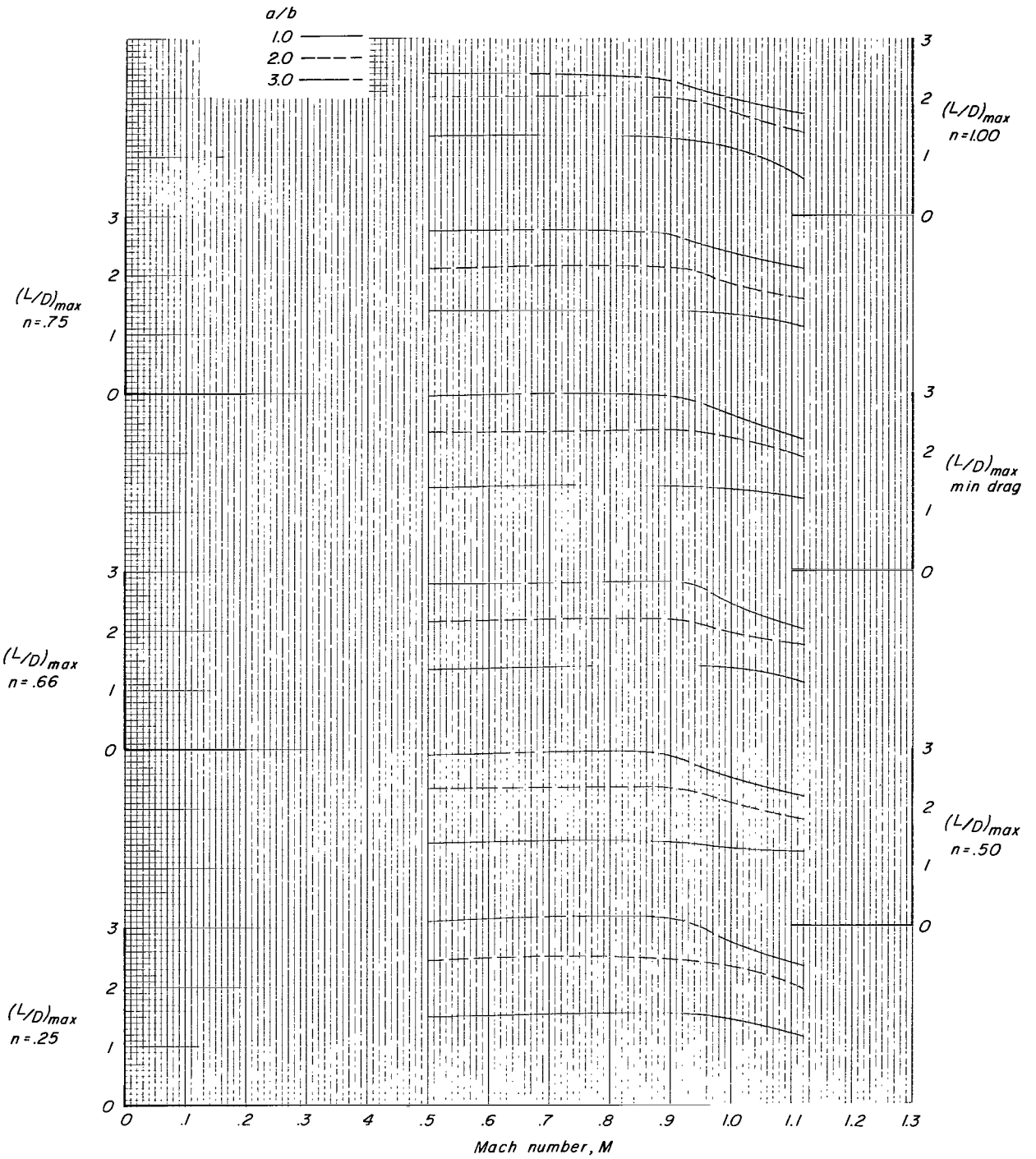

(a) Effects of Mach number on $(L/D)_{max}$.

Figure 12.- Summary of $(L/D)_{max}$ parameter.

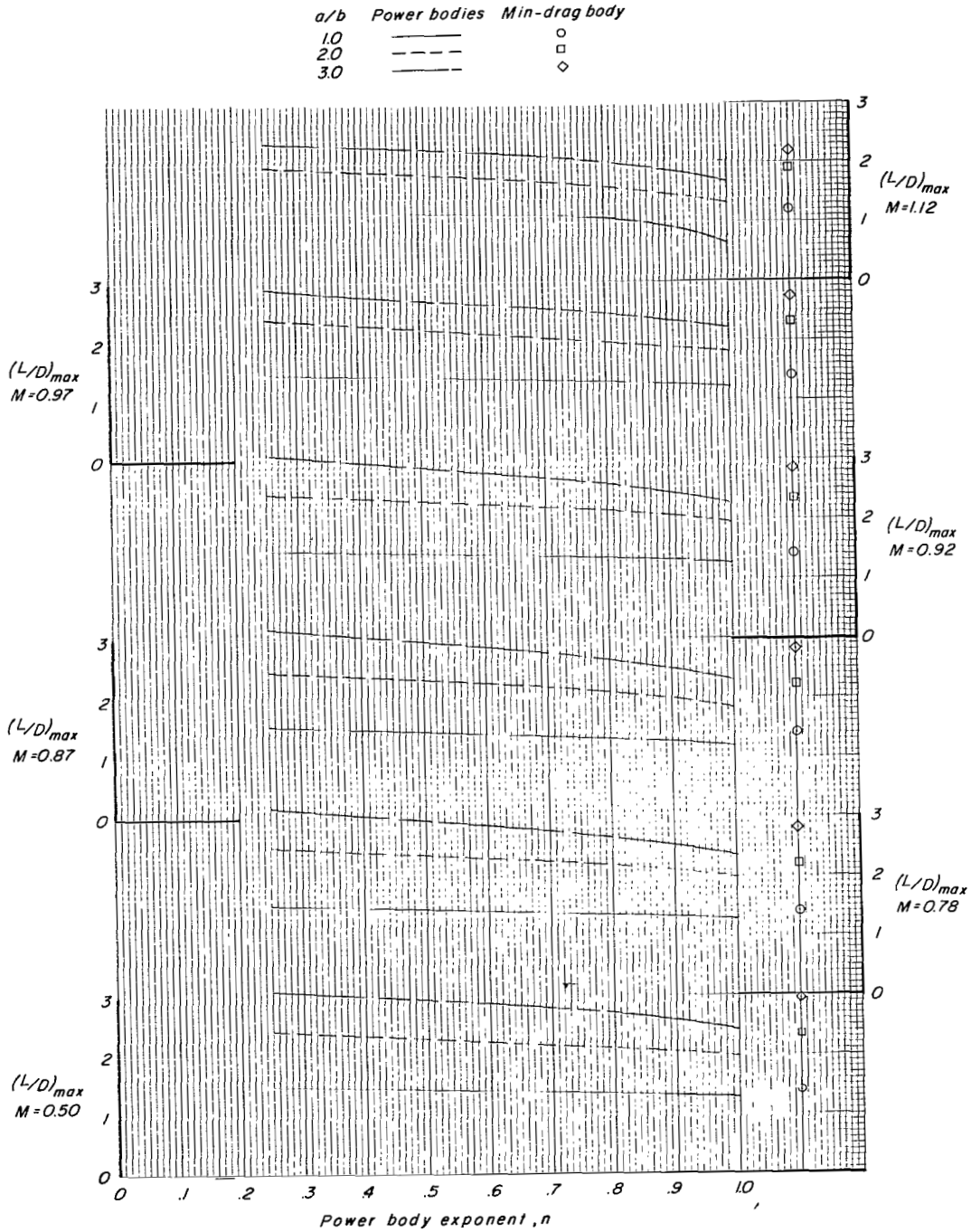

(b) Effects of power-body exponent on $(L/D)_{max}$.

Figure 12.- Continued.

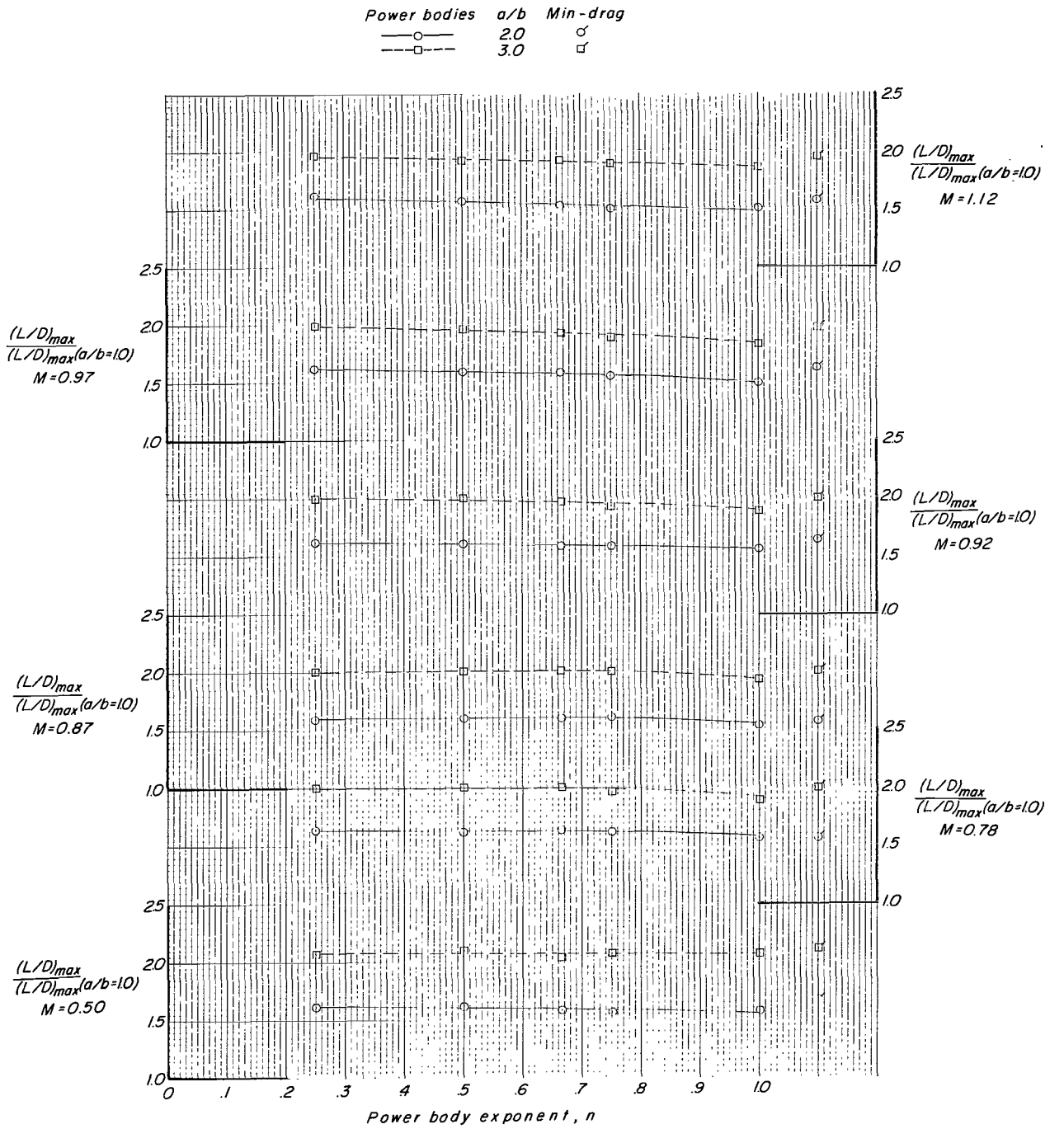

(c) Effects of power-body exponent on $\frac{(L/D)_{max}}{(L/D)_{max}(a/b = 1.0)}$.

Figure 12.- Concluded.

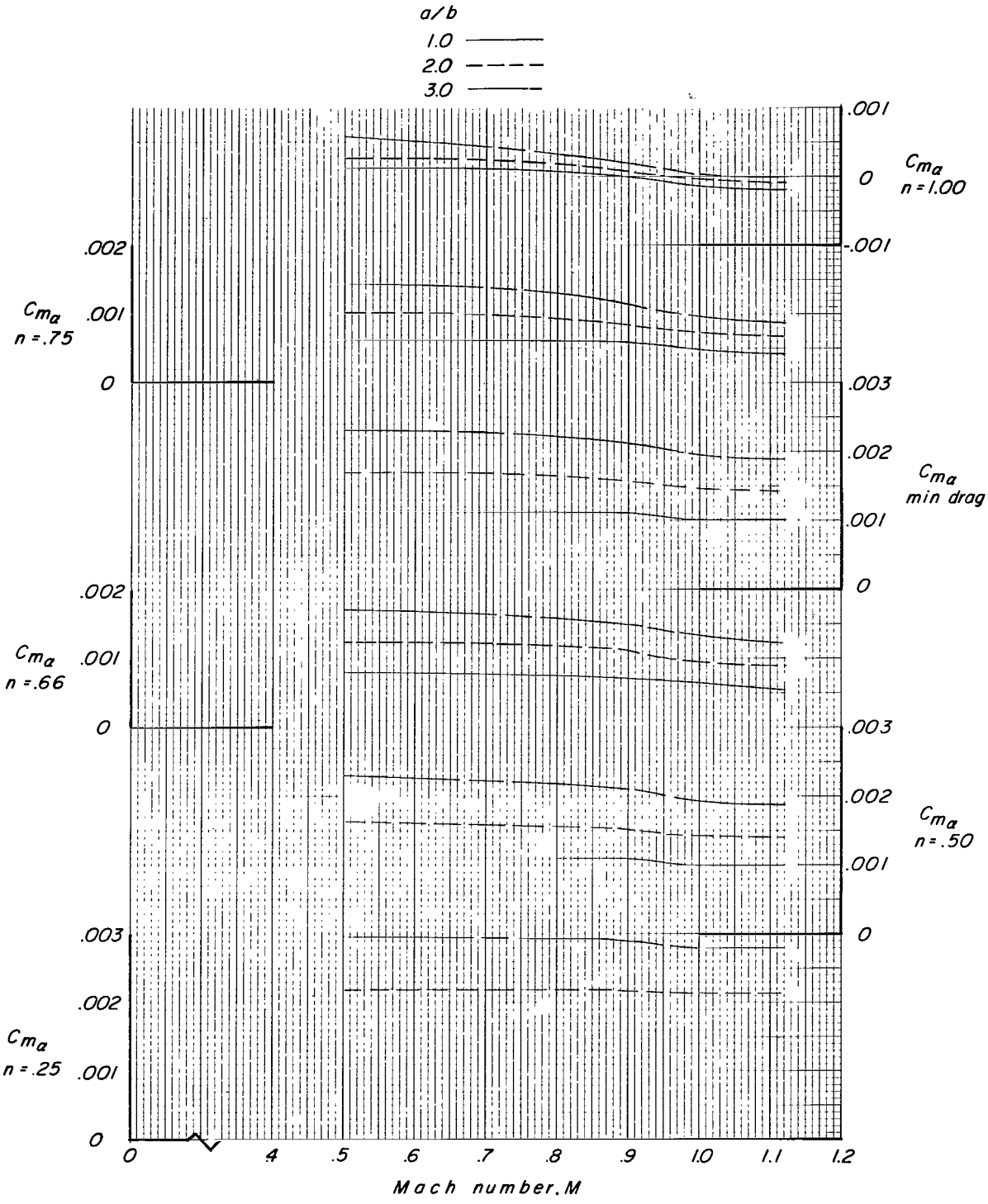

Figure 13.- Effects of increasing Mach number on the longitudinal stability parameter C_{m_α} for the power-law bodies and minimum-wave-drag body.

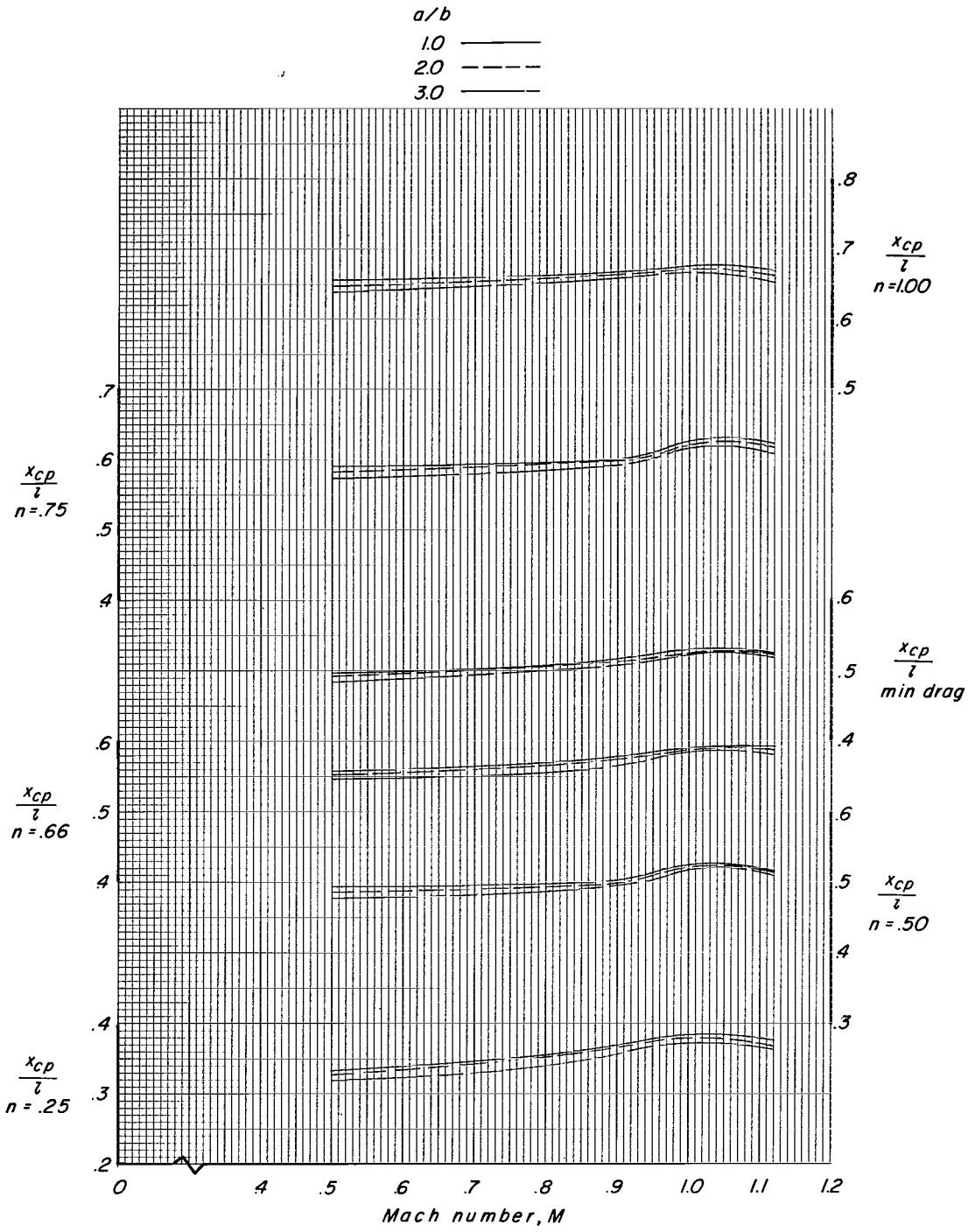

(a) Effects of Mach number on x_{cp}/l.

Figure 14.- Summary of x_{cp}/l parameter.

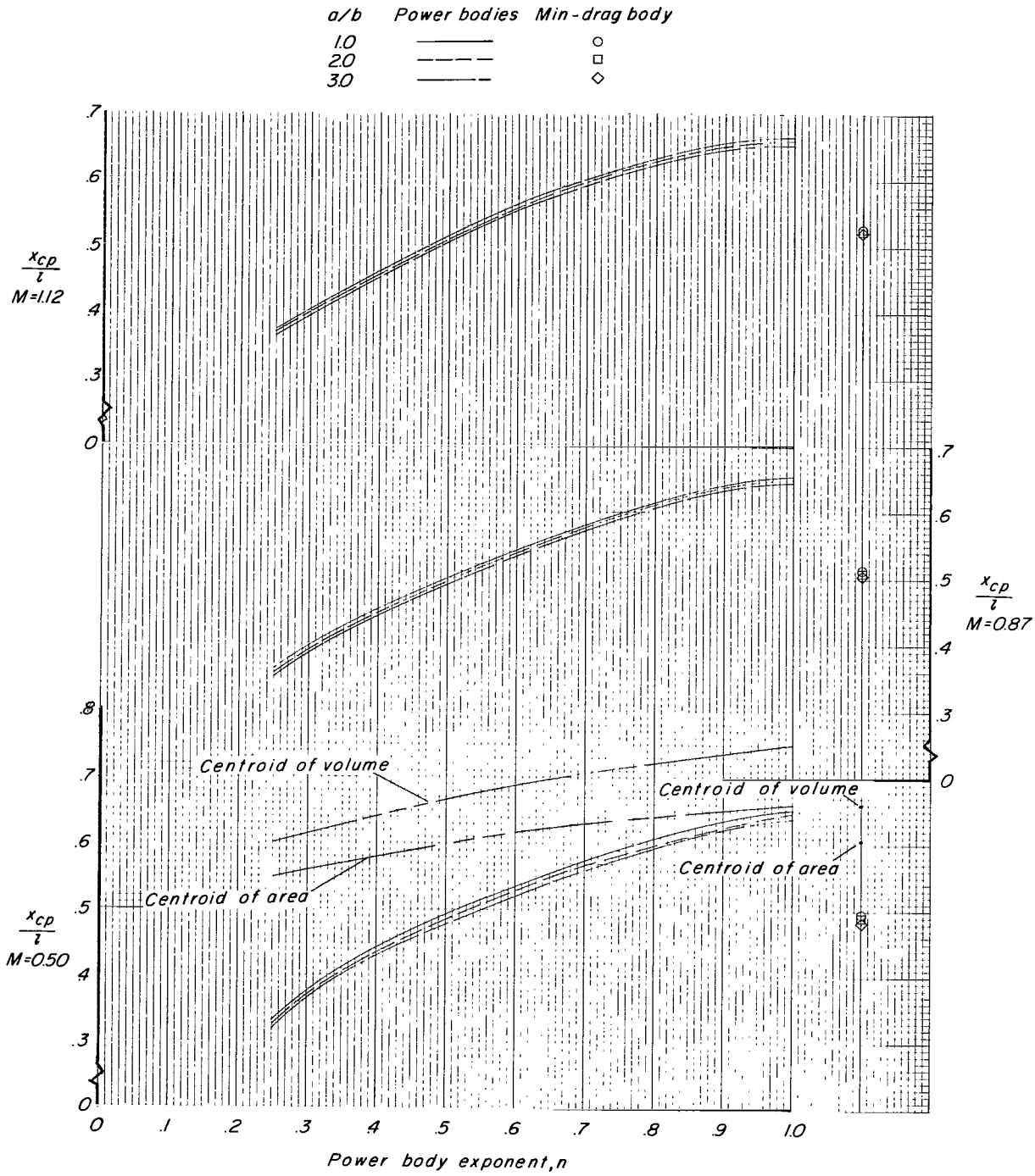

(b) Effects of power-body exponent on x_{cp}/l.

Figure 14.- Concluded.

"The aeronautical and space activities of the United States shall be conducted so as to contribute . . . to the expansion of human knowledge of phenomena in the atmosphere and space. The Administration shall provide for the widest practicable and appropriate dissemination of information concerning its activities and the results thereof."

—NATIONAL AERONAUTICS AND SPACE ACT OF 1958

NASA SCIENTIFIC AND TECHNICAL PUBLICATIONS

TECHNICAL REPORTS: Scientific and technical information considered important, complete, and a lasting contribution to existing knowledge.

TECHNICAL NOTES: Information less broad in scope but nevertheless of importance as a contribution to existing knowledge.

TECHNICAL MEMORANDUMS: Information receiving limited distribution because of preliminary data, security classification, or other reasons.

CONTRACTOR REPORTS: Technical information generated in connection with a NASA contract or grant and released under NASA auspices.

TECHNICAL TRANSLATIONS: Information published in a foreign language considered to merit NASA distribution in English.

TECHNICAL REPRINTS: Information derived from NASA activities and initially published in the form of journal articles.

SPECIAL PUBLICATIONS: Information derived from or of value to NASA activities but not necessarily reporting the results of individual NASA-programmed scientific efforts. Publications include conference proceedings, monographs, data compilations, handbooks, sourcebooks, and special bibliographies.

Details on the availability of these publications may be obtained from:

SCIENTIFIC AND TECHNICAL INFORMATION DIVISION

NATIONAL AERONAUTICS AND SPACE ADMINISTRATION

Washington, D.C. 20546